QA: N/A

Subject:
Planning Guidance for EBS Test Number 3-Drip Shield Test.

Date:
May 7, 1999
LV.EBSPM.JHP.05/99-005

From:
J. H. Pye

To:
Distribution

cc:
See Below

Location/Phone
Sum1/423
(702) 295-4250

This is a revision of IOC LV.EBSPM.JHP.04/99-004.

This guidance is issued in response to the License Application Design Selection (LADS) recommendation that the Enhanced Design Alternative 2 (EDA 2) be selected as the License Application (LA) baseline design for the repository. This option deploys a drip shield and diffusion limiting invert comprised of gravel fill as apart of the Engineered Barrier System (EBS).

This guidance is intended as a supplement to the Engineered Barrier Systems Test Plan, entitled "Engineering Plan: Evaluation of Alternative Design Features Engineered Barrier Systems, BB0000000-01717-4600-00001, Rev 01 A, January 20, 1999". Specifically this guidance is to provide sufficient direction for the design of the EBS Test # 3 to assess the performance of the drip shield as a means to prevent water from contacting the simulated waste packages. Conceptual engineering sketches show how the 2-cm. thick drip shield could be installed in the emplacement drifts are presented in Figure 1 and 2.

The primary objectives of the EBS Pilot Scale Test # 3 are to demonstrate, at approximately ¼ scale, the movement of the moisture (water dripping from the crown of the emplacement drift) in the EBS system. For this test, the EBS system is defined as the supports for the simulated waste package, the drip shield, the invert material, and the tunnel walls. The EBS Test # 3 will be performed in the EBS Pilot Scale Test Facility located in the North Las Vegas DOE complex on Losse Road.

General guidance for conduct of this test is as follow:

A. Test Set Up

- An existing Pilot Scale Test Cell will be used for this test. This test cell is fabricated from mild carbon steel. It has nominal dimensions of 1.4-m diameter and 4-m in length. The cell is predrilled with holes for instrumentation access, water injection ports and wicks to remove water.

- Modify test cell as needed by either plugging some of the predrilled holes or drilling additional holes for removing moisture or for installing instruments.
- 240 V power will be required for the heaters.
- The invert will be formed from the crushed welded tuff from the Yucca Mountain ECRB excavation. The particle size for the invert material will have size range from 0.0187-0.0787 in (material retained on the sieve #4 and passing through the sieve #10).
- J-13 water from the Yucca Mountain will be used for irrigation. Approximately 500 gallons of J-13 water will be required for the test.
- The simulated waste package will be fabricated from mild carbon steel to a dimension of nominally 39.1-cm (1/4 scale of the 21 PWR waste packages). The pedestal for the simulated waste will be also fabricated from mild carbon steel and welded in place with a V-shaped support. The base of the V support will be nominally 21 cm from the bottom of the inner surface of the test cell.
- The simulated drip shield will be constructed from ANSI 304 stainless steel, which has a thermal conductivity similar to titanium grade 7. The simulated drip shield will be fabricated in three sections with sleds on each side at the bottom. The segment seam covers will be fabricated from 304 stainless steel and placed over the adjacent drip shield segments. It may be necessary to weld the seam cover segments to either end of the drip shield segment or slide it over the adjacent section of the drip shield.
- The final test configuration will be based on a ¼ scale dimensional analysis and pretest predictive modeling. Where necessary simplifying assumptions will be made and documented by Sandia National Laboratories (Sandia).
- Lawrence Livermore National Laboratory (LLNL) will provide/install 36 metal coupons on the surface of the simulated waste package and the drip shield. The metal coupons will be installed in-groups of 4 at three different locations along the length of the drip shield. The test coupons will be installed so that there is no galvanic coupling with other components of the test apparatus. This can be accomplished by using electrically insulating washer and sleeves.
- The coupons will be fabricated by LLNL from Alloy 22, a Ni-Cr-Mo alloy; Ti-Gr 16, a Ti-0.05 Pd alloy, and A516 GR 70, carbon steel. The test coupons will be approximately 5 cm x 5 cm 0.16 cm thick.
- Water samples will be collected by the Test Coordination Office (TCO) from the injection tanks and the water exiting from the test cell according to the QA procedures listed in the Field Work Package (FWP). LLNL will analyze the samples and provide information to the test participants.
- LLNL and Los Alamos National Laboratory (LANL), in coordination with the TCO, will also take, aseptically collected. Chemical samples for microbial activity within the test cell from the invert material before and after the test in accordance with the applicable QA procedures listed in the FWP.
- Collect five samples of the invert material prior to the start of the test.
- Twenty-five samples, in triplicate, of the invert material are to be collected at the end of the test.

- The collected invert material samples will be from the surface of the invert material and approximately 15 cm. below the surface. The samples will be collected from outside boundary of the drip shield. Samples are to be collected from at least five locations below the entire length of the drip shield and from at least five locations from the invert material exposed to the dripping water along the length of the test cell.
- The collected samples will be placed in double ziplock bags and immediately placed on dry ice and transferred to a –70-C. freezer for further analysis by LANL.
- The sample size for each of the invert material sample will be approximately 100 gm.
- The sample size of each water sample will be about 10 ml.
- The chemistry of water and the invert materials will be determined by LLNL.
- USGS will provide the hydrologic properties of the invert materials before and after the test.
- UFA Ventures, Inc. will provide the laboratory derived diffusion coefficient for the invert material on samples provided to the UF A Ventures Inc. by the USGS.

B. Test Conditions

- The water will be injected on a rectilinear grid covering both waste package and invert, nominal pattern as shown in Figure 3. The configuration of the simulated drip shield and the waste package is presented in Figure 4.
- The Heating system in the simulated waste package will be capable of raising the simulated waste package to a temperature of 100°C and the test cell canister boundary heaters will be capable of raising the test cell boundary wall temperature to 60°C.
- The test cell will be insulated to minimize the effects of outside temperature changes on the test.
- As tracer FD&C Blue 1 food color or equivalent will be used in the injected water. This dye is commercially known as Brilliant Blue FCF, Acid Blue 9.
- The water injection rate will be nominally 250 ml/hr/m of the length of the test cell.
- Initial moisture content of the invert material will be determined by the USGS from the samples collected as the invert material is placed in the test cell after it has been air-dried.
- Sandia will perform the pre and post test analysis of the test.
- Camera runs, sampling and observations guidance shall be revised, as necessary, to reflect test activities for this test as compared to the earlier pilot scale tests performed in the Atlas facility (Test # 1 and 2).

C. Conduct of Test

The EBS Test #3 heating system(s) and heating/irrigation schedule is a very complex issue. Very preliminary analyses by Sandia suggest that large temperature gradients will be present within the canister if only a single line heat source located within the simulated waste package is used. These calculations showed that with a simulated waste package temperature of 80 degrees C, the drip shield would be at 70 degrees C and the outer canister would be at 45 degrees C. The gradient of 35 degrees C

exceeds by 15 degrees from the target temperature gradient. Therefore, the boundary heaters will be installed to the outside wall of the test cell to maintain a temperature gradient of approximately 20 degrees C.

The EBS Test #3 will be conducted in two Parts. Part 1of the test will evaluate the thermal influence of the drip shield in the ¼ scale configuration without irrigation. Part 2 of the test will evaluate the

Performance of the drip shield system at elevated temperature.

C. 1 - EBS Test #3-Part 1- Evaluate the Thermal Influence of the Drip Shield

Construct the test with a subset of the instrumentation, Figures 5-9, necessary for the EBS Test #3-Part 2.

This part of the test will primarily concentrate on the thermal instrumentation (RTD's) placed on the midpoint centerline configuration (Y=2m), Figures 10-14. Both sets of the heaters and controllers will also be installed. The drip shield and associated instrumentation will not be installed during this portion of the test. The test will follow the same heating schedule as for the Part 2 of the test as described in C.2.

- Initiate Q data collection.
- Set system temperature on both inside and outside to nominally 60°C.
- Let system come to thermal equilibrium.
- Increase simulated waste package temperature to nominally 80°C in 5°C increments.
- Allow the test to reach equilibrium at each 5°C increment to a final temperature of approximately 80°C inside the simulated waste package and the outside wall of the test cell to approximately 60°C.

At the completion of the Part-1 of the test, the system will be allowed to cool to approximately ambient Conditions at which time the front cover from the test cell will be removed and the drip shield and additional instrumentation will be installed.

C.2 -EBS Test # 3 - Part 2. Start of Dripping Water at Elevated Temperature

- Install all the remaining instruments and reinstall the front cover.
- Insulate the test cell.
- Activate the Data Acquisition System.
- Evaluate the heating system prior to beginning the test.
- Bring system up to operating temperature of nominally 60°C.
- Evaluate time to "steady-state" and thermal flux through system.
- Initiate Q data collection.
- Set system temperature on both inside and outside to nominally 60°C.
- Let system come to thermal equilibrium

- Increase simulated waste package temperature to nominally 80°C in 5°C increments.
- Let system reach equilibrium at each 5°C increment and at final temperature of nominally 80°C inside and 60°C to the outside wall of the test cell.
- Begin irrigation at a rate of nominally 250ml/hr/m length of the test cell.
- Allow system to equilibrate.
- Increase both inside and outside temperatures in 5°C increments.
- Allow system to equilibrate at each temperature increment.
- Perform the water collection and visualization at each increment of the temperature.
- Collect other samples as required.

The power to each of the inner and outer heater systems may be controlled by a silicon-rectified controller(s) which "pulse" power or a similar device on an as needed basis. Each of the heaters will require the use of power monitors connected to the DAS as shown in Figure 15.

D. Data Collection

The data will be collected using data loggers, automatic data collection system from instruments installed in the invert material and installed inside the test cell. Sandia will establish the instruments to be installed and their location within the test. The type of instruments that might be installed are listed below:

Thermocouples
Thermocouple Pyschrometers and Vaisala RH gages for relative humidity
Scales for monitoring water balance
RTD's
Thermistors
Heat Dissipation Probes
Wicks
Lysimeters
Cameras
Tensiometers
Pressure Transducers
TDR's

E. Data Reporting

The data will be reported as described in the FWP and the Test Plan. Sandia will prepare a test report at the conclusion of the test. The report will include data analysis, as built test information conclusions and recommendations. The data produced by participants other than Sandia will be appended to the report. The Appendices will include work performed, test data, test results, any conclusions and recommendations. All data will be submitted to project technical database in accordance with the current project QA Procedures.

F. Safety Considerations

Job Safety Analysis (JSA) will be performed by the TCO to identify any hazards related to this test. Since this test will have hot surfaces and higher voltage power as compared to the EBS Test # 1 and # 2. the JSA should identify potential hazards and provide required mitigation.

G. Test Termination

Decision to terminate the test will be made by the EBS Performance Testing Department. Sandia and other participants will be provided test termination guidance. The TCO will receive written guidance that the scope of the test has been completed so that the Field Record Packages may be closed and submitted.

H. Point of Contact

For questions and clarifications please call Hemi Kalia at (702) 295-4339 or me at (505) 295-4250. respectively. Thank you.

JHP/HNK/mmc

Distribution:
R. W. Andrews, M&O, Las Vegas, NV
K. K. Bhattacharyya, M&O, Las Vegas, NV
John Case, M&O, Las Vegas, NV
D. A. Chesnut, M&O, Las Vegas, NV
Veraun Chipman, M&O, Las Vegas, NV
James Conca, M&O/LANL, Las Vegas, NV
J. J. Danneels, M&O/SNL, Albuquerque, NM
R. E. Finley, M&O/SNL, Albuquerque, NM
G. E. Gdowski, M&O/LLNL, Livermore, CA
L. E. Hersman, M&O/LANL, Los Alamos, NM
R. L. Howard, M&O, Las Vegas, NV
H. N. Kalia, M&O/LANL, Las Vegas, NV
William Lowry, M&O, Las Vegas, NV
M. T. Peters, M&O, Las Vegas, NV
L. D. Rickertson, M&O, Las Vegas, NV
R. L. Schreiner, M&O, Las Vegas, NV
S. F. Schuermann, QATSS, Las Vegas, NV
Christine Stockman, M&O/LLNL, Livermore, CA
S. H. Swenning, QATSS, Las Vegas, NV
D. J. Weaver, M&O, Las Vegas, NV
RPC=Total Pages 21

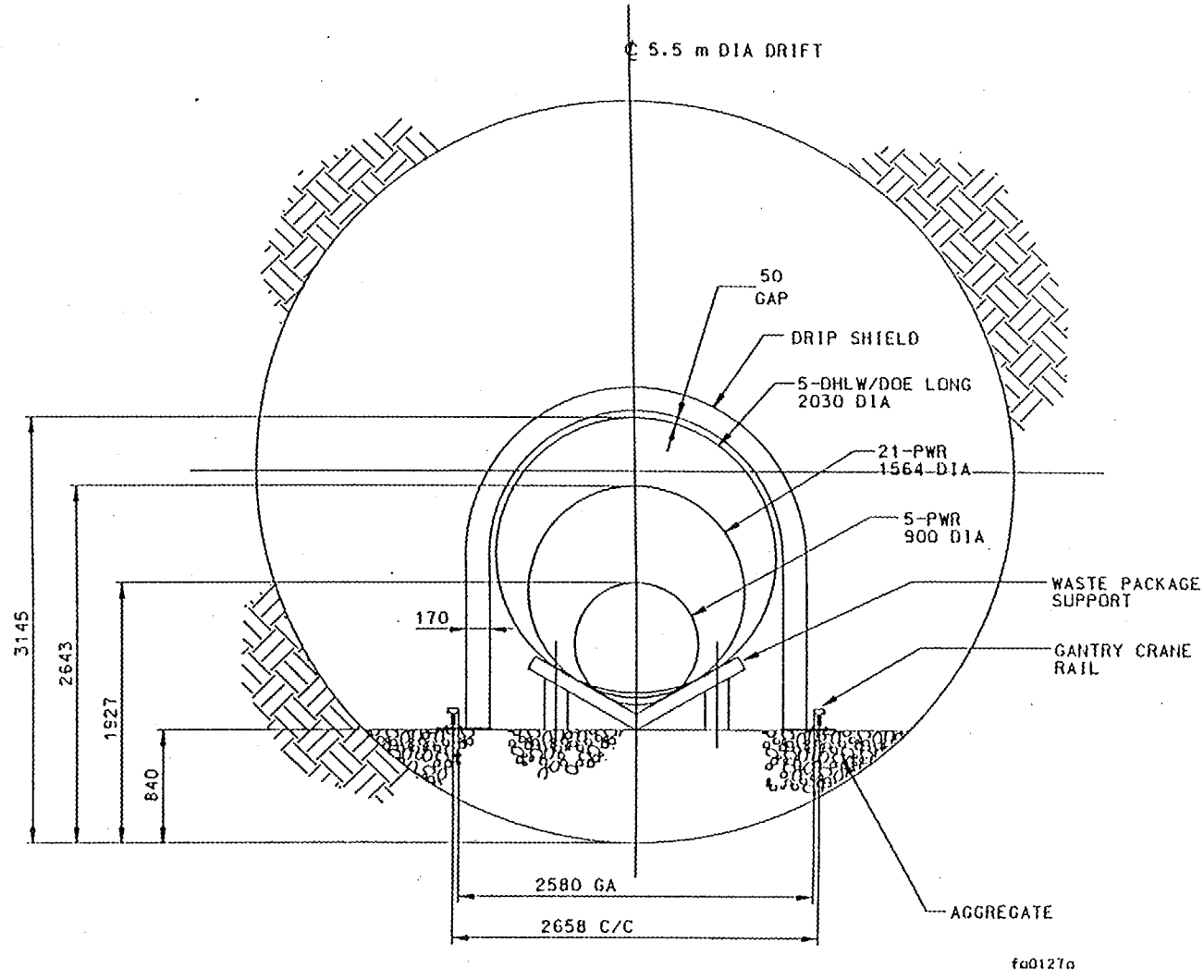
℄ 5.5 m DIA DRIFT
50
GAP
DRIP SHIELD
5-DHLW/DOE LONG
2030 DIA
21-PWR
1564 DIA
5-PWR
900 DIA
WASTE PACKAGE
SUPPORT
GANTRY CRANE
RAIL
170
3145
2643
1927
840
2580 GA
2658 C/C
AGGREGATE
fa0127a
fa0127a.PPT

Figure 1

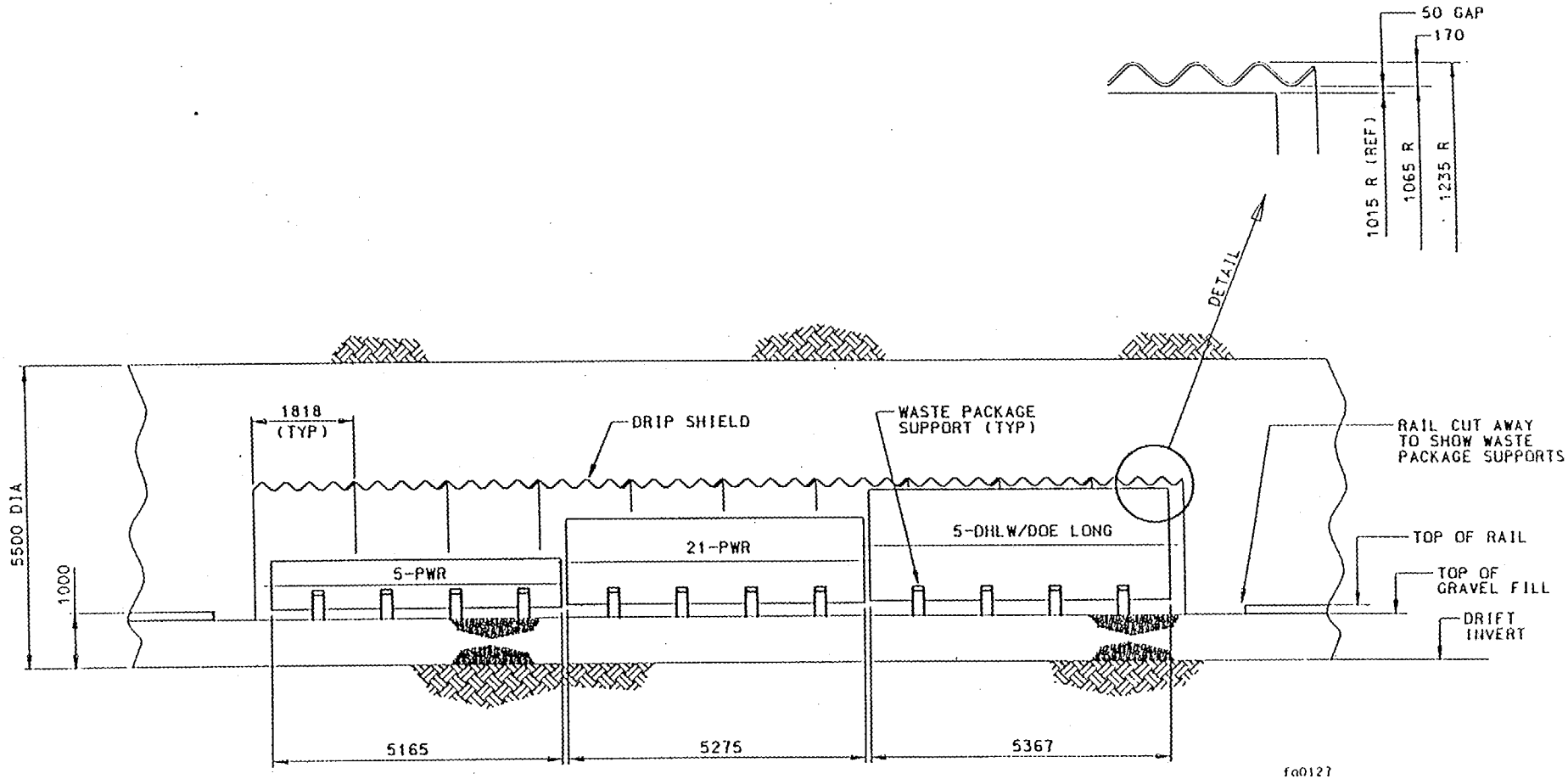

LONGITUDINAL SECTION

SCALE: NTS

Fa0127.PPT

Figure 2

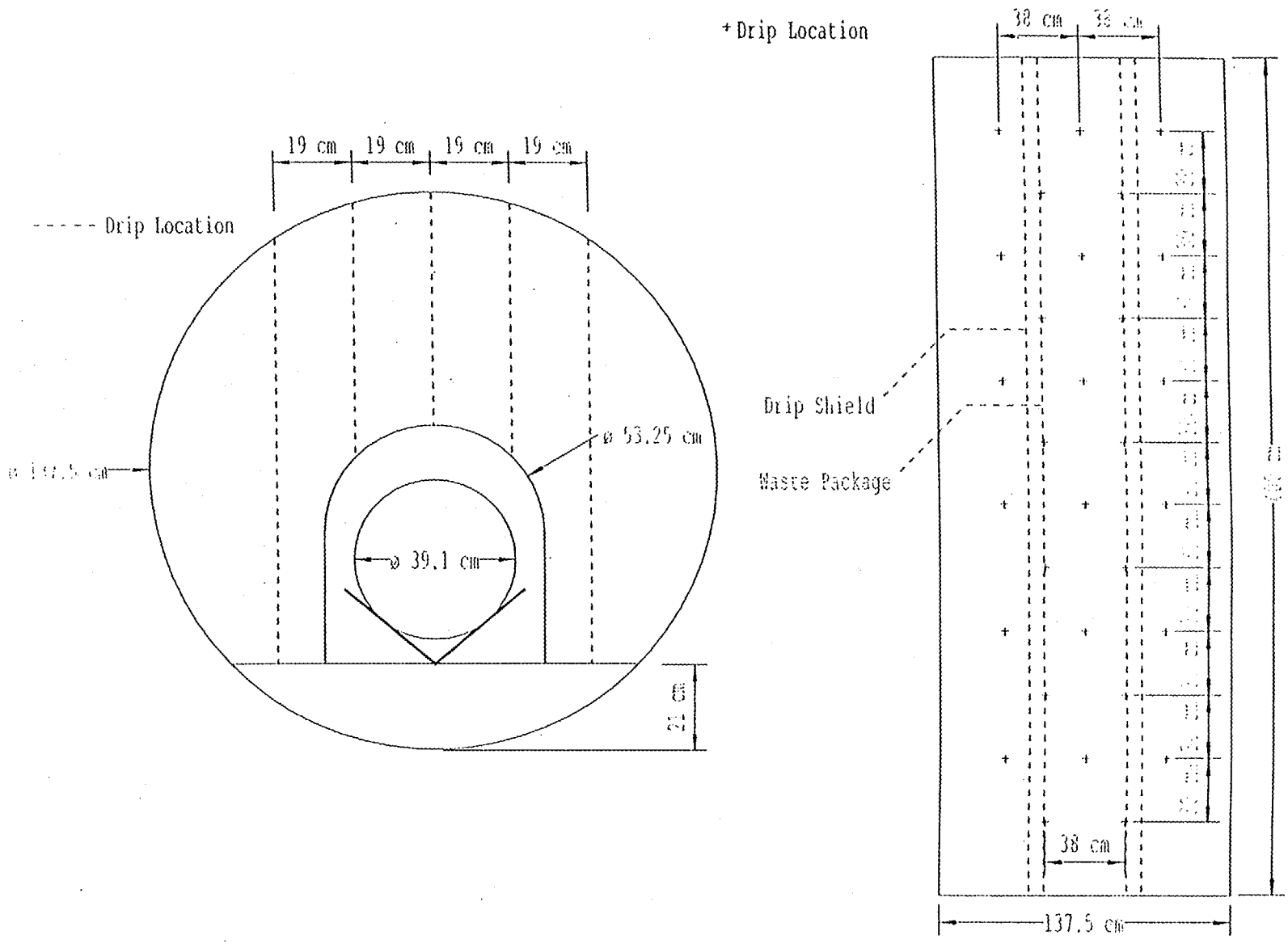
19 cm
19 cm
19 cm
19 cm
Drip Location
ø 53.25 cm
ø 39.1 cm
Drip Location
38 cm
38 cm
Drip Shield
Waste Package
38 cm
137.5 cm

Figure 3

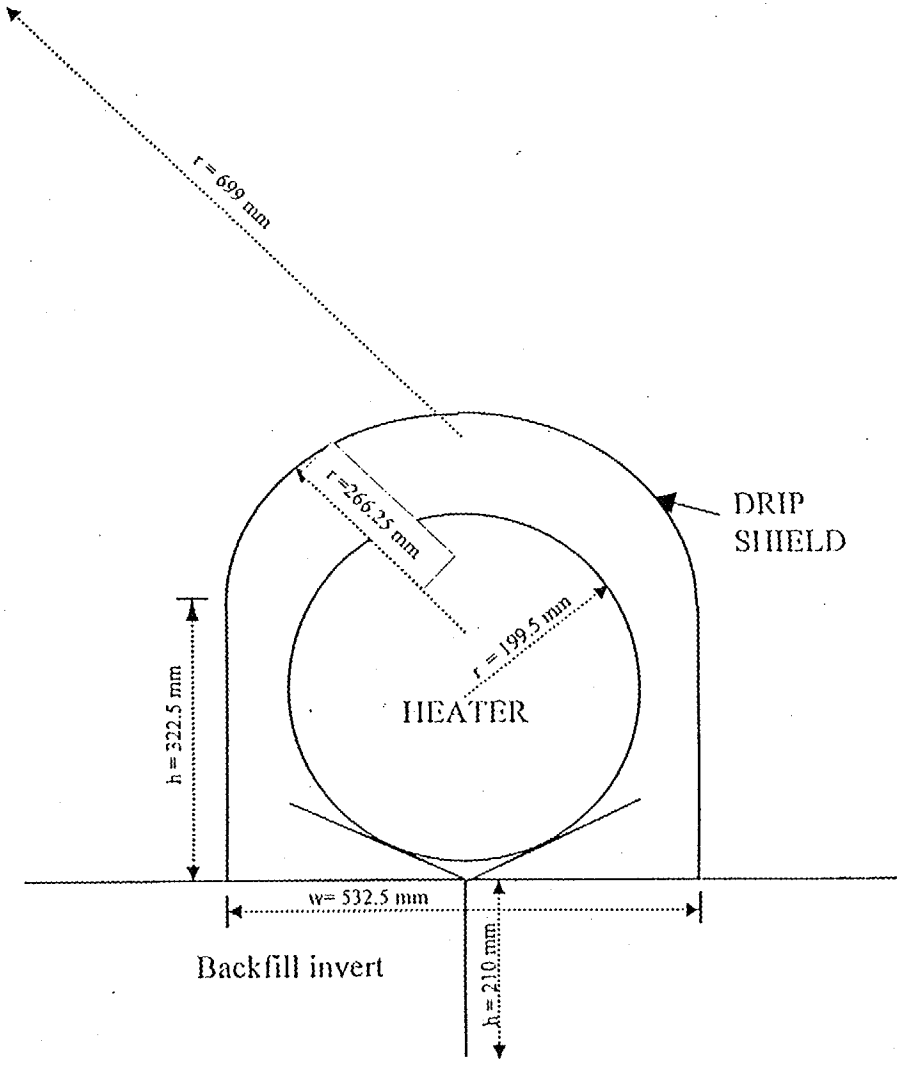
r = 699 mm
CANISTER
r =266.25 mm
DRIP
SHIELD
r = 199.5 mm
HEATER
h = 322.5 mm
w= 532.5 mm
Backfill invert
h = 210 mm

Figure 4

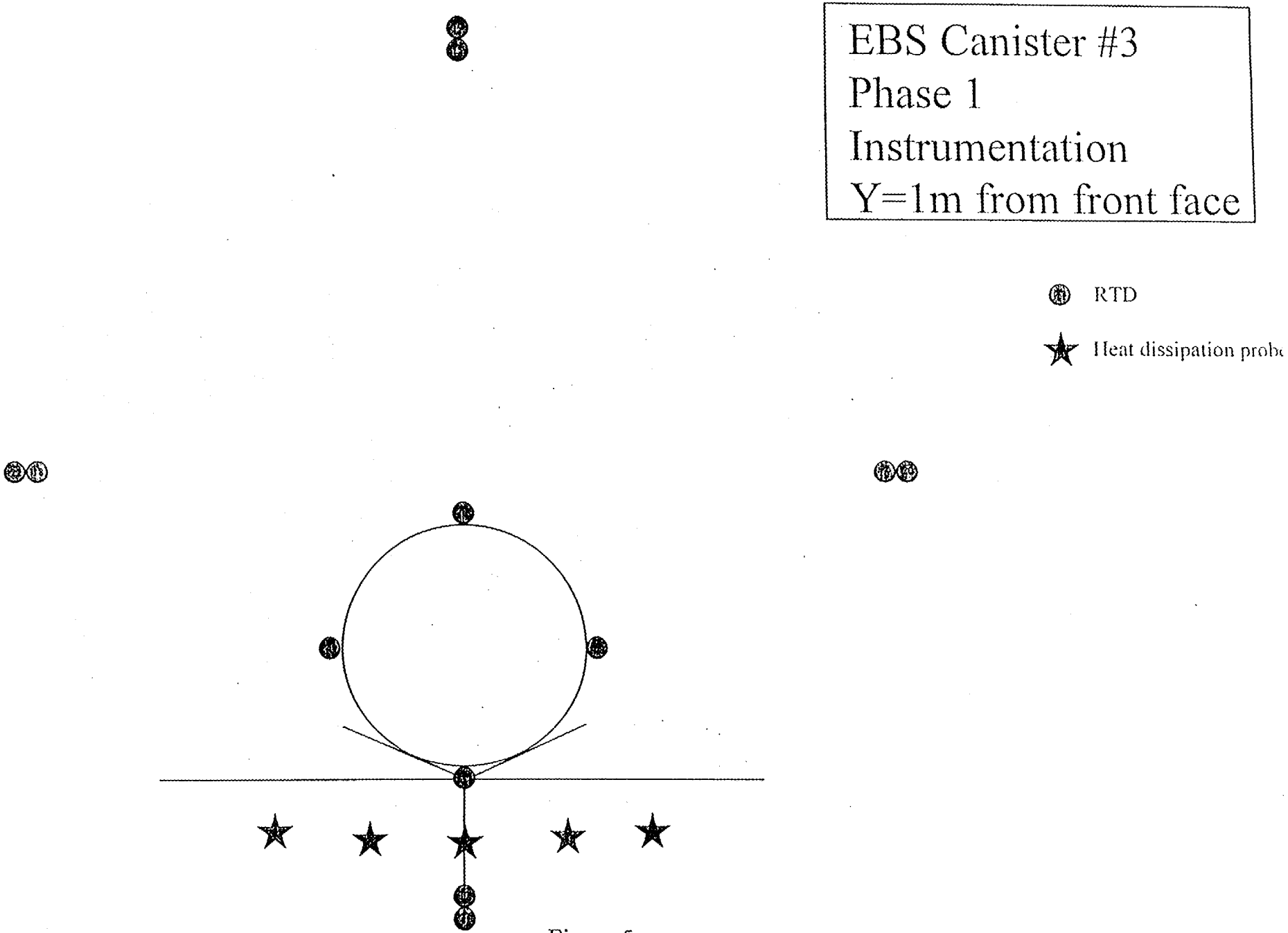
EBS Canister #3
Phase 1
Instrumentation
Y=1m from front face
RTD
Heat dissipation probe

Figure 5

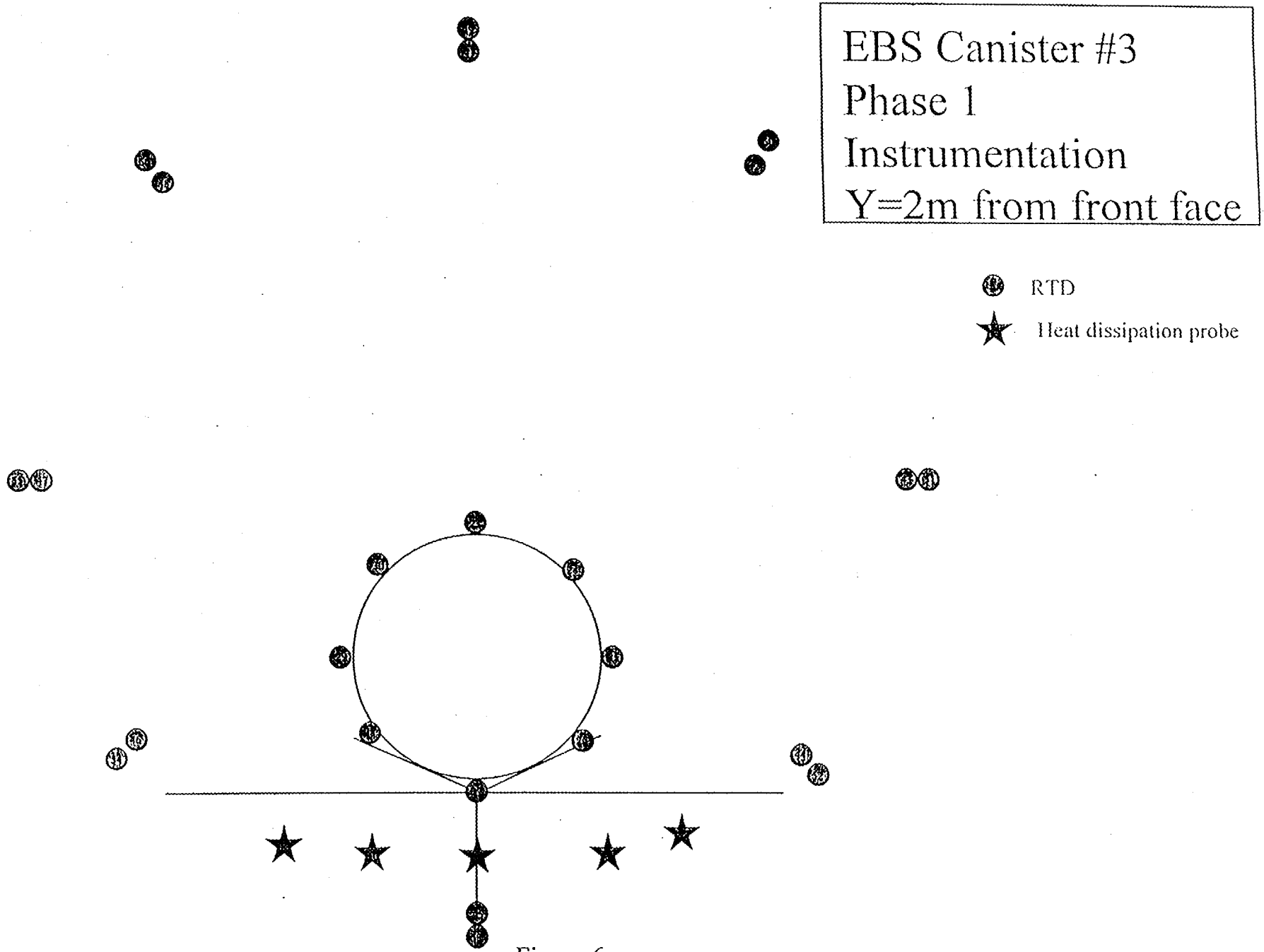
EBS Canister #3
Phase 1
Instrumentation
Y=2m from front face
RTD
Heat dissipation probe

Figure 6

EBS Canister #3
Phase 1
Instrumentation
Y=3m from front face

RTD

Heat dissipation probe

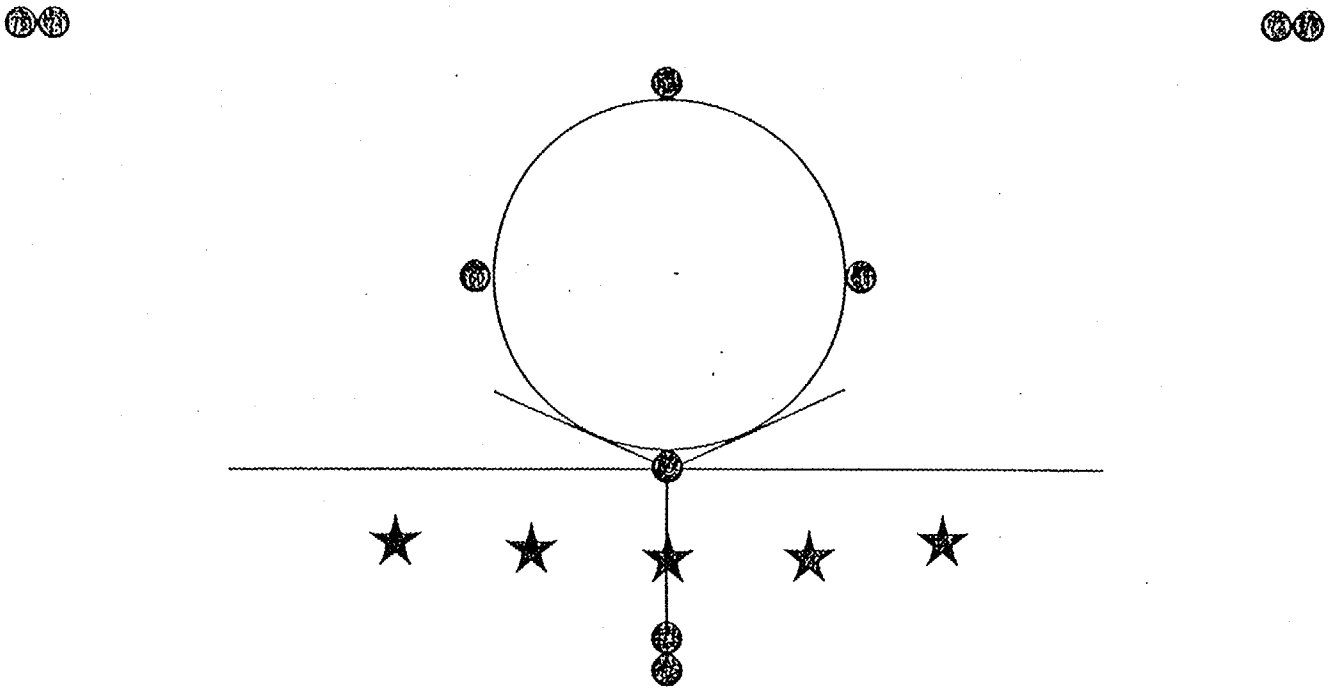

Figure 7

EBS Canister #3
Phase 1
Instrumentation
Front Face

CANISTER

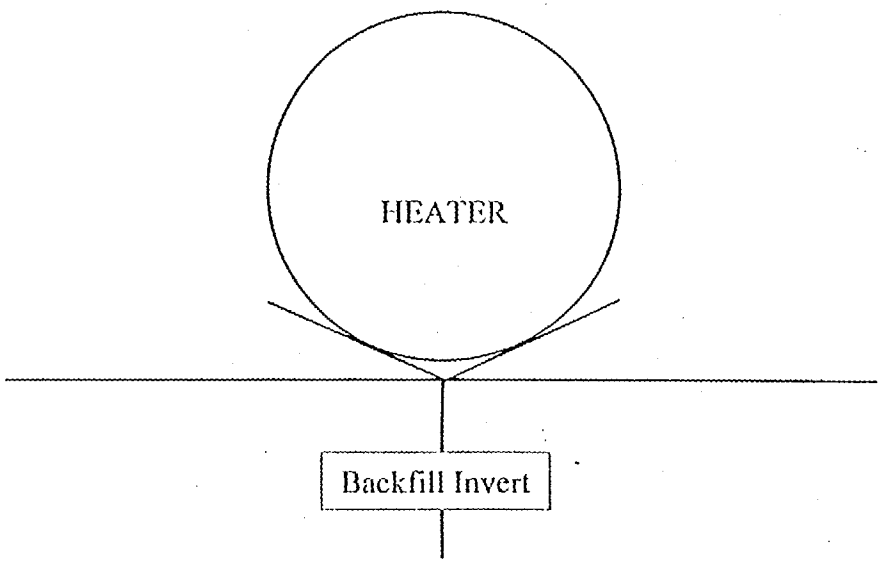

Figure 8

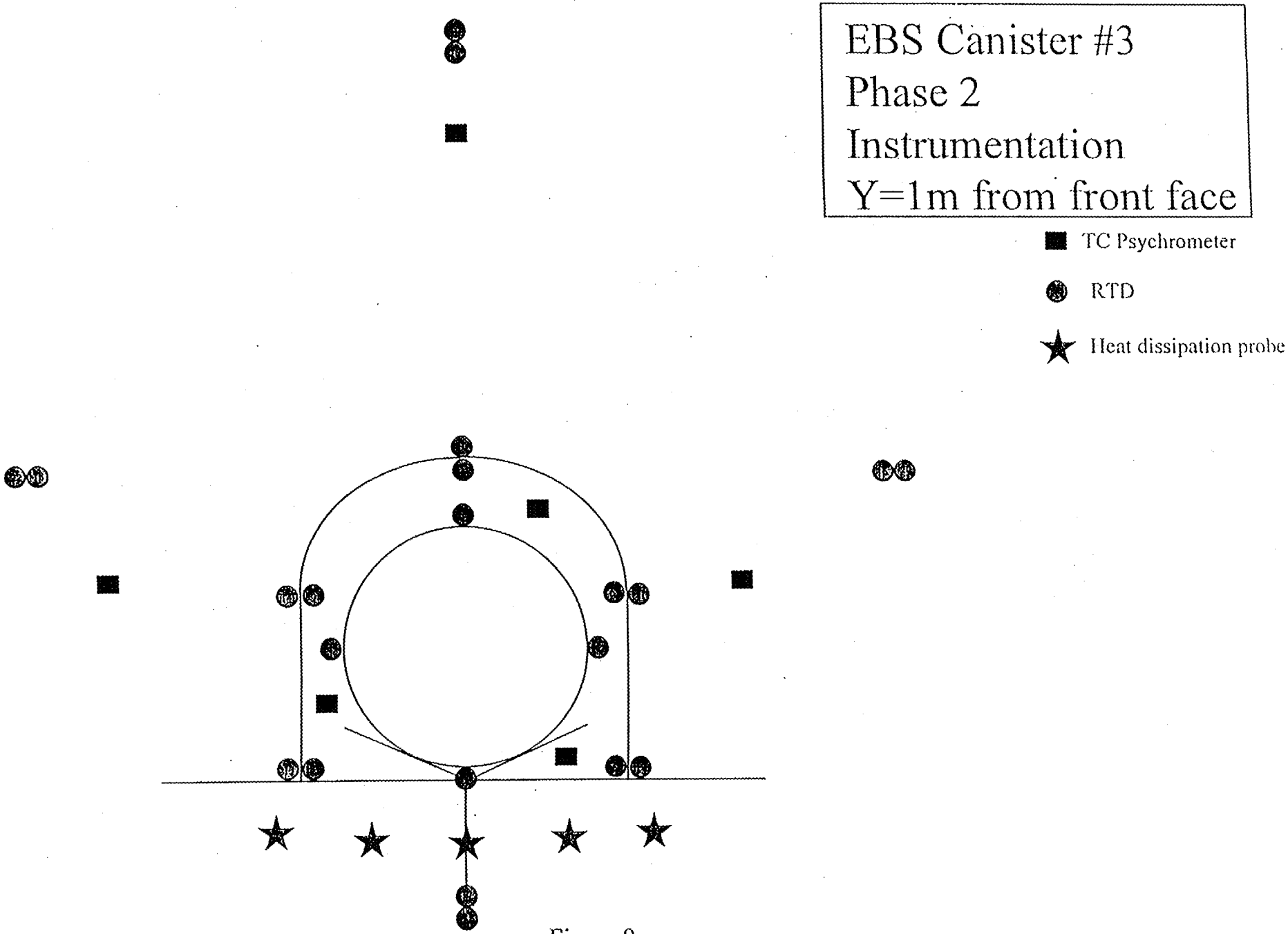
EBS Canister #3
Phase 2
Instrumentation
Y=1m from front face
TC Psychrometer
RTD
Heat dissipation probe

Figure 9

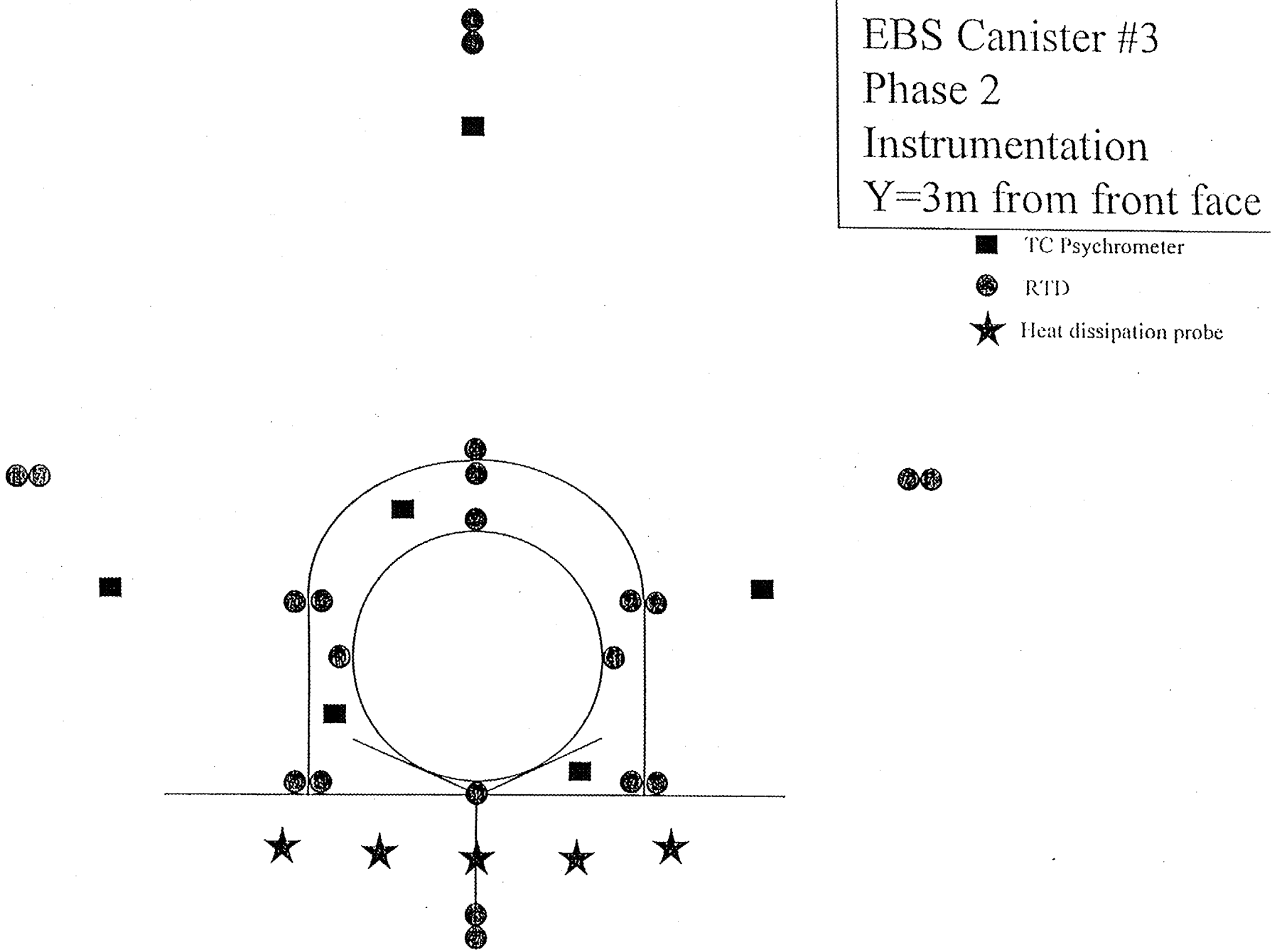
EBS Canister #3
Phase 2
Instrumentation
Y=3m from front face
TC Psychrometer
RTD
Heat dissipation probe

Figure 10

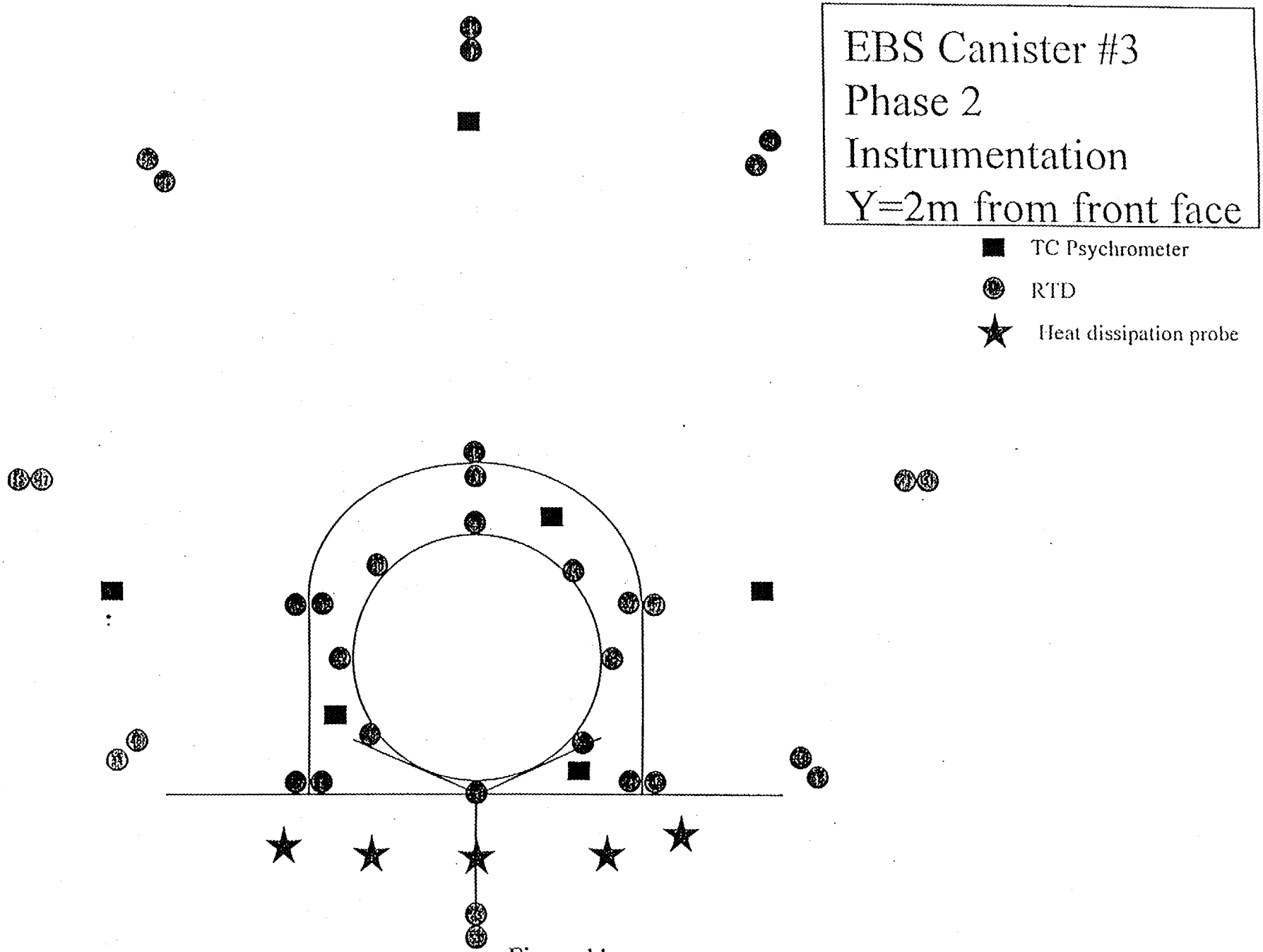
EBS Canister #3
Phase 2
Instrumentation
Y=2m from front face
TC Psychrometer
RTD
Heat dissipation probe

Figure 11

EBS Canister #3
Phase 2
Instrumentation
Front Face

CANISTER

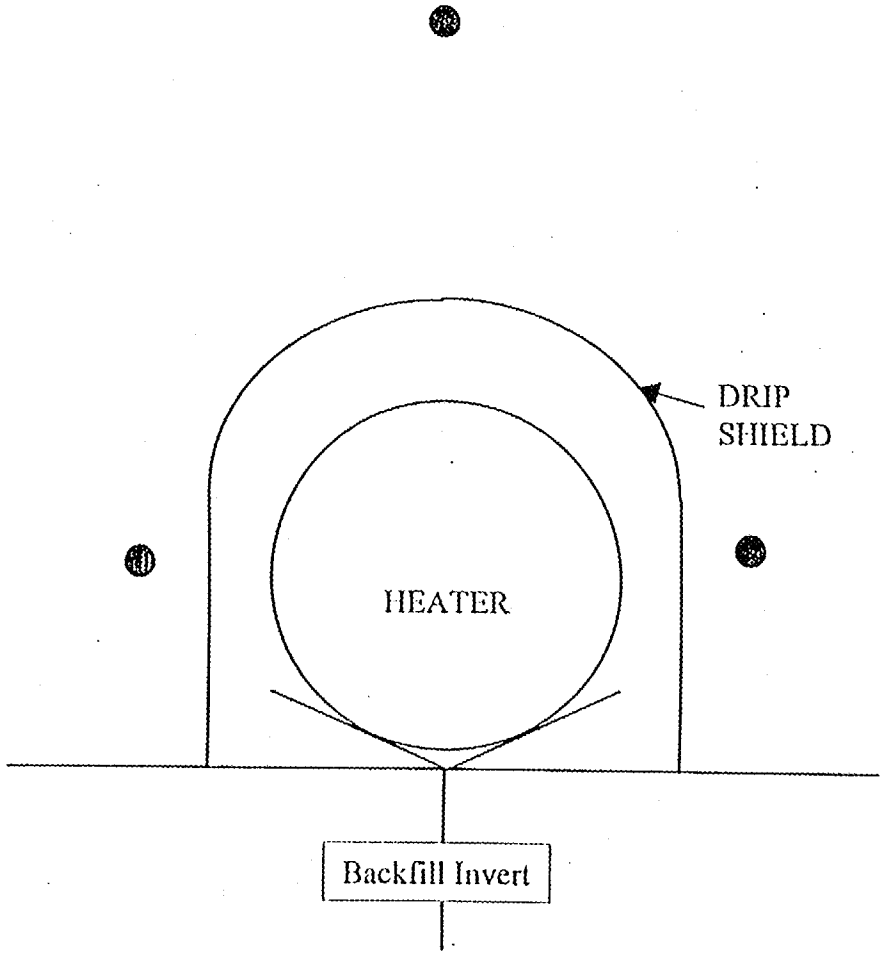

Figure 12

EBS Canister #3
Phase 2
Instrumentation
Back Face

CANISTER

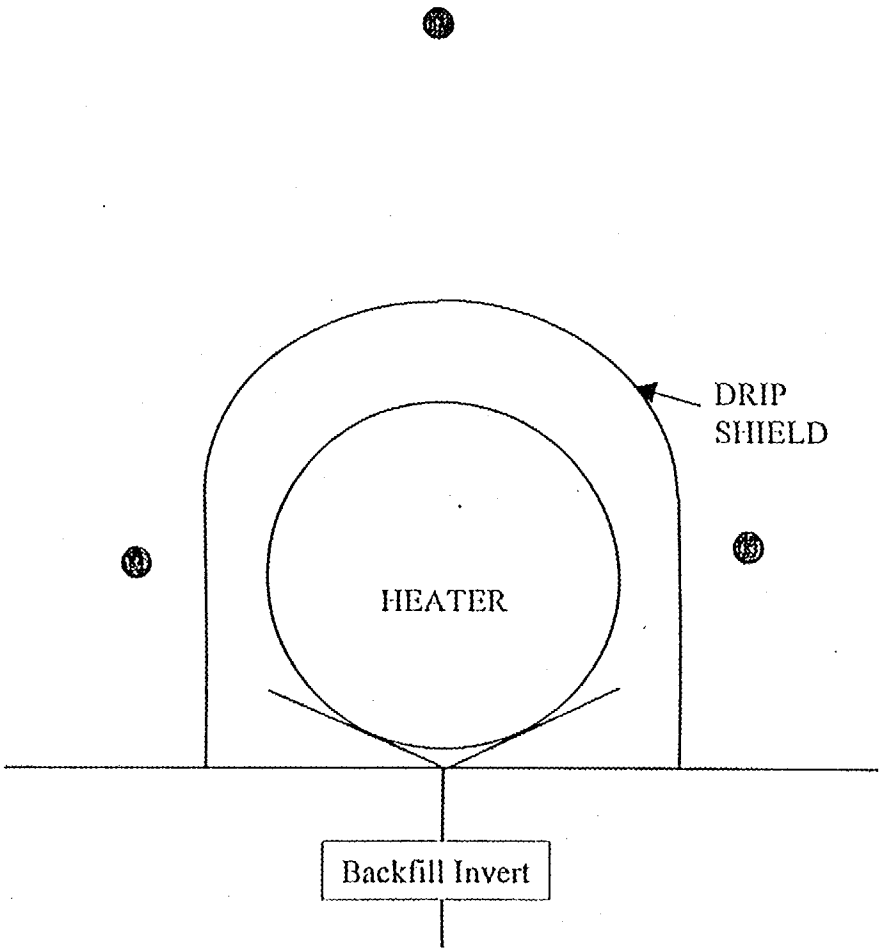

Figure 13

EBS Canister #3
Phase 1
Instrumentation
Back Face

CANISTER

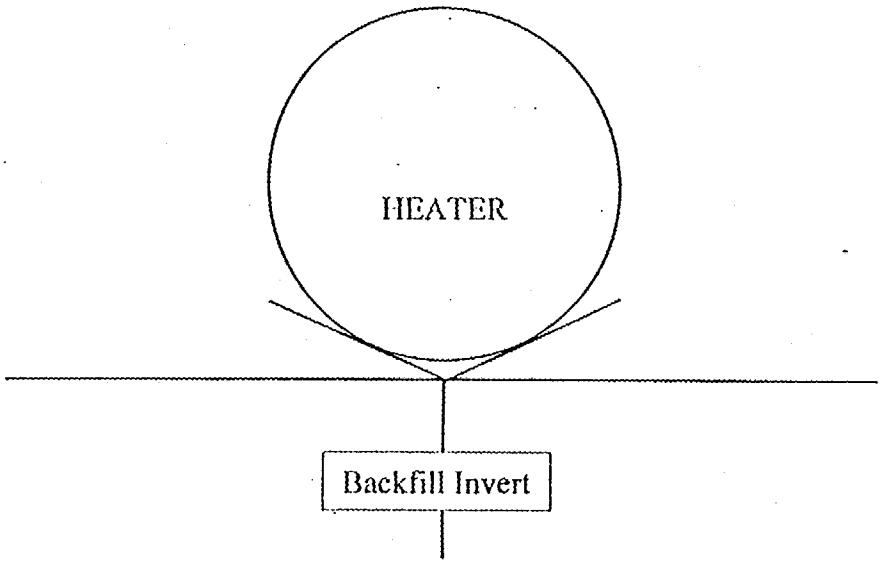

Figure 14

Possible Power Control System

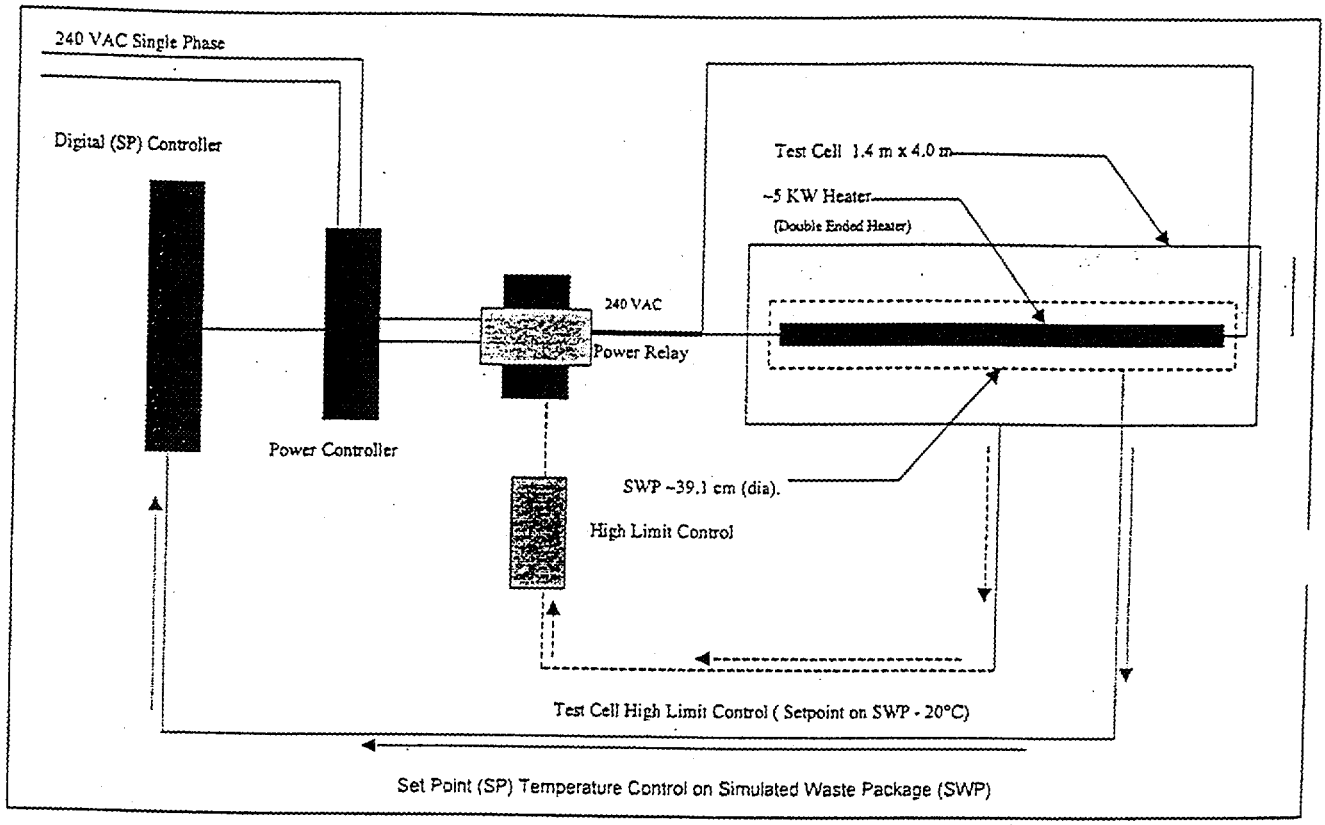

Figure 15

DRAFT DISCLAIMER

This contractor draft document was prepared for the U.S. Department of Energy (DOE), but has not undergone programmatic, policy, or publication review, and is provided for information only. The document provides preliminary information that may change based on new information or analysis, and is not intended for publication or wide distribution; it is a lower level contractor document that may or may not directly contribute to a published DOE report.

This document has not undergone technical reviews at the contractor organization, nor has it undergone a DOE policy review. Therefore, the views and opinions of authors expressed may not state or reflect those of the DOE. However, in the interest of the rapid transfer of information, we are providing this document for your information, per your request.

REVIEW OF THE EXPECTED BEHAVIOUR OF ALPHA TITANIUM ALLOYS UNDER YUCCA MOUNTAIN CONDITIONS

D.W. SHOESMITH

Department of Chemistry
University of Western Ontario
London, Ontario
Canada N6A 5B7

PRELIMINARY
DRAFT

TABLE OF CONTENTS

ABSTRACT

The possible failure processes, crevice corrosion, pitting and hydrogen-induced cracking (HIC) have been reviewed for the candidate titanium alloys (Ti-12, Ti-16 and Ti-7) under anticipated conditions in the Yucca Mountain nuclear waste repository. Both pitting and crevice corrosion are very remote possibilities under these conditions. For Ti-12, a limited amount of crevice corrosion is possible but repassivation will occur. Hydrogen absorption leading to HIC, within an acidified but passive crevice, is the most likely failure mechanism.

Both Ti-12 and Ti-16 have been shown capable of tolerating substantial amounts of hydrogen (~400 $\mu g \cdot g^{-1}$ for Ti-12, and > 1000 $\mu g \cdot g^{-1}$ for Ti-16) before any effect on the materials fracture toughness is observed. The rate of absorption to a hydrogen content

which exceeds these values will be the key feature determining if, or when, the material becomes susceptible to cracking.

In order for Ti to absorb hydrogen it is inevitably necessary to subject the material to substantial cathodic polarization, either by coupling to a more active material or by the application of galvanic protection. Absorption occurs when the passive TiO_2 is rendered permeable to hydrogen by cathodically inducing redox transformations in the oxide ($Ti^{4+} \rightarrow Ti^{3+}$). However, the presence of intermetallic particles (Ti_2Ni in Ti-12, Ti_xPd in Ti-7/Ti-16) could allow hydrogen absorption at lower cathodic polarizations since these particles could act as hydrogen absorption "windows" in the oxide. This has been shown to occur for Ti-12 but does not appear to occur for Ti-16. On the contrary, there is speculative evidence to suggest that the intermetallics present in Ti-16 inhibit hydrogen absorption.

If failure of Ti by hydrogen absorption leading to HIC is to occur then the cathodic titanium must couple to an available anode. For Ti-12, the Ti_2Ni intermetallics are corrosive and their corrosion could couple to hydrogen absorption. For Ti-16 the intermetallics are inert and thus do not appear to be a feasible pathway for hydrogen absorption. A second possibility is that in the presence of F^- enhanced passive dissolution could couple to hydrogen absorption. The evidence from dental and flue gas scrubber studies suggest this is unlikely, especially with the Pd-containing alloys. The evidence, however, is not totally conclusive. Other anions, SO_4^{2-} and HCO_3^-, and the species, silica, expected to be present in copious amounts in concentrated groundwaters at Yucca Mountain, are very likely to counterbalance any aggressiveness of F^-.

The final possibility that could lead to hydrogen absorption by Ti alloys is their coupling to other waste package materials; i.e. Alloy-22 and 316L stainless steel. An active couple between a Ti alloy and Alloy-22 is very unlikely, and for such a couple involving 316L to be active would require the loss of passivity on the steel. This remains a possibility until tests prove otherwise.

Based on these studies the order of preference of these alloys as materials for waste packages would be

Ti-16 □ Ti-7 >> Ti-12.

However, before a confident recommendation that Ti-16 be chosen over Ti-7, a better understanding of the presently baffling behaviour of the intermetallic particles in this material is required.

1 INTRODUCTION

Advanced waste package designs are under consideration for use in the Yucca Mountain Repository. The present reference design employs a dual wall arrangement, in which a 2 cm-thick nickel alloy inner barrier is encapsulated within a 10-cm thick mild steel outer barrier. The pros and cons of this design have been discussed in detail (Van Konynenburg 1998) elsewhere and a case for its usage presented (USDOE 1998).

The major corrosion issue with this reference design is the possible formation of hot, saline ferric ion solutions in contact with the inner barrier alloy (Alloy-22). The source of this environment is the corrosion of the outer barrier carbon steel. Besides potentially producing a corrosive environment on the inner barrier corrosion resistant alloy it has proven difficult to justify that the carbon steel outer barrier itself will provide long term protection of the inner barrier from corrosion. While many of these reservations are unduly pessimistic, it is judicious to consider alternative materials which avoid these uncertainties.

With these reservations in mind, it has been proposed that the carbon steel be replaced by a second corrosion resistant material which will not suffer any common mode corrosion failure with Alloy-22. While final decisions on package design remain to be made, the advanced waste package is likely to comprise a combination of Alloy-22 and titanium alloy corrosion barriers and a supporting structure fabricated from stainless steel, possibly the 316 grade.

The purpose of this report is to review the corrosion performance of possible titanium alloys for this application. The alloys under consideration are the Pd-containing alloys Grades-7 and -16, and, to a lesser degree, the nickel/molybdenum containing Grade-12

alloy. The ASTM nominal maximum compositions (expressed as a weight %) for these alloys are given in Table 1. The commercial purity Grade-2 alloy composition is given for comparison, and its corrosion behaviour is often used throughout this report as a reference point against which to discuss the corrosion behaviour of the other alloys.

The review will concentrate on potential corrosion processes possible in aqueous environments at Yucca Mountain. A brief review of passive oxide (TiO_2) properties, and how they could be affected by the key environmental variables of redox potential, pH and temperature will be given. Then the key corrosion processes which could occur will be addressed individually. Finally, the expected corrosion performance of these alloys under the specific environmental conditions anticipated at Yucca Mountain will be considered.

Table 1 ASTM Nominal Compositions (weight %) for Various Grades of Titanium

Grade	N	C	H	Fe	O	Mo	Ni	Pd
2	0.03	0.10	0.015	0.30	0.25			
12	0.03	0.10	0.015	0.30	0.25	0.3	0.8	
7	0.03	0.10	0.015	0.30	0.25			0.2
16	0.03	0.10	0.01	0.30	0.25			0.05

2 PROPERTIES OF PASSIVE FILMS ON TITANIUM

It is universally accepted that the protectiveness of the passive oxide film is the key feature which confers on titanium its ability to resist corrosion. Here, a number of pertinent oxide properties, and how they are likely to be affected by environmental variables, are discussed. A more extensive discussion has been presented elsewhere (Shoesmith and Ikeda 1997).

Figure 1 summarizes the changes expected in passive oxide properties as a function of potential, pH and temperature. Apart from specific features of anticipated groundwater

composition, these three parameters are the most significant under waste repository conditions.

- The potential experienced by the titanium surface will be dictated by the redox conditions of the exposure environment. These will generally be oxidizing due to the ubiquitous presence of air, but could be affected by the formation of galvanic couples between titanium and the other waste package materials. Reducing conditions could be established within occluded sites to which the access of oxygen is transport limited.

- The pH, while generally anticipated to be neutral to slightly alkaline could be influenced by minor corrosion processes within occluded sites such as crevices.

- The temperature within the waste repository could range from well over 100°C to eventually ambient. From the perspective of aqueous corrosion only temperatures which allow the establishment of aqueous conditions are of significance. For higher temperatures, the unsealed nature of the waste vault will reduce local humidities to low, and hence innocuous, levels. Taking into account the anticipated electrolyte concentration processes possible due to periodic wetting and drying of the waste package surface, a maximum temperature for aqueous conditions of ~125°C appears feasible (G. Gordon, personal communication).

2-1 Effect of potential

The passive oxide grown under open-circuit conditions at room temperature may be amorphous or crystalline depending on the conditions of growth. However, the maintenance of an amorphous oxide structure over extremely long exposure times seems unlikely. The thickness of the oxide and its degree of crystalline order may vary spatially (Kuldelka et al. 1995) and a small degree of non-stoichiometry (in the form of oxygen vacancies (O_v^{II}) and Ti^{3+} interstitial ions (Ti_I^{III})) gives the oxide n-type semiconducting properties.

Anodic polarization leads to oxide thickening and a decrease in the number density of defects. Amorphous films recrystallize to anatase over the potential range 4 to ~7 V (*vs* SCE[1]) and cracks and faults begin to appear in the oxide (Shibata and Zhu 1995). The amount of water absorbed by the oxide, which generally leads to an improvement in passivity, does not increase with increasing applied potential. Films grown potentiostatically at high potentials (□8 to 9 V), and subsequently examined in NaBr solutions, show an increase in pit generation rate without a corresponding increase in pit repassivation rate. This pitting process is specific to Br^- and not observed in Cl^- solutions. For high anodic potentials, in the region of 8 to 9 V, the breakdown of the film leads to recrystallization and a more rapid thickening of the film with potential than observed at lower potentials. Potentials this positive are unattainable under natural corrosion conditions.

Polarization to cathodic potentials leads to a combination of reductive transformations within the oxide and the absorption of hydrogen once the potential is sufficiently negative of the flatband potential for surface degeneracy to be established. For E < -1.0 V (*vs* SCE), hydrogen evolution occurs and the formation of surface hydrides is observed. Measurements of the amount of hydrogen absorbed suggest a potential threshold of ~-0.6 V above which no absorption occurs.

2-2 Effect of temperature

The effect of temperature on films grown either electrochemically or under natural corrosion conditions is similar in many respects to that of potential. A similar +

breakdown/recrystallization process to yield anatase/rutile occurs in the temperature range 50°C to 70°C but, in contrast to the effect of potential, is accompanied by the absorption of water. For T > 70°C, the rate of film thickening increases as observed at

---

[1] Unless otherwise stated all potentials in this report will be quoted against the saturated calomel electrode (SCE).

high potentials, but the amount of absorbed water also increases markedly. Subsequent examination at room temperature in NaBr solutions shows this absorption of water improves the passivity of the oxide as indicated by a marked increase in pitting potential (Shibata and Zhu 1994).

2-3 Effect of pH

The pH has no effect on oxide stability for E □ -0.3 V but, for sufficiently acidic conditions, an active region and an active to passive transition are observed between ~-0.7 V and -0.3 V (Kelly 1979). At room temperature in chloride solutions, a pH between 1 and 0 is required before active conditions can be established (Watanabe *et al.* 1989). For a temperature of 70°C, a pH < 1 is required. For natural corrosion conditions, the dissolution of the oxide film in acidic solutions is slow (~20 μm/y at pH < 0 and 45°C) and in solutions of pH > 1, extremely slow (~2 μm/y at pH~1 and 45°C) (Blackwood *et al.* 1988). Cathodic polarization in acidic solutions leads to the reductive dissolution of the oxide (Ti^{IV} (oxide) → Ti^{III} (solution)) (Ohtsuka *et al.* 1987), a process which is accompanied by the absorption of hydrogen into the oxide.

To avoid the two processes most likely to lead to localized corrosion, crevice corrosion and hydrogen-induced cracking (HIC), practical operating guidelines have been established. For crevice corrosion, it is accepted that attack will not occur on titanium alloys below a temperature of 70°C, regardless of solution pH or chloride concentration. For HIC a number of criteria must be simultaneously satisfied: a source of hydrogen atoms must be present; the temperature must be in excess of 80°C; and either the pH must be < 3 or > 12, or the potential at the surface must be < -0.7 V (Schutz and Thomas 1987). Further consideration of these guidelines will be included when discussing the corrosion behaviour of the individual alloys.

3 CRITICAL CORROSION PROCESSES

If Ti alloys are to fail rapidly due to corrosion then the most likely processes are crevice corrosion, pitting, and hydrogen induced cracking (HIC) under either aqueous or vapour

phase conditions. Processes such as microbially induced corrosion and radiolytically-induced corrosion are extremely unlikely and have been considered in detail elsewhere (Shoesmith and Ikeda 1997, Shoesmith and King 1999). The possibility of direct hydrogen absorption leading to HIC due to radiolysis effects is considered briefly below.

3-1 Vapour phase corrosion

Many aspects of Ti behaviour under vapour phase conditions have been discussed elsewhere (Shoesmith and Ikeda 1997), and will not be readdressed in any detail here. The oxide film on Ti has been shown to provide an excellent barrier to corrosive attack by a wide range of dry and moist gases (Schutz and Thomas 1987). Titanium alloys are widely used in hydrogen-containing environments and, in the presence of traces of moisture or oxygen the surface oxide provides a highly effective barrier to hydrogen absorption (Cotton 1970, Covington 1979).

The possibility of Ti corrosion under vapour phase conditions at Yucca Mountain seems either remote, or an easily avoidable possibility. If placed on the outside of the waste package, Ti should not be exposed to the high temperature pressurized steam environment that could lead to hydrogen absorption. Yucca Mountain is an unsealed site and very low drift humidities are expected for waste package temperatures over 100°C. Only when the temperature drops below 100°C would saturated vapour conditions be anticipated, and these temperatures would be too low for water decomposition leading to hydrogen absorption to occur.

If titanium were the inner barrier material, then a number of environmental features could make the material susceptible to hydrogen absorption. The temperatures would initially be well above 200°C and any residual water within the package could produce a pressurized steam environment. This combination, coupled with high gamma radiation fields within the waste package, could cause hydrogen absorption. The evidence from studies in aqueous solutions show that hydrogen absorption can occur for gamma dose rates $> 10^2$ Gy/h at these temperatures (Westerman 1990). Absorption occurred more readily for Ti-12 than for Ti-2. This problem would seem easily avoidable by either

careful drying of the waste form prior to sealing the waste package or by the addition to the waste package of relatively small amounts of water absorbing materials.

Table 2 Crevice corrosion test data for Pd-containing titanium alloys in acidic oxidizing NaCl brines (30 days exposure) (Schutz and Xiao, 1993)

Test Environment	Alloy	Crevice Attack Frequency	Comments
20% NaCl; pH = 2; 260°C (naturally aerated)	Ti-16 Ti-7	0/12 0/12	No attack No attack
20% NaCl; pH = 2; 90°C (Cl_2 saturated)	Ti-16 Ti-7	0/12 0/12	No attack No attack
20% NaCl; pH = 1; 90°C (Cl_2 saturated)	Ti-2 Ti-16 Ti-7	12/12 0/12 0/12	Severe attack No attack No attack
Boiling 10% $FeCl_3$; pH = 1.0 to 0.3; 102°C	Ti-2 Ti-16 Ti-7	12/12 0/12 0/12	Severe attack No attack No attack

3-2 Crevice Corrosion

The alloying additions to Ti-12, Ti-16 and Ti-7 are deliberately made to enhance their crevice corrosion resistance. The evidence to support the conclusion that they perform admirably in this function is extensive and well documented. Figure 2 shows critical crevice temperatures for Ti-12, Ti-16 and Ti-7, and the closely related Ti-Ru alloy, determined in a number of aggressive acidic and extremely oxidizing chloride environments. While in some cases Ti-12 may suffer crevice corrosion at temperatures as low as 70°C, both the Pd-containing alloys and the Ti-Ru alloy show no corrosion for T < 200°C, even in 10% $Fe^{III}Cl_3$ solution at pH = 2. The Ti-Ru alloy is similarly resistant to this form of corrosion (Schutz 1996). Critical crevice temperatures for Ti-2 are also

included in Figure 2. The results of a comparison of the crevice corrosion resistance of these alloys, based on the immersion of a number of specimens in various aggressive environments, is given in Table 2.

A closer examination of the crevice corrosion behaviour of Ti-2, Ti-12 and Ti-16, using a galvanic coupling technique (Ikeda *et al.* 1989) confirms that the crevice corrosion resistance of these alloys improves according to the sequence

$$\text{Ti-2} << \text{Ti-12} < \text{Ti-16}.$$

Figure 3 shows values of the coupled crevice current (I_c) and potential (E_c) recorded in 0.27 mol·L^{-1} NaCl at 150°C (Ti-2 and Ti-12) or 100°C (Ti-16) (Shoesmith *et al.* 1995). It is clear that the crevice propagation rate ($\alpha\, I_c$) and the extent (Q_c, equal to the area under the I_c-t curve) of crevice propagation decrease by many orders of magnitude from Ti-2 to Ti-12 and Ti-16. The distinctly different behaviours observed for the Ti-2 materials reflect the diverse properties of materials that differ in the amount and distribution of impurities, particularly iron (Ikeda *et al.* 1990, Ikeda *et al.* 1994). The shift in E_c to more positive values as $I_c \rightarrow 0$ is a clear indication that crevice repassivation has occurred. For Ti-16 crevice propagation is not observed, although a small number of attempts to initiate crevice corrosion were observed, Figure 3D.

The results of these electrochemical experiments are confirmed by weight change measurements, Figure 4 (Bailey *et al.* 1996), shown here as a function of chloride concentration at 150°C. No data for Ti-16 are shown since no weight change was observed on this material. It should be noted that, for Ti-12, the extent of crevice propagation (Figure 4) is severely limited by relatively rapid repassivation (Figure 3). This limitation on the extent of crevice propagation on Ti-12 was demonstrated to occur even in extremely aggressive Mg^{2+}-containing brines at 150°C (Westerman 1990). The unexpected dependence of weight change on chloride concentration ([CL^-]) has been addressed elsewhere (Bailey et al. 1994).

It is generally accepted that the function of the alloying additions (Ni in Ti-12, Pd in Ti-16 and Ru in Ti-Ru) is to supply cathodic sites within the creviced area which catalyze proton reduction in the reducing acidic environment existing at actively propagating sites. This catalysis of proton reduction pushes the crevice potential into the passive region for titanium thereby forcing it to repassivate, (Figure 5). While the general nature of the repassivation process is understood, the chemical/electrochemical details are not so well defined.

The most commonly accepted explanation for both the Ni/Mo-containing Ti-12 and the Pd-containing Ti-7 and Ti-16 is that corrosion of the alloy in the acidic crevice environment leads to the release of Ni^{2+} or Pd^{2+} which are then subsequently redeposited to produce Ni or Pd sites which act as proton reduction catalysts (Cotton 1967, Satoh *et al.* (1987), Sedriks *et al.*1972, Hall *et al.* 1985, Schutz and Xiao 1993, Shida and Kitayama 1988, Kitayama *et al.* 1990, McKay 1987). Figure 6A attempts to illustrate this mechanism schematically.

For Ti-12, the alternative opinion is that the Ni is localized in Ti_2Ni intermetallics which act as cathodes galvanically-coupled to the surrounding Ti α-grains (Glass 1983, Kido and Tsujikawa 1989) (Figure 6B). While the evidence for the presence of Ni^{2+} in solution during passive corrosion in strong acidic solutions (to simulate the crevice environment) is good, that for dissolved Pd^{2+} is marginal. Cotton (1967) found only ~0.9 $\mu g \cdot g^{-1}$ of dissolved Pd for Ti-6 corroding in boiling H_2SO_4. A similar redeposition mechanism to produce noble metal cathodes has been claimed for Ti-Ru (van der Lingen and de Villiers Steyn 1994). Again, however, the amount of dissolved Ru found in solution (~0.4 $\mu g \cdot g^{-1}$) after corrosion in strong acids (10% H_2SO_4, 5% HCl) (Sedriks 1975) is marginal.

Although no real evidence is available to prove the point, it is tempting to hypothesize that Ti-12 and, to a lesser degree Ti-2 with a high Fe content, may be repassivated by a process involving dissolution of Fe^{2+} and Ni^{2+} followed by their redeposition (Figure 6A), whereas Ti-7 and Ti-16 repassivate by the galvanic coupling of intermetallic precipitates to the titanium matrix, (Figure 6B). The former process might be expected to

be less efficient than the latter, thereby accounting for the limited propagation of crevice corrosion on Ti-12 and Ti-2 (high Fe).

For Pd-containing alloys there is the additional possibility that the alloying element leads to the anodic ennoblement of the alloy as a consequence of either metal dissolution or oxide growth. In both cases the preferential oxidation of Ti to produce either soluble Ti^{3+}/Ti^{4+} or TiO_2, would lead to enrichment of Pd in the surface of the alloy and, hence to its ennoblement, Figure 7.

The analytical evidence for the accumulation of Pd in the surface of Pd-containing alloys after corrosion in acid solutions is indisputable (Hubler and McCafferty 1980, Shida and Kitayama 1988). Whether this is due to the redeposition of dissolved Pd^{2+} or the accumulation of Pd or Pd-containing particles after the preferential dissolution of Ti (Hubler and McCafferty 1980, Amstrong *et al.* 1973) is not proven.

Whether or not the fine details of the function of the alloying element in reinforcing passivity within crevices is important is open to debate, and in the final analysis may not be. However, whether or not the alloying elements are present in α-phase solid solution, β-phase solid solution and/or intermetallic precipitates could have a significant influence on the ability of the alloy to absorb hydrogen when exposed to acidic conditions and/or galvanically coupled to another more easily corrodible material. This possibility is discussed in detail below.

3-3 Pitting

The pitting of titanium has been studied in some detail (Posey and Bohlmann 1967, Koizumi and Furuya 1973) and a review has been recently written (Shoesmith and Ikeda 1997). Commercially pure titanium (Ti-2) is extremely resistant to pitting in keeping with the excellent properties of the passive TiO_2 film under oxidizing conditions, Figure 1. Commonly pitting potentials at room temperature are in excess of 7 V, and even for temperatures greater than150°C are in the region of 2 V.

The fear on adding alloying elements is that the formation of intermetallic precipitates will provide sites for pit initiation, or that the stabilization of an α/β alloy phase structure could lead to inhomogeneities in the passive film which could render it susceptible to pitting breakdown at much lower potentials. Thus the pitting potentials of Al/V containing alloys of titanium are often as low as 2 V at low temperatures and □ 1 V for temperatures > 100°C (Posey and Bohlmann 1967). However, these authors showed that the addition of the alloying elements present in Ti-12 (Ni, Mo) and Ti-7/Ti-16 (Pd) did not adversely affect the pitting potential of titanium. These observations, and also the influence of the common titanium impurity Fe, are summarized in Figure 8. The pitting potential is shown to be normally distributed around a conservatively low mean value of ~7 V with a σ value taken to be ~1 V (Shibata and Zhu, 1994). Also indicated with a horizontal arrow is the expected small influence of chloride concentration. This figure was constructed for a temperature of ~100°C, and pitting potentials would be expected to be even higher at lower temperatures (Posey and Bohlmann 1976). The range of corrosion potentials achievable under waste repository (vault) conditions is much less than the pitting potentials values and one can be confident in claiming that pitting of Ti-12, Ti-16 or Ti-7 will not occur under waste repository conditions.

3-4 Hydrogen-induced cracking (HIC)

It is clear from the properties of the passive film on Ti, Figure 1, that cathodic polarization leading to hydrogen absorption and eventually HIC is a much more probable failure process than pitting. Whether or not failure by this process is feasible will depend on the hydrogen content required to degrade the fracture toughness of the material, the ease of absorption of this amount of hydrogen, and whether the environment can polarize the titanium to a potential sufficiently negative for hydrogen absorption.

It has been demonstrated by Sorensen and coworkers (Sorensen 1990) that the alloy Ti-12 requires a hydrogen content of > 500 $\mu g \cdot g^{-1}$ before any measurable loss of ductility occurs. Using the slow strain rate technique on precracked compact tension specimens precharged with known amounts of hydrogen, Clarke *et al.* (1994, 1995) showed that the fracture toughness of both Ti-2 and Ti-12 is not significantly affected until their hydrogen

contents exceed a critical value (H_c). An example of the data obtained, expressed as a plot of stress intensity factor as a function of hydrogen concentration is shown in Figure 9. The as-received materials, containing 20 to 50 $\mu g \cdot g^{-1}$ of hydrogen, are very tough and under high stress, fail by ductile overload. This ductile tearing is also observed during slow crack growth for both materials. The value of H_c is the hydrogen concentration above which slow crack growth is no longer observed and only fast crack growth occurs. Extensive discussions of such data are available elsewhere (Shoesmith *et al.* 1997).

A generalized form of such a plot is shown in Figure 10, illustrating how they can be used to identify the critical hydrogen content (H_c) above which the fracture toughness is affected and one cannot then be sure these alloys will not fail by fast crack growth. Based on such measurements, values of H_c of 500 to 800 $\mu g \cdot g^{-1}$ (Ti-2) and 400 to 600 $\mu g \cdot g^{-1}$ (Ti-12) have been determined. More recent measurements (Ikeda, unpublished data) show that H_c for Ti-16 is at least 1000 $\mu g \cdot g^{-1}$ and may be much greater.

To assume fast crack growth is inevitable once H_c is attained is a conservative assumption. Implicit in this assumption is that the waste package will always be subject to sufficient stress to lead to cracking. Since some creep of the material might be expected over long disposal periods this is by no means certain to be the case. A second assumption is that the hydrogen will be evenly distributed as hydride precipitates throughout the material.

The criterion for failure by HIC then becomes the time required for the alloy to absorb this amount of hydrogen. In their ability to enforce repassivation within crevices the alloying elements must exist as, or create, catalytic cathodic sites. This raises the question as to whether, and in what form, these elements can catalyze the absorption of hydrogen into the Ti matrix. While this process could be rapid under propagating crevice conditions (Noël *et al.* 1996, Shoesmith *et al.* 1997) it will be much slower under passive

conditions but could still be a factor if sufficiently cathodic polarization of titanium could be achieved.

The absorption of hydrogen into titanium is not readily achieved, since the oxide is highly impermeable, and it is necessary to induce, by cathodic polarization, redox transformations within the oxide. It is this need which accounts for the criterion of a potential < 0.7 V specified by Schutz and Thomas (1987), and demonstrated in long term hydrogen absorption measurements by Murai *et al.* (1977), Figure 11. Figure 12 attempts to illustrate the nature of the parallel oxide redox transformation-hydrogen absorption process, which occurs once the potential is sufficiently negative of the flatband potential for surface degeneracy to be established. A more detailed discussion of this process has been given elsewhere (Shoesmith and Ikeda 1997).

Once the potential is sufficiently negative for these transformations to occur, titanium hydrides are thermodynamically stable with respect to the metal (Beck 1973) and the passive film can only be considered as a transport barrier. Beyond this threshold potential, the rate of absorption of hydrogen by the metal is effectively independent of potential down to ~ -1.0 V (*vs* SCE), Figure 11. Indeed, there is a significant amount of evidence to claim that hydrogen is not transported through the oxide film at any significant rate until potentials < -1.0 V (*vs* SCE) are achieved. This is clearly evident in electrochemistry-in-situ neutron experiments on titanium, Figure 13. Hydrogen has a strong negative scattering length for neutrons and, when present in the oxide, reduces its scattering length density (Tun *et al*, 1999). The results in Figure 13 show that hydrogen is present in the oxide close to the oxide/solution interface but not close to the metal/oxide interface, and that a cathodic polarization of > -1.0 V is required for hydrogen to penetrate to the metal/oxide interface when its entry into the metal becomes inevitable. A fuller discussion of these results is available elsewhere (Tun *et al.* 1999)

A more definitive demonstration that significant hydrogen transport through TiO_2 does not occur until E < -1.0 V (*vs* SCE) was obtained using an electrochemically controlled bilayer system comprising a layer of TiO_2 deposited on Pd metal (Pyun and Yoon 1996). By using this bilayer in back to back electrochemical cells, hydrogen could be injected

into the TiO_2 at the TiO_2/solution interface ($H^+ + e \rightarrow H_{abs}$), and its transport detected by its reoxidation ($H_{abs} \rightarrow H^+ + e$) at the Pd/solution interface. Any H_{abs} crossing the boundary from TiO_2 to Pd is subsequently transported very rapidly to the Pd/solution interface and detected by oxidation. The results in Figure 14 show that no detectable hydrogen transport through the TiO_2 layer into the Pd occurred until the potential applied to the TiO_2/solution interface was < -1.0 V (*vs* SCE). These results are consistent with industrial observations which show significant hydride formation and embrittlement of Ti is not observed until E < -1.0 V (Schutz and Thomas 1987).

The fear when alloying elements capable of catalyzing proton reduction are added to titanium is that they will also catalyze hydrogen absorption. If, for instance, intermetallic precipitates are present, over which a coherent layer of TiO_2 does not act as first a chemical, then a transport barrier, then possible "hydrogen windows" exist within the oxide. Under these circumstances, transformation of the redox properties of the passive oxide may not be a necessary prerequisite for hydrogen absorption which could therefore occur at potentials more positive than -0.6 V. Whether or not this proves to be the case would depend on the catalytic properties of the cathodic sites, but, inevitably, the alloying elements added, Ni, Pd, Ru, are known to facilitate proton reduction (Greef *et al.*) and to possess significant solubilities for hydrogen. An attempt to illustrate this scenario schematically is shown in Figure 15

A substantial body of evidence exists to show that the presence of these alloying elements can lead to the absorption of hydrogen into titanium. This evidence is summarized, referenced, and discussed in Appendix A. The nature and distribution of the alloying element has a large effect on this behaviour. For Ti-12 (containing both Ni and Fe (as an impurity)) and Ti-2 (similarly contaminated with Fe) both the corrosion behaviour and the extent and rate of hydrogen absorption depend on the location and chemical form of the alloying element (Ni) and impurity element Fe.

Both Ni- and Fe-containing β-phase and Ti_2Ni and Ti_xFe intermetallic particles are susceptible to corrosion in acidic environments. The evidence in support of this claim is given in Appendix B. While it remains to be demonstrated whether Ni/Fe β-phase can

act as a catalytic cathode, there is little doubt in the case of the intermetallics, or in their ability to absorb hydrogen. Consequently, for sufficiently acidic conditions the corrosion of the β-phase or intermetallic will lead to hydrogen absorption. It is likely, however that absorbed H would remain localized at the intermetallic sites unless the predominately α-phase alloy contains β-phase ligaments, commonly located along α-phase grain boundaries, which enhance transport of hydrogen into the bulk of the alloy. An attempt to illustrate this process is given in Figure 16. In the absence of these transport pathways, the intermetallic particles may become saturated in H, a condition for which the efficiency of further hydrogen absorption appears to approach zero.

For the Pd-containing alloys the formation of β-phase is negligible and intermetallic particles, when present, appear inert to corrosion (Appendix B). The rate and efficiency of hydrogen absorption increases with increasing Pd content, though, in the absence of any apparent separation of the Pd into discrete intermetallics (Ti-7) the mechanism of absorption remains unclear. Electrochemical evidence for catalysis of the proton discharge step,

$$H^+ + E \rightarrow H_{ads}$$

a characteristic feature of proton reduction on noble metals, is clear. Presumably, in the absence of separated intermetallic particles, this discharge step, and the subsequent H absorption step, occur at the atomic level. Since absorption can occur for $E > -0.6$ V redox transformations within the oxide do not appear to be a prerequisite.

For Ti-16, H absorption was not observed for potentials as low as –1.0 V, despite the presence of a large number of randomly dispersed intermetallic particles (Appendix A). While the degree of catalysis of proton discharge and the efficiency of H absorption are expected to decrease as the Pd content decreases (i.e., from Ti-7 to Ti-16), this observation is still surprising. Since the material investigated contained a substantial amount of Fe (as an impurity) it is likely that the particles contain Fe. However, since they are apparently inert, whereas Ti_xFe is not, there is the possibility that Pd

cosegregated to yield TiPdFe particles. The composition and properties of these particles remain to be elucidated.

CORROSION PROCESSES POSSIBLE UNDER WASTE REPOSITORY CONDITIONS

From the above discussion it is clear that pitting will not be a failure mechanism and that active crevice corrosion, leading to waste package failure, is extremely unlikely for the alloys chosen. For Ti-12, the initiation of crevice corrosion would be possible but any significant propagation would be prevented by repassivation of the alloy. This has been demonstrated even for high temperature conditions in very aggressive Mg^{2+}-containing brines. For the Ti-16 and Ti-7 alloys the possibility of active crevice corrosion is extremely remote.

In the absence of active crevice corrosion, the most likely corrosion scenario for Ti under repository conditions is that it will absorb H in the occluded areas existing between inner and outer barrier walls of the waste package. For this to happen the Ti, or at least the intermetallics within it, must function as cathodes coupled to some anode within the system. For such a couple to be actively established the development of acidic conditions within these occluded areas would be required.

Three potential anodes appear possible:

(i) the presence in the alloy of a reactive phase or intermetallic; e.g. β-phase and/or Ti_2Ni in Ti-12;

(ii) galvanic coupling to another waste package material. Considering the proposed waste package design, this would be either nickel alloy-22 or 316 stainless steel;

(iii) general active or enhanced passive corrosion of Ti if the presence in the groundwater of F^- can lead to a significant increase in passive current density.

4-1 Generation of acidity within creviced sites

A key question which must be answered when considering these three possibilities is whether acidic conditions can be generated within creviced (occluded) regions even though active crevice corrosion conditions cannot be established. Noël (1999) has already shown that, for tight crevices between Ti and teflon spacers, crevice acidification did occur at 100°C. While these crevices were coupled to large Ti counter electrodes (to yield an anode/cathode ratio of ~ 1:40) which could have helped drive the acidification process, it is clear that the creviced Ti face became etched, Figure 17. This etching was observed on Ti-2 specimens exposed to neutral NaCl solutions prior to the initiation of active crevice corrosion and on Ti-2 specimens exposed to neutral sulphate solutions on which crevice corrosion did not initiate. Etching was also observed on the creviced face of Ti-16 specimens in chloride solutions, again despite the maintenance of passivity.

The fall in resistance observed in impedance experiments on Ti-2 and Ti-12 when the temperature is increased to □ 65°C (Appendix B and Figure B2) can be interpreted to indicate that a film breakdown/recrystallization process occurs once this temperature is exceeded. These results and this claim are consistent with those of Shibata and Zhu (1995). This process leads to the introduction of grain boundaries, and possibly even more open pathways, by which metal dissolution can occur. Under occluded crevice conditions, this leads to cation hydrolysis and the development of local acidity as illustrated schematically in Figure 18. That this development of acidity precedes the initiation of crevice corrosion on Ti-2 has been clearly demonstrated by Noël (1999), and is the reason why the industrial guideline for avoiding crevice corrosion, *i.e.*, T □ 70°C (Schutz and Thomas 1987), applies. For the Ti-16 and Ti-7 alloys the development of this occluded acidity does not lead to the initiation of crevice corrosion.

The need for film breakdown/recrystallization to produce localized acidity suggests that such an acidification process would require temperatures higher than ~65°C. However, even at temperatures in the range 25°C to 35°C, a drop in pH of a few units from neutral (7) has been observed in laboratory-formed femoral taper crevices between Ti6Al4V and Cr-Co-Mo alloys (Gilbert and Jacobs 1997).

4-2 Passive oxide dissolution

Under neutral conditions passive oxide dissolution rates are immeasurable (Mattsson and Olefjord 1990, Mattsson *et al.* 1990). Over a 6-year exposure period to water-saturated bentonite clay at 95°C, the maximum dissolution rate was < 0.4 nm/year. This value effectively represents an analytical detection limit since no dissolved Ti was found.

For more acidic conditions, Blackwood *et al.* (1988) measured dissolution rates of passive titanium oxides using electrochemical methods that determined the amount of oxide removed from the metal surface rather than by attempting to measure the amount of dissolved Ti^{3+}/Ti^{4+} in solution. These rates were measured in acidic sulphate, perchlorate, phosphate and chloride solutions at 45°C and, generally for pH ≤ 2, Table 3). Dissolution was chemical in nature; *i.e.*, did not involve electrochemical interaction between the oxide and the substrate metal and led to the uniform thinning (as opposed to pitting) of the oxide film. The rate was close to first order with respect to proton concentration. Extrapolation of these rates according to this pH dependence predicts negligibly small dissolution rates in neutral solutions, consistent with the observations of Mattsson and coworkers.

Table 3. Rates of Oxide Dissolution at 45°C (from Blackwood *et al.* 1988)

Electrolyte	Concentration ($mol \cdot dm^{-3}$)	Dissolution Rate (μm/year)
H_2SO_4	3.0	19.53
H_2SO_4	1.0	16.12
H_2SO_4	0.25	8.15
H_2SO_4	0.02	2.01
$H_2SO_4/NaHSO_4$	1.0/1.0	11.21
H_2SO_4/K_2SO_4		2.72
H_3PO_4	3.0	2.60
$HClO_4$	3.0	9.2
HCl	3.0	17.17
Oxalic acid	1.0	12.52

Table 3. Simulated Corrosion Test Environments for the Yucca Mountain Repository

	Concentration (µg·g-1)						
Parameter	SDW (60°C)	SDW (90°C)	SCW (60°C)	SCW (90°C)	SAW (60°C)	SAW (90°C)	SCMW (60°C)
pH	9.5	9.9	9.2	9.2	2.7	2.7	7.8
Ca^{2+}	3.5	3.4	16	15	58	58	400
Mg^{2+}	1.2	ND	29	3.4	52	53	4
K^{+}	36	38	4600	4,500	4,300	4,3000	85
Na^{+}	430	460	36,000	44,000	43,000	43,000	10
Si	17	16	18	58	30	50	10
SO_4^{2-}	170	180	13,000	13,000	41,000	40,000	1,200
Cl^{-}	68	74	7,4000	7,500	28,000	27,000	11
NO_3^{-}	62	64	7,000	7,200	23,000	24,000	10
F^{-}	14	15	300	1,400	0	0	<0.1
HCO_3^{-}	720	700	44,000	51,000	0	0	<1
Equiv. NaCl	112	122	12,199	12,363	46,157	44,508	18

ND – not detected

SDW – simulated dilute well water (10×J-13)

SCW – Simulated concentrated well water (1000×J-13)

SAW – simulated acidified well water

SCMW – simulated cement-modified water

Table 5. Expected Groundwater Concentrations After Wetting/Evaporation Cycles

	Concentration (mg/L)			
Ion	J-13	Long Term Test Solution 1000x	Beaker Evaporation 1000x	90°C/85%RH
SO_4	18.4	13000	15700	29500
Cl	7.14	7200	6120	14800
NO_3	8.78	6440	6730	14200
F	2.18	1580	1520	3400
HCO_3	128.9	47326	31471	
Na	45.8	42500	37700	77400
K	5.04	3580	3720	9700
Ca	13.0	3	7	25
Mg	2.01	1	0	0
$SiO_{2(aq)}$	61.0	109.14	7124	22500
pH	7.4	10.1	9.9	10

Long term test solution - similar to SCW in Table 4

Beaker evaporation - J-13 solution evaporated to 1000x concentration in the presence of crushed tuff

90°C/85%RH – Evaporation performed for a constant relative humidity

Within an acidified crevice (at 45°C), these rates indicate that a maximum rate of 10-20 μm/year for a pH ~ 1 falling to < 1-2 μm/y for pH ~ 2 would be possible. Clearly, substantial and enduring acidification would be required for passive dissolution rates at creviced sites to reach significant values.

4-3 Effect of fluorides

The corrosion of Ti and its alloys in the presence of F^- has mainly been studied for dental and flue gas scrubber applications. In the first application the environment is saline and neutral, but low temperature, and in the second much more aggressively saline, hot (> 100°C) and potentially acidic. For the low temperature dental applications, Ti-2 was tested in 1% NaCl solutions ranging in pH from 6 to ~3 containing between 1000 and 100 μg/g of F^- (Reclaru and Meyer 1988). For flue gas scrubber applications the environments tested were much more concentrated with Ca and $MgCl_2$ concentrations between 0.1 and 12.7% (*i.e.*, $[Cl^-]$ up to 15,700 $\mu g \cdot g^{-1}$ with $[SO_4^{2-}]$ in the range 9000 to 26,000 $\mu g \cdot g^{-1}$). The temperature was up to 177°C and the pH down to ~1. Fluoride concentrations were in the range 0 to 12,000 $\mu g \cdot g^{-1}$ (Thomas and Bomberger 1983, Schutz and Grauman 1986). These concentrations are similar to those used in corrosion testing, Table 4 and those established in J-13 well water evaporation tests, Table 5.

In the dentistry related studies in 1% NaCl containing ~ 1000 $\mu g \cdot g^{-1}$ of F^- passivity was maintained, and the galvanic currents generated by coupling to various Au/Ag dental alloys were insignificant (1 to 10 $nA \cdot cm^{-2}$) (Reclaru and Meyer 1988). Although it is not made specifically clear it appears that Ti formed the cathode in these couples. When galvanically coupled to 316L stainless steel a galvanic current of ~ 400 $nA \cdot cm^{-2}$ was obtained with Ti acting as the anode. As will be seen when discussing the galvanic coupling of Ti below, this observation (*i.e.*, Ti acting as the anode) is not uncommon. In the absence and presence of F^- the potential of this couple was 9 mV and –30 mV (*vs* SCE), respectively. In neither case is the potential sufficiently negative to allow H absorption by Ti-2. When the pH is decreased, the presence of F^- leads to an increase in passive current density, and, under creviced conditions the potential drops to much more

negative values, indicating that in the presence of F^-, crevice corrosion of Ti-2 could occur even at low temperatures.

In the simulated flue gas scrubber environments, the influence of F^- was much more muted (Thomas and Bomberger 1983, Schutz and Grauman 1986). As observed in the dental studies, the passivity of Ti-2 was lost for pH < 3 when F^- was present. For Ti-12 this pH-threshold for the loss of passivity was < 1.5. Although Ti-16 and Ti-7 were not tested, it would follow from these observations that an even lower pH would be required before F^- exerted any significant influence on these two alloys. An interesting synergism was observed between Cl^- and F^-, the influence of F^- on corrosion decreasing as $[Cl^-]$ increased (Thomas and Bomberger 19830. This was attributed to a common ion effect with Ca^{2+} leading to the precipitation of CaF_2. The presence of flyash eliminated any influence of the F^- ion, an effect attributed to the introduction of Fe^{3+}, a known inhibitor of Ti corrosion, and to the presence of SiO_2 which would complex F^- thereby reducing its free concentration drastically.

At F^- concentrations of ~ 100 $\mu g \cdot g^{-1}$, Schutz and Grauman (1986) found that F^- did not influence the electrochemically-determined repassivation potentials for Ti-2, Ti-12 and Ti-7 at 82°C for pH values as low as 1.5. Values remained > 7 V (*vs* SCE). Crevice corrosion tests showed no susceptibility except at 177°C, and for Ti-7 passivity was maintained even at this temperature. In tests involving a galvanic couple to carbon steel, only Ti-12 showed any significant H absorption. Some enhancement of H absorption was noticed for Ti-7 galvanically-coupled to carbon steel, but only when the couple was driven under oxidizing conditions and presumably when the additional demand for cathodic current was partially met by proton reduction.

More general laboratory studies have concentrated on strongly acidic solutions, when the influence of fluoride (as HF) is significant in the millimolar range (10-100 $\mu g \cdot g^{-1}$). Wilhelmsen and Grande (1987) concluded that acidic fluoride (HF) stimulated the passive dissolution of titanium at these concentrations but that the F^- ion had no effect on

passive behaviour. Their electrochemical data clearly indicates that F^- will only be aggressive in acidic solutions. This conclusion was supported by Auger spectroscopy measurements which showed that incorporation of F^- into the passive film leading to increased passive currents and increased film thicknesses only occurred at low pH (≤ 0). Unfortunately, no experiments were conducted at slightly higher pHs than 0. In alkaline solutions (pH ~ 13) no influence on passive currents or incorporation into the oxide was observed.

This pH dependence of the influence of F^- is consistent with expectations for the dissolution of oxides. If F^- is to accelerate the transfer of Ti^{4+} to solution (as TiF_6^{2-}) then it must be accompanied by the neutralization of O^{2-} ions by H^+. As the pH increases one would expect the latter anion transfer process to become rate determining, and hence for the ability of F^- to accelerate TiO_2 dissolution to decrease (Segall *et al.* 1988).

The possibility of an aggressive F^- solution developing within a crevice on the waste package seems unlikely. While crevice acidification is to be expected, and recent beaker and evaporation tests (Table 5) show F^- concentrations could reach 3400 $\mu g \cdot g^{-1}$, a number of factors suggest this will not lead to particularly aggressive consequences. Firstly, for significant temperatures (60 to 90°C) HF could be sufficiently volatile to prevent its concentration in solutions. Secondly, the concentration of other groundwater species will impede the development of extreme acidic conditions within the crevice, and nullify the ability of F^- and Cl^- to produce active crevice conditions.

Both sulphate and carbonate suppress crevice corrosion by neutralizing acidity (Shoesmith *et al.* 1995). The buffering ability of HCO_3^- is obvious, while that for SO_4^{2-} is more likely due to its ability to complex dissolved Ti^{III}/Ti^{IV} species, thereby preventing their hydrolysis to produce protons. Also, SO_4^{2-} enhances the ability of Ti to maintain passivity by an autopassivation process. This autopassivation process couples the reduction of Ti^{IV} to Ti^{III} with active metal dissolution, and its acceleration in SO_4^{2-}-containing solutions reinforces passivity (Kelly 1982).

This ability of SO_4^{2-} to drive the repassivation of Ti was observed by Sedriks (1975) on Ti-Ru (0.1 to 0.3%), but misinterpreted as the ability of dissolved Ru to redeposit to form catalytic cathodes. In boiling H_2SO_4, he observed a decrease with time of the corrosion rate to effectively zero. A similar decrease in boiling HCl was not observed. This drop in rate is clearly an anion effect, and not a consequence of the accumulation in solution of dissolved Ru. It can be attributed to the build up of sulphate-complexed Ti^{IV} which eventually enforces repassivation. Since Cl^- does not complex Ti^{4+} as strongly as SO_4^{2-}, the Ti^{4+} reduction step is much slower and repassivation much more difficult to enforce (Kelly 1982).

Our own experiments on Ti-2 crevice corrosion (Shoesmith *et al.* 1995) clearly indicate the ability of SO_4^{2-} to suppress active crevice corrosion and cause repassivation when present in excess over Cl^-. Given the large sulphate concentrations likely to exist within waste package crevices (Tables 4 and 5) the dominance of SO_4^{2-} over Cl^- and F^- can be expected.

A final feature which could nullify any adverse influence of F^- within waste package crevices would be the presence of substantial amounts of silica. Evaporation testing under a condition of constant relative humidity (90°C/75% RH, Table 5) lead to the formation of a silica gel. While unproven, it was claimed that, in the flue gas scrubber tests (Thomas and Bomberger 1983, Schutz and Grauman 1986), SiO_2, present as flyash lead to a reduction in the free concentration of F^- and the elimination of its influence on titanium corrosion.

4-4 Galvanic coupling to other materials

According to Schutz (1986), in its normal passive condition Ti would generally be the cathode in galvanic couples with other materials. However, for the materials of interest in waste package applications, the corrosion potentials measured in ambient seawater are very close when the materials are in their passive condition, Table 6. The small potential differences between these alloys indicates that negligible galvanic interaction should

occur as long as passivity is maintained. Also, it is not surprising that, given the similarity of expected potential values under passive conditions, Ti can sometimes function as the anode as observed by Reclaru and Meyer (1998). Other factors important in determining which is the anode and cathode in a galvanic couple include the relative surface areas and geometry of the coupled materials as well as the conductivity of the coupling environment. More generally Schutz (1988) has reported that the coupling of Ti to many materials in hot chloride brines can often lead to an enhanced resistance to crevice corrosion of the more crevice susceptible member of the couple. Such behaviour was reported for nickel alloys (Monel, 625, C-276) and for stainless steels (304, 316).

Table 4. Galvanic Series in Flowing Seawater (4m/s) at 24°C (from Schutz (1986))

Material	Corrosion Potential (V *vs* SCE)
Ti	-0.10
316 SS (passive)	-0.05
304 SS (passive)	-0.08
Alloy C (passive)	-0.08
316 SS (active)	-0.18
314 SS (active)	-0.53

Wang *et al.* (1999) also reported that Ti-2 could form the anode or cathode when coupled to various materials in hot (50°C to 90°C) 6% NaCl. Brass and alloy 600 were found to anodically polarize Ti, while 316 stainless steel and Monel could polarize Ti either anodically or cathodically depending on temperature and pH. However, the reliability of these last results is uncertain since it is not clear whether the pretreatment of the specimens used in the experiments caused their surface hydriding or not, or whether

similarly polarized couples would be obtained for alternative geometries and coupled surface areas.

Foroulis (1989) also found that Ti could form the anode or cathode in galvanic couples depending on the aggressiveness of the solution to which the couple was exposed, although the test environments used were not really relevant to waste repository conditions. The tests were generally conducted in hot (80°C) acidic sulphate and sulphidic solutions (pH = 0.5 to 5) or in ammonium sulphide solutions (pH 9-10.6). Whether or not the Ti was the anode or cathode depended on whether chlorides or cyanides were present. When these ions were present Ti tended to be more cathodic by 200 to 300 mV. This was attributed to the loss of passivity on the coupled material due, in this case to the breaking of a sulphide film, when Cl^- was present. In sulphidic solutions containing CN^- and Cl^-, the Ti tended to be cathodic and the corrosion rates of carbon steel, 304 stainless steel and I-600 were enhanced by a factor of 1 to 2. In solutions free of CN^-, Ti was anodic to these materials and no adverse corrosion effects were observed on either of the materials in the couple.

What is clear from this discussion is that galvanic couples involving Ti and other passive materials are unlikely to lead to significant corrosion of either material. The prospect of a galvanic couple between titanium and alloy-22 leading to any significant damage of either material can be judged remote. However, given the corrosion potential for 304 stainless steel when active in seawater (Table 6) the possibility of Ti being the cathode in a couple with this material is a possibility in an acidified crevice containing a concentrated groundwater, eg., SAW in Table 3. Whether or not stainless steel can become active under these conditions remains to be determined. For significantly negative potentials (-0.53 V *vs* SCE, Table 6) to be established would require the active crevice corrosion of the stainless steel not just the establishment of low density pitting, a condition for which such negative potentials should not be established. However, it would be judicious, given this possibility, to choose a stainless steel resistant to crevice corrosion, if the possibility of a crevice with Ti is unavoidable.

5 SUMMARY AND CONCLUSIONS

The possible failure processes, crevice corrosion, pitting and hydrogen-induced cracking (HIC) have been reviewed for the candidate titanium alloys (Ti-12, Ti-16 and Ti-7) under anticipated conditions in the Yucca Mountain nuclear waste repository. Both pitting and crevice corrosion are extremely remote possibilities under these conditions for these alloys. For Ti-12 it is possible that a limited amount of crevice corrosion could occur but repassivation has inevitably been observed after ~ 1 mm of penetration in even the most aggressive of saturated brines.

All three alloys could suffer hydrogen absorption making the possibility of hydrogen-induced cracking worth investigation. Based on slow strain rate testing of pre-hydrided compact tension specimens, both Ti-12 and Ti-16 have been shown capable of tolerating a substantial hydrogen concentration before any decrease in fracture toughness is observed. For Ti-12 the fracture toughness starts to decrease once the hydrogen content reaches a value of ~ 400 $\mu g \cdot g^{-1}$, whereas for Ti-16 this threshold is at least ~ 1000 $\mu g \cdot g^{-1}$. It may be larger for Ti-16 but testing has so for been limited.

The feature which determines whether this degradation in fracture toughness will lead to waste package failure is the rate of hydrogen absorption by the alloy. For the commercially pure Ti-2 hydrogen absorption is extremely slow, and probably negligible, for potentials more positive than –0.6 V (vs SCE). This potential coincides with that required to induce the redox transformation, Ti^{4+} to Ti^{3+}, in the passive TiO_2 oxide, a process that renders the oxide conductive and permeable to hydrogen. Generally, such a potential is only achieved when titanium is over-protected cathodically, or galvanically coupled to an actively corroding metal such as carbon steel.

However, the presence of intermetallics in the alloys being considered (and possibly also β-phase in Ti-12) could allow hydrogen absorption into the metal at potentials less negative than this –0.6 V threshold. Both Ti-12 and Ti-7 have been shown to absorb hydrogen at potentials above this threshold, but the few experiments performed to date on Ti-16 indicate that no absorption occurs until < -1.0V. This last alloy definitely contains many randomly dispersed intermetallic particles. To date their identity has not been

elucidated, and why they do not appear to act as hydrogen absorption sites not determined.

From this review it was concluded that the only feasible failure mechanism for these titanium alloys would be hydrogen absorption leading to HIC within an acidified crevice under passive conditions. For this to occur the titanium would need to act as a cathodic site and would require a coupled cathode. The titanium could supply its own anode in two ways.

(1) The intermetallic could be corrosive under the acidified crevice conditions thereby acting as both anode and cathode. The intermetallic Ti_2Ni (in Ti-12) has been demonstrated capable of acting in this manner and Ti-12 has been shown to more readily absorb hydrogen than the commercial alloy Ti-2. However, the intermetallic particles in Ti-16 appear to be inert, a claim based on impedance measurements. Consequently, they would not be expected to be corrosive in the same manner as Ti_2Ni in Ti-12, and hence incapable of providing an anodic site.

(2) The presence of F^- in the concentrated groundwaters anticipated at Yucca Mountain could accelerate passive dissolution, and hydrogen could be absorbed at the cathodic intermetallic site. For this to be feasible, the pH would have to be □ 3 (for Ti-2) with substantial amounts of F^- present. The evidence from dental and flue gas scrubber experiments indicates that this can occur but is unlikely in the presence of the other groundwater anions expected to be present, particularly SO_4^{2-} and HCO_3^-, and in the presence of substantial amounts of silica. These last three species inhibit the development of acidity within crevices and, in the case of silica, appear to remove F^- from the solution. There is also the possibility that, under acidic elevated temperature conditions, F^- may be removed as the volatile HF. For the alloy Ti-12, a pH < 1.5 appears necessary before F^- exerts any measurable influence on the passive corrosion rate. Although not tested one would, therefore, expect an even lower pH threshold for the Ti-16 and Ti-7 alloys. While one can be optimistic that, at the levels anticipated on the waste packages in Yucca Mountain, F^- will not exert a significant influence on the corrosion of Ti-

12, Ti-7 and Ti-16, definitive proof that this anion will have no influence is presently unavailable.

The third potential anode would be provided by the coupling of a more active material to the passive titanium. Within the present waste package design this would be either Alloy 22 or 316L stainless steel. If all the three materials remain passive, then it is possible the Ti alloys could be either anodes or cathodes in the couple. Evidence exists to show both combinations are possible and that the activities of the couples are generally innocuously low. However, the test environments have not been as aggressive as those anticipated at Yucca Mountain. While it is unlikely that Alloy 22 will form an active anode, the possibility cannot presently be ruled out with stainless steels. In environments where the passivity of the stainless steel can be degraded (sulphidic environments have been tested), galvanic couples to Ti were observed and the steel corrosion rates accelerated, but only by a factor of 1 to 2.

The formation of such a galvanic couple would be expected to lead to the absorption of hydrogen by the Ti-12 and Ti-7 alloys but possibly not by the Ti-16 alloy. For Ti-12, absorption would be expected to be more extensive than with the other alloys, and the transport of absorbed hydrogen into the bulk of the alloy facilitated by the presence of β-phase ligaments along predominantly α-phase grain boundaries. Since the efficiency of hydrogen absorption decreases as the Pd content of the alloy decreases, Ti-16 would be expected to absorb hydrogen less readily than the Ti-7 alloy. Indeed, some speculative evidence exists suggesting that the intermetallic particles presence in Ti-16 may prevent absorption.

Based on these studies the order of preference of these alloys as candidate materials for waste packages at Yucca Mountain would be

Ti-16 □ Ti-7 >> Ti-12

However, before a confident recommendation that Ti-16 be chosen over Ti-7, a real understanding of the presently baffling behaviour of the intermetallic particles in this material is required.

REFERENCES

T. Watanabe. T. Shindo and H. Naito. 1988. Effect of iron content on the breakdown potential for pitting of titanium in NaCl solutions. In Proceedings of the Sixth World Conference on Titanium, Cannes, France, 1988, June 6-9, 1735-1740.

S. Kitayama, Y. Shida and M. Oshiyama. 1990. Development of new crevice corrosion resistant Ti alloys. Sumitomo Search 41, 23-32.

T. Shibata and Y.-C. Zhu. 1995. The effect of film formation conditions on the structure and composition of anodic oxide films on titanium. Corrosion Science 37(2), 253-270.

J. L. Gilbert and J. J. Jacobs. 1997. The mechanical and electrochemical processes associated with taper fretting crevice corrosion: A review. In Modularity of Orthopedic Inplants (editors D. E. Marlowe, J. E. Parr and M. B. Mayor) ASTM STP 1301, 45-59, American Society for Testing and Materials, Philadelphia, PA.

J. J. Noël. 1999. The electrochemistry of titanium corrosion. Ph. D. Thesis, University of Manitoba.

R. Greef, R. Peat, L.M. Peter, D. Pletcher, J. Robinson. 1985. Instrumental methods in Electrochemistry. Ellis Horwood Ltd. Chichester, U. K.

T. M. Murai, M. Ishikawa and C. Miura. 1977. Absorption of hydrogen and titanium under cathodic polarization. Boshoku Gijutsu. 26, 177-183.

T. R. Beck. 1973. Electrochemistry of freshly-generated titanium surfaces - I. Scraped-rotating-disk experiments. Electrochimica Acta 18, 807-814.

S-I Pyun and Y-G Yoon. 1996. Hydrogen transport through TiO_2 films prepared by plasma enhanced chemical vapour deposition (PECVD) method. In Hydrogen Effects in Materials (edited by A. W. Thompson and N. R. Moody), The Minerals, Metals and Materials Society, 261-269.

Z. Tun, J. J. Noël and D. W. Shoesmith. 1999. Electrochemical modification of the passive oxide layer on a Ti film observed by in-situ neutron reflectometry. J. Electrochem. Soc. 146, 988-994.

C. F. Clarke, D. Hardie and B. M. Ikeda. 1994. the effect of hydrogen content on the fracture of pre-cracked titanium specimens. Corrosion Science 36, 487-509.

C. F. Clarke, D. Hardie and B. M. Ikeda. 1995. Hydrogen induced cracking of Grade-2 titanium, Atomic Energy of Canada Ltd. Report, AECL-11284, COG-95-113.

D. W. Shoesmith, D. Hardie, B. M. Ikeda and J. J. Noël. 1997. Hydrogen absorption and the lifetime performance of titanium nuclear waste containers. Atomic Energy of Canada Ltd. Report, AECL-11770, COG-97-035-I.

J. J. Noël, M. G. Bailey, J. P. Crosthwaite, B. M. Ikeda, S. R. Ryan and D. W. Shoesmith. 1996. Hydrogen absorption by Grade-2 Titanium. Atomic Energy of Canada Ltd. Report, AECL-11608, COG-96-249.

R. W. Schutz and D. E. Thomas. 1987. Corrosion of titanium and titanium alloys. In Metals Handbook, Ninth edition, volume 13 (corrosion), ASM International, Metals Park, OH, 669-706.

D. W. Shoesmith and B. M. Ikeda. 1997. The resistance of titanium to pitting, microbially induced corrosion, and corrosion in unsaturated conditions. Atomic Energy of Canada Ltd. Report, AECL-11709, COG-95-557-1.

F. A. Posey and E. G. Bohlman. 1967. Pitting of titanium alloys in saline waters. Desalination 3, 269-279.

T. Koizumi and S. Furuya. 1973. Pitting corrosion of titanium in high temperature halide solution. In Proceedings of the Second International Conference; Titanium Science and Technology (edited by R. I. Jaffe and H. M. Burte), Plenum Press, New York, NY, 2383-2393.

N. R. Sorensen. 1990. Laboratory studies of the corrosion and mechanical properties of titanium Grade-12 under WIPP repository conditions. In Corrosion of Nuclear Fuel Waste Containers. Proceedings of a Workshop, Winnipeg, Feb. 9-10 (1988) (edited by D. W. Shoesmith), Atomic energy of Canada Ltd. Report, AECL-10121, 29-44.

T. Kido and S. Tsujikawa. 1989. Effect of Ni and Mo on initial conditions for crevice corrosion of low alloy titanium, Japanese J. of Iron and Steel, 75(8), 96- .

E. van der Lingen and H. de villiers Steyn. 1994. Titanium Applications Conference, Boulder, CO, Oct. 2-5, 1994, Titanium Development Association, Boulder, CO, USA, 450-461.

A. J. Sedriks. 1975. Corrosion resistance to Ti-Ru alloys. Corrosion 31(2), 60-65.

G. K. Hubler and E. McCafferty. 1980. The corrosion behaviour and RBS analysis of Pd-implanted titanium. Corrosion Science, 20, 103-116.

R. D. Armstrong, R. E. Firman and H. R. Thirsk. 1973. Ring-disc studies of Ti-Pd alloy corrosion. Corrosion Science 13, 409-420.

R. E. Westerman. 1990. Hydrogen absorption and crevice corrosion behaviour of titanium Grade-12 during exposure to irradiated brine at 150°C. In Corrosion of nuclear fuel waste containers: Proceedings of a workshop. Atomic Energy of Canada Ltd. Report, AECL-10121, 67-84.

J. B. Cotton. 1967. The role of palladium in enhancing corrosion resistance of titanium. Platinum Metals Rev. 11, 50-52.

K. Satoh, K. Shimogori and F. Kamikubo. 1987. The crevice corrosion resistance of some titanium materials. A review of the beneficial effects of palladium. Platinum Metals Review, 31(3), 115-121.

A. J. Sedriks, J. A. S. Green and D. L. Novak. 1972. Electrochemical behaviour of Ti-Ni alloys in acidic solutions. Corrosion 28(4) 137-142.

J. A. Hall, D. Banerjee and T. L. Wardlaw. 1985. The relationships of structure and corrosion behaviour of Ti0.3Mo0.8Ni (Ticode-12). In Titanium, Science and Technology, Proceedings of the Fifth International Conference of Titanium (edited by G. Lütjering, U. Zwickler and W. Bunk), Sept. 10-14 (1984), Munich, Germany, 2603-2610.

B. M. Ikeda, M. G. Bailey, D. C. Cann and D. W. Shoesmith. 1990. Effect of iron content and microstructure on the crevice corrosion of Grade-2 titanium under nuclear waste vault conditions; In Advances in Localized Corrosion (edited by H. S. Isaacs, U. Bertocci, J. Kruger and S. Smialowska), 439-444, NACE International, Houston, TX.

D. W. Shoesmith, F. King and B. M. Ikeda. 1995. An assessment of the feasibility of indefinite containment of Canadian nuclear fuel wastes. Atomic Energy of Canada Ltd. Report, AECL-10972, COG-94-534.

M. G. Bailey, B. M. Ikeda, M. J. Quinn and D. W. Shoesmith. 1996. Crevice corrosion behaviour of titanium Grades-2 and -12 in hot aqueous chloride solution - The effect of chloride concentration. Atomic Energy of Canada Ltd. Report, AECL-10971, COG-95-279.

B. M. Ikeda, M. G. Bailey, C. F. Clarke and D. W. Shoesmith. 1989. Crevice corrosion of titanium under nuclear fuel waste conditions, Atomic Energy of Canada Ltd. Report, AECL-9568 (1989).

B. M. Ikeda, R. C. Styles, M. G. Bailey and D. W. Shoesmith. 1994. The effect of material purity on crevice corrosion of titanium in NaCl solution. In Compatibility of Biomedical Implants, (edited by P. Kovacs and N. S. Istephanous), Electrochemical Society Proceedings, Vol. 94-15, Electrochemical Society, Pennington, NJ, 368-380.

J. B. Cotton. 1970. Using titanium in the chemical plant. Chemical Engineering Progress, 66(10), 57-62.

L. C. Covington. 1979. The influence of surface condition and environment on the hydriding of titanium. Corrosion 35(8), 378-382.

T. Murai, M. Ishikawa and C. Miura. 1977. Absorption of hydrogen into titanium under cathodic polarization. Boshoku Gijutsu 26, 177-183.

T. Shibata and Y.-C. Zhu. 1994. The effect of film formation temperature on the stochastic processes of pit generation on anodized titanium. Corrosion Science 36(10), 1735-1749.

E. J. Kelly. 1979. Anodic dissolution and passivation of titanium in acidic media. J. Electrochem. Soc. 126, 2064-2074.

T. Watanabe, M. Kondo, H. Naito and K. Sakai. 1989. Electrochemical properties and corrosion characteristics of titanium in chloride solutions. Nippon Steel Technical Report 39/40, 29-35.

D. J. Blackwood, L. M. Peter and D. E. Williams. 1988. Stability and open circuit breakdown of the passive oxide film on titanium. Electrochimica Acta 33, 1143-1149.

T. Ohtsuka, M. Masuda and N. Sato. 1987. Cathodic reduction of anodic oxide films formed on titanium. J. Electrochem. Soc. 134, 2406-2410.

A. J. Sedriks. 1975. Corrosion resistance of Ti-Ru alloys. Corrosion, 31, 60-65.

R. W. Schutz. 1986. Titanium. In Process Industries Corrosion. The Theory and Practice, National Association of Corrosion Engineers, Houston, TX, 503-527.

R. W. Schutz. 1988. Titanium alloy crevice corrosion: Influencing factors and methods of prevention. In Proceedings of the Sixth International Conference on Titanium, (edited by P. Lacombe, R. Tricot and G. Beranger) June 6-9, 1988, Cannes, France. Societé Française de Métallurgie, Les Ulis Cedex, France; Vol. IV, 1917-1922.

Z. W. Wang, C. L. Briant and K. S. Kumar. 1999. Electrochemical, galvanic, and mechanical responses of Grade-2 Titanium in 6% sodium chloride solution. Corrosion, 55, 128-138.

Z. A. Foroulis. 1989. Corrosion and hydrogen embrittlement of titanium in aqueous sulphate and sulphidic solutions. Anti-corrosion Methods and Materials, June 1989, 4-9.

W. Wilhelmsen and A. P. Grande. 1987. The influence of hydrofluoric acid and fluoride on the corrosion and passive behaviour of titanium. Electrochimica Acta 32, 1469-1474.

R. L. Segall, R. St. C. Smart and P. S. Turner. 1988. Oxide surfaces in solution. In Surface and Near-surface Chemistry of Oxide Materials (edited by J. Nowotny and L.-C. Dufour), Elsivier Science Publishers, Amsterdam, 527-576.

D. W. Shoesmith, B. M. Ikeda, M. G. Bailey, M. J. Quinn and D. M. LeNeveu, 1995. A model for predicting the lifetimes of Grade-2 titanium nuclear waste containers. Atomic Energy of Canada Ltd. Report, AECL-10973, COG-94-558.

E. J. Kelly. 1982. Electrochemical behaviour of titanium. In Modern Aspects of Electrochemistry (edited by J. O. M. Boikrs, B. E. Conway, and R. E. White), Plenum Press, New York, 14, 319-424.

H. Mattson and I. Olefjord. 1990. Analysis of oxide formed on Ti during exposure in bentonite clay-I. The oxide growth. Werkstoffe and Korrosion, 41, 383-390.

H. Mattsson, C. Li and I. Olefjord. 1990. Analysis of oxide formed on Ti during exposure in bentonite clay-II. The structure of the oxide. Werkstoffe and Korrosion 41, 578-584.

R. W. Schutz. 1996. Ruthenium enhanced titanium alloys. Minor ruthenium additions produce cost effective corrosion resistant commercial titanium alloys. Platinum Metals Rev. 40(2), 54-61.

D. W. Shoesmith and F. King. 1999. The effects of gamma radiation on the corrosion of candidate materials for the fabrication of nuclear waste packages. Atomic Energy of Canada Ltd. Report. AECL-11999.

L. Reclaru and J-M. Meyer. 1988. Effects of fluorides on titanium and other dental alloys in dentistry. Biomaterials 19, 85-92.

D. E. Thomas and H. B. Bomberger. 1983. The effect of chlorides and fluorides on titanium alloys in simulated scrubber environments. Materials Performance, Nov. 1983, 29-36.

R. W. Schutz and J. S. Grauman. 1986. Corrosion behaviour of titanium and other alloys in laboratory FGD scrubber environments. Materials Performance, April 1986, 35-42.

US Department of Energy, Office of Civilian Radioactive Waste Management. 1988. Viability Assessment of a Repository at Yucca Mountain; volume 3: Total System Performance Assessment, DOE/RW-058/V3, Yucca Mountain Site Characterization Office, North Las Vegas, NV.

R. A. Van Konynenburg, R. D. McCright, A. K. Roy and D. A. Jones. 1988. Engineered Materials Characterization Report for the Yucca Mountain Site Characterization Project. Lawrence Livermore National Laboratory Report, UCRL-ID-119564.

S. Kudelka, A. Michaelis and J. W. Schultze. 1995. Electrochemical characterization of oxide layers on single grains of a polycrystalline Ti-sample. Ber. Bunsenges. Phys. Chem. 99, 1020-1027.

R. W. Schutz and M. Xiao. 1993. Optimized Lean-Pd titanium alloys for aggressive reducing acid and halide service environments. Proceedings of 12th International Corrosion Congress, Sept. 1993, Vol. 3A, 1213-1225, NACE International, Houston, TX.

Y. Shida and S. Kitayama. 1988. Effect of Pd addition on the crevice corrosion resistance of titanium. Proceedings of 6th International Conference on Titanium, 1988.

P. McKay. 1987. Crevice corrosion kinetics on titanium and a Ti-Ni-Mo alloy in chloride solutions at elevated temperature. In Corrosion Chemistry Within Pits Crevices and Cracks (edited by A. Turnbull) National Physical Laboratory, Teddington, UK, 101-127.

R. S. Glass. 1983. Effect of intermetallic Ti_2Ni on the electrochemistry of Ticode-12 in hydrochloric acid. Electrochimica Acta, 28(11), 1507-1513.

LEGENDS TO FIGURES

Figure 1. Summary of the changes expected in passive oxide properties as a function of pH, potential and temperature.

Figure 2. Critical crevice temperatures for Ti-12, Ti-16 and Ti-7, and the closely related Ti-Ru alloy, determined in a number of aggressive acidic and extremely oxidizing chloride environments (reported from Schutz (1995)).

Figure 3. Coupled currents (I_c) and crevice potentials (E_c) measured in 0.27 $mol \cdot L^{-1}$ NaCl on artificially formed crevices of various Ti-alloys: (A) Ti-2 (Fe-0.024 wt%) at 150°C; (B) Ti-2 (Fe-0.13 wt%) at 150°C; (C) Ti-12 at 150°C; (D) Ti-16 at 100°C (from Shoesmith *et al.* 1997).

Figure 4. Weight changes due to crevice corrosion for Ti-2 ((, low iron content), Ti-2 (o, high iron content) and Ti-12 (±) as a function of chloride concentration at 150°C (from Bailey *et al.* 1996)

Figure 5. Schematic illustrating the polarization curve for titanium and its relationship to the cathodic polarization curves for proton reduction on Ti-2 and on a titanium alloy containing a catalytic alloying element (e.g., Ti-12, Ti-16).

Figure 6. Schematics illustrating the two mechanisms proposed to explain the crevice corrosion resistance conferred on Ti by alloying with Ni (Ti-12) or Pd (Ti-7, Ti-16):

(A) redeposition of dissolved alloying element to produce a galvanically-coupled catalytic site for H^+ reduction;

(B) galvanic coupling of an inert catalytic site for H^+ reduction.

Figure 7. Schematic illustrating the anodic ennoblement of a Pd-containing Ti-alloy due to surface enrichment by Pd of temporarily active or passive sites.

Figure 8. Summary of the effect of various parameters on the pitting potential for Ti (from Shoesmith *et al.* 1997)

Figure 9. Variation of the critical stress intensity factor with hydrogen content for Ti-2 (transverse-longitudinal (T-L) orientation): o – slow crack growth (K_s); • - fast fracture (K_H) (from Clarke *et al.* 1994).

Figure 10. Schematic showing the combinations of stress intensity factor and hydrogen concentration leading either to fast crack growth (brittle failures (K_H)), slow crack growth (K_s) due to either sustained load cracking or ductile rupture, or to no failure (from Shoesmith *et al.* 1995).

Figure 11. The hydrogen absorption rate as a function of applied potential measured on Ti-2 electrodes in flowing artificial seawater with a flow velocity of 2.0 ms^{-1} at 30°C (from Murai *et al.* 1977).

Figure 12. Schematic illustrating the cathodic transformations occurring in TiO_2 films which lead to the absorption of hydrogen.

Figure 13. Profiles of scattering length density (SLD) as a function of depth recorded by in-situ neutron reflectometry on an anodically treated (2.0V) sputter-deposited Ti film in neutral 0.2 $mol{\cdot}L^{-1}$NaCl. While the SLD was being measured the electrode was potentiostatted at the indicated potentials. The differently shaded areas show the oxide region free of hydrogen and that containing hydrogen (from Tun *et al.* 1999).

Figure 14. The ratio of the input current to output current as a function of the potential applied across a TiO_2 layer deposited on Pd metal. The ratio was measured in 0.1 $mol{\cdot}L^{-1}$ NaOH. The input current is the current measured for H^+ reduction at the TiO_2/solution interface. The output current is that measured for H oxidation across the Pd/solution interface (from Pyun and Yoon 1996).

Figure 15. Schematic illustrating the low efficiency of hydrogen absorption under passive conditions and the possibility of a much more highly efficient absorption process through catalytic intermetallic windows in the passive oxide.

Figure 16. Schematic illustrating how the corrosion of a Ti_2Ni intermetallic particle can lead to the absorption of hydrogen and how the presence of β-phase ligaments along α-

phase grain boundaries can assist the transport of this absorbed hydrogen into the bulk of the alloy.

Figure 17. The creviced face of a Ti specimen exposed to 0.27 $mol \cdot L^{-1}$ NaCl at 100°C without the initiation of active crevice corrosion. The rectangular area between the two bolt holes shows the section of the titanium beneath the PTFE crevice former. The darkened area within this creviced area is the stained area due to the development of acidic conditions within the crevice.

Figure 18. Schematics illustrating the processes occurring within a creviced site at, (A) low temperature (< 65°C, and (B) temperatures greater than 65°C. At low temperatures film growth predominates and passivity is maintained. At higher temperatures, film breakdown/recrystallization processes occur leading to cation hydrolysis and the development of acidity within the creviced site.

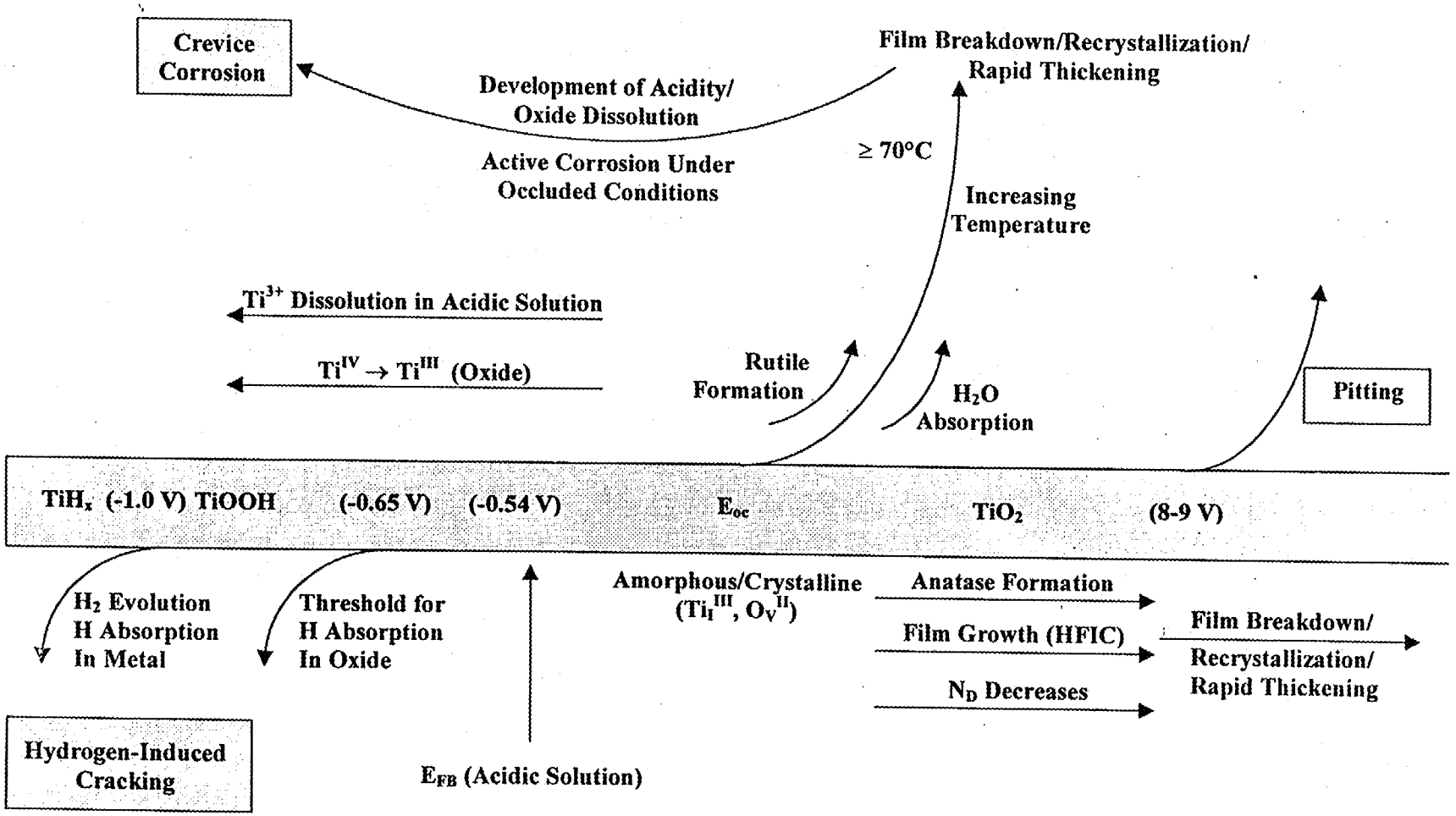
Crevice Corrosion
Development of Acidity/ Oxide Dissolution
Active Corrosion Under Occluded Conditions
Film Breakdown/Recrystallization/ Rapid Thickening
≥ 70°C
Increasing Temperature
Ti3+ Dissolution in Acidic Solution
TiIV → TiIII (Oxide)
Rutile Formation
H2O Absorption
Pitting
TiHx (-1.0 V) TiOOH (-0.65 V) (-0.54 V) Eoc TiO2 (8-9 V)
H2 Evolution H Absorption In Metal
Threshold for H Absorption In Oxide
Amorphous/Crystalline (TiI III, OV II)
Anatase Formation
Film Growth (HFIC)
ND Decreases
Film Breakdown/ Recrystallization/ Rapid Thickening
Hydrogen-Induced Cracking
EFB (Acidic Solution)

Figure 1

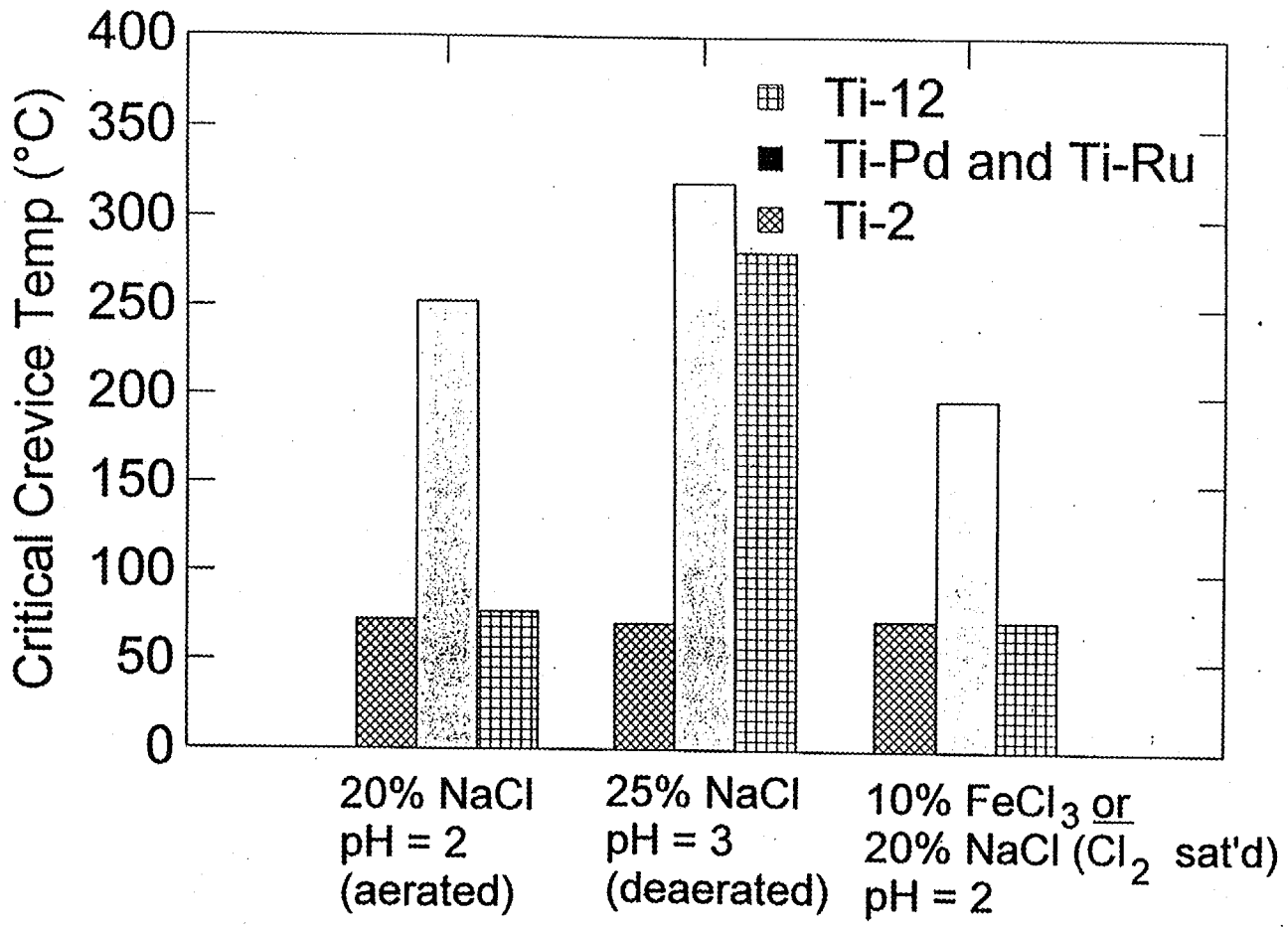
Critical Crevice Temp (°C)
400
350
300
250
200
150
100
50
0
Ti-12
Ti-Pd and Ti-Ru
Ti-2
20% NaCl
pH = 2
(aerated)
25% NaCl
pH = 3
(deaerated)
10% FeCl3 or
20% NaCl (Cl2 sat'd)
pH = 2

Figure 2

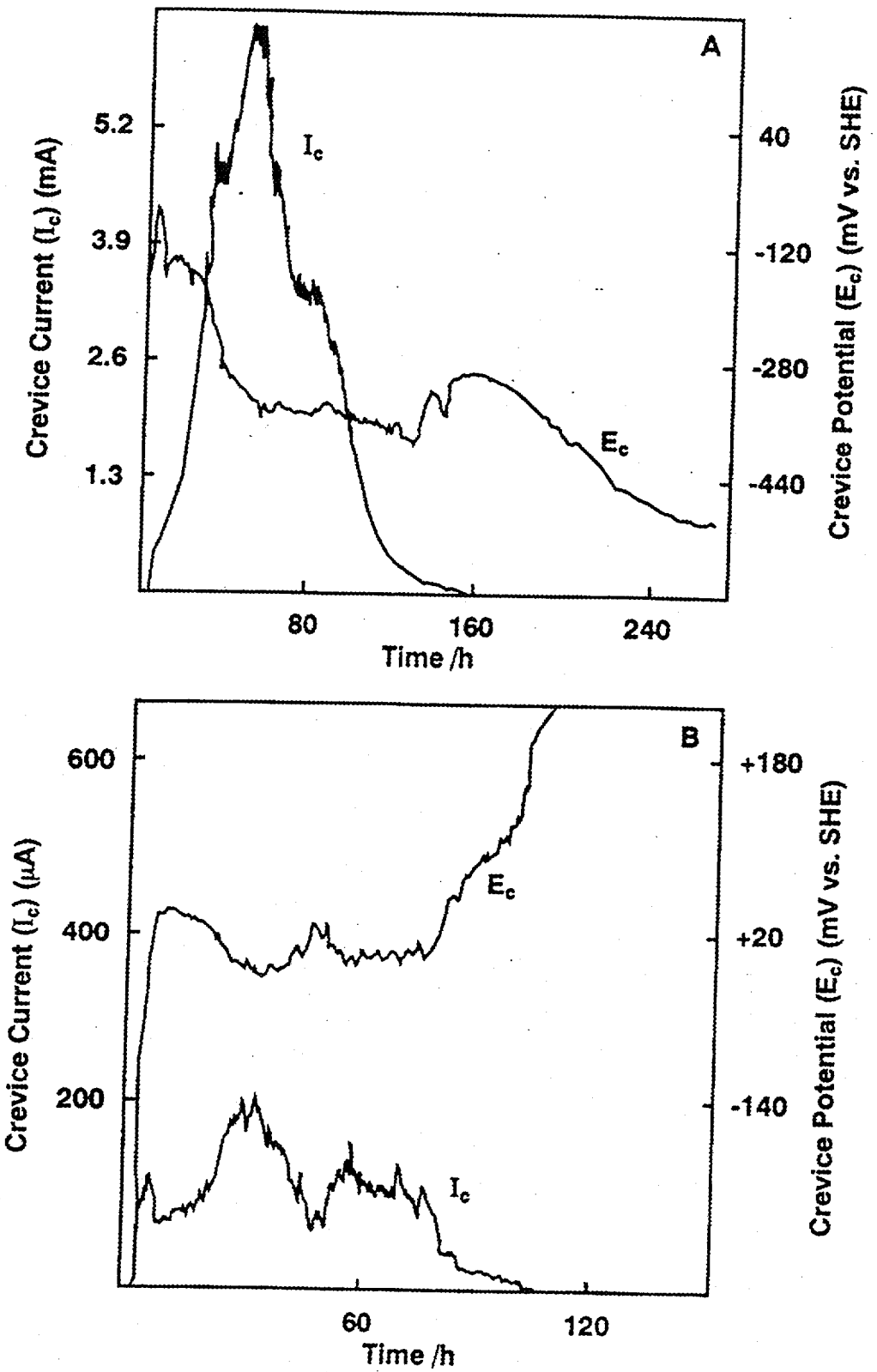

Figure 3A and 3B

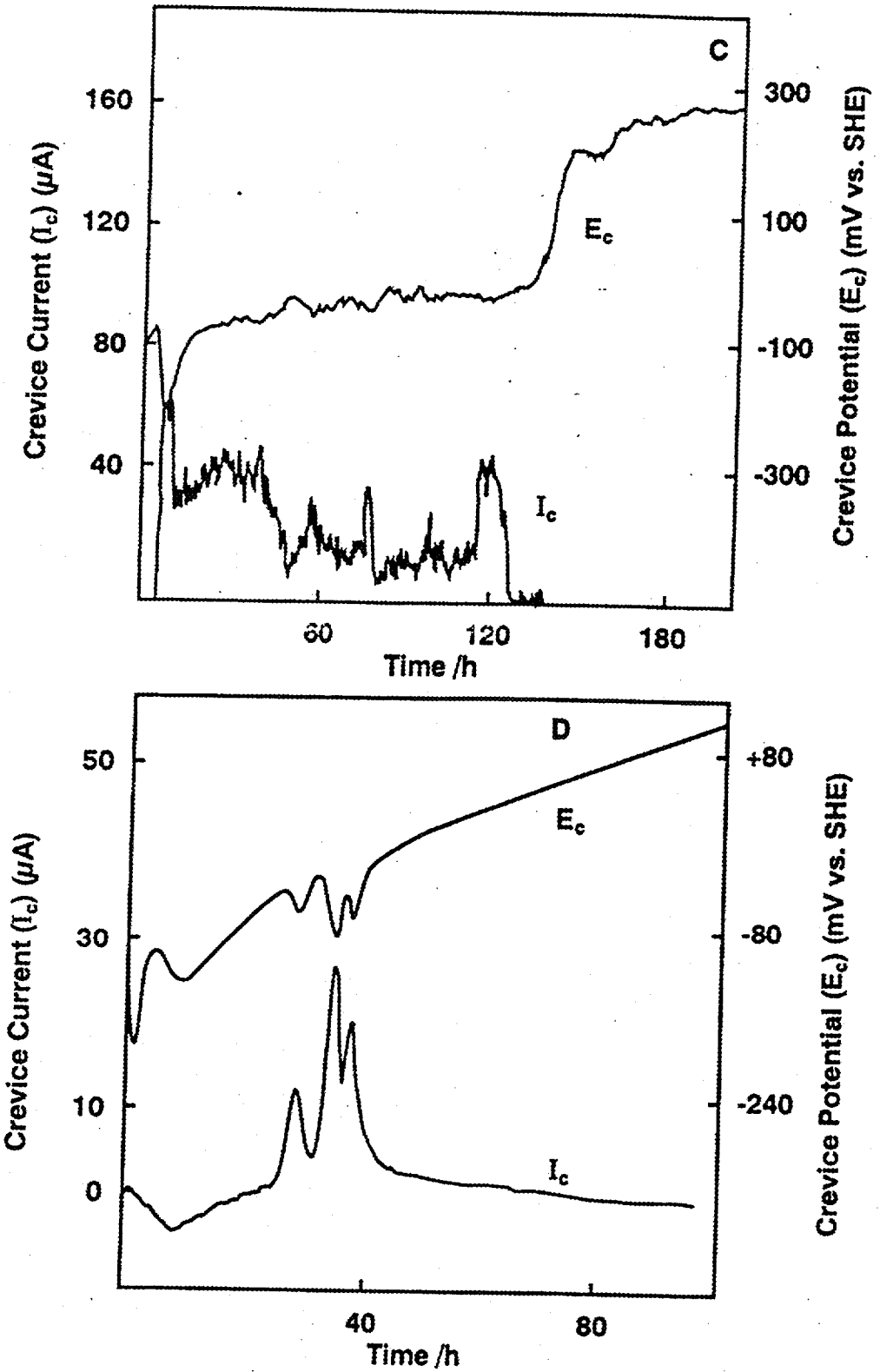

Figure 3C and 3D

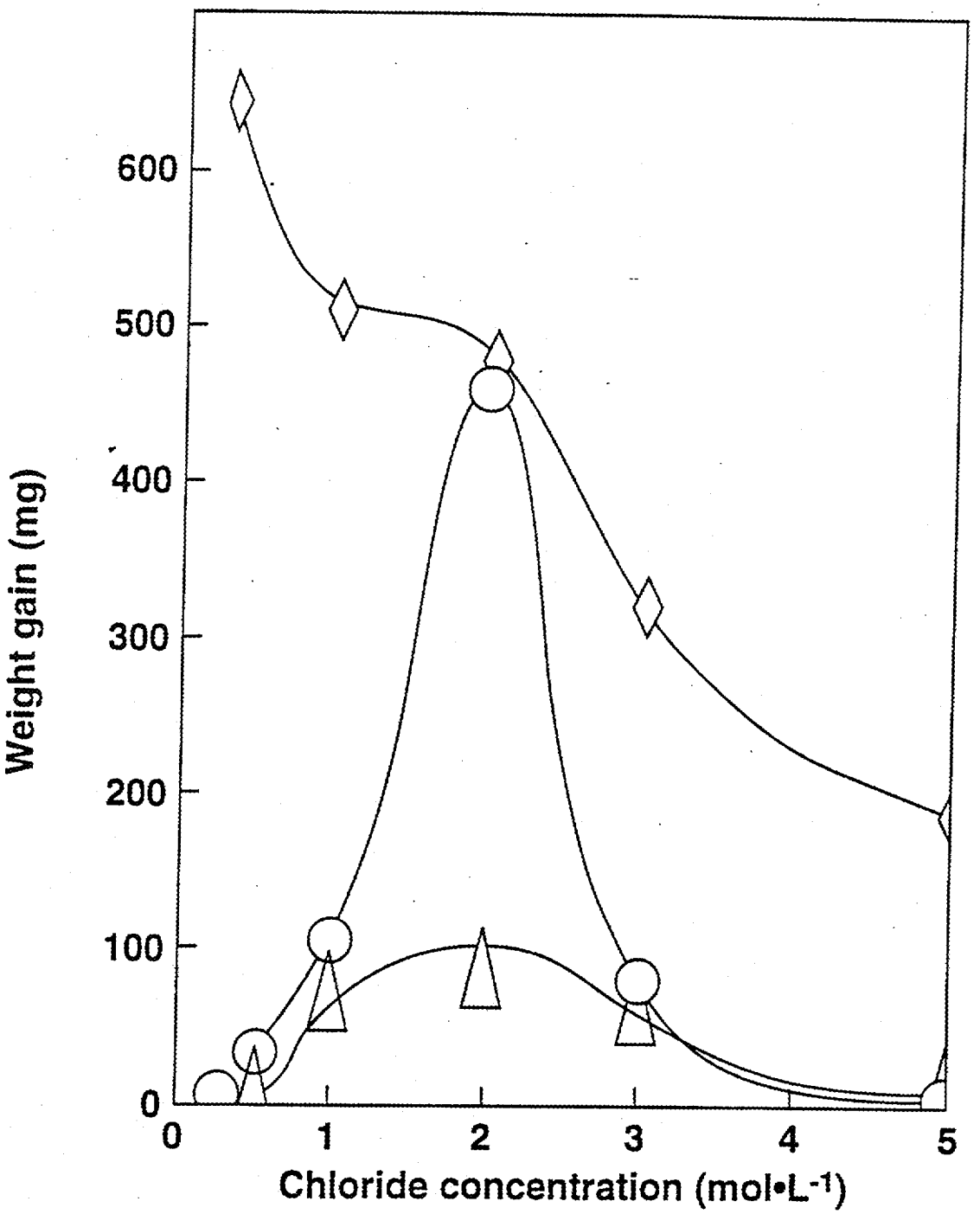
Weight gain (mg)
600
500
400
300
200
100
0
0
1
2
3
4
5
Chloride concentration (mol•L-1)

Figure 4

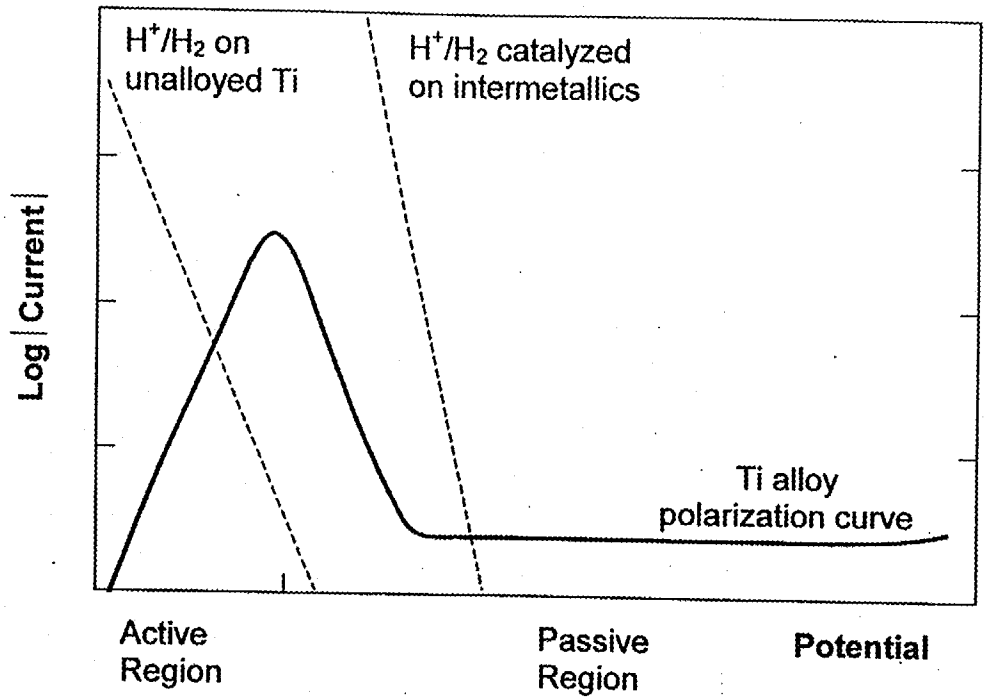
H+/H2 on
unalloyed Ti
H+/H2 catalyzed
on intermetallics
Log |Current|
Ti alloy
polarization curve
Active
Region
Passive
Region
Potential

Figure 5

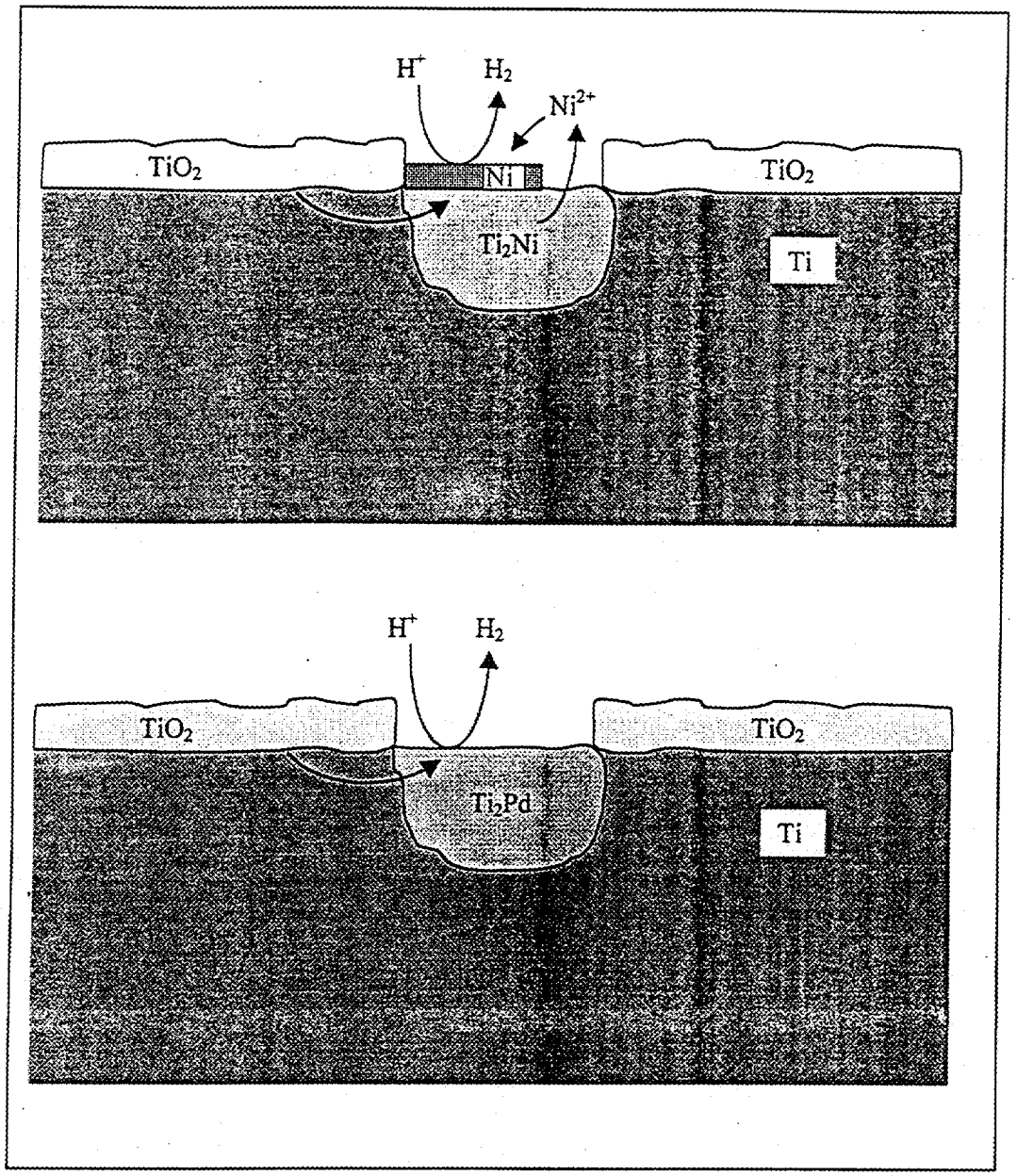

Figure 6

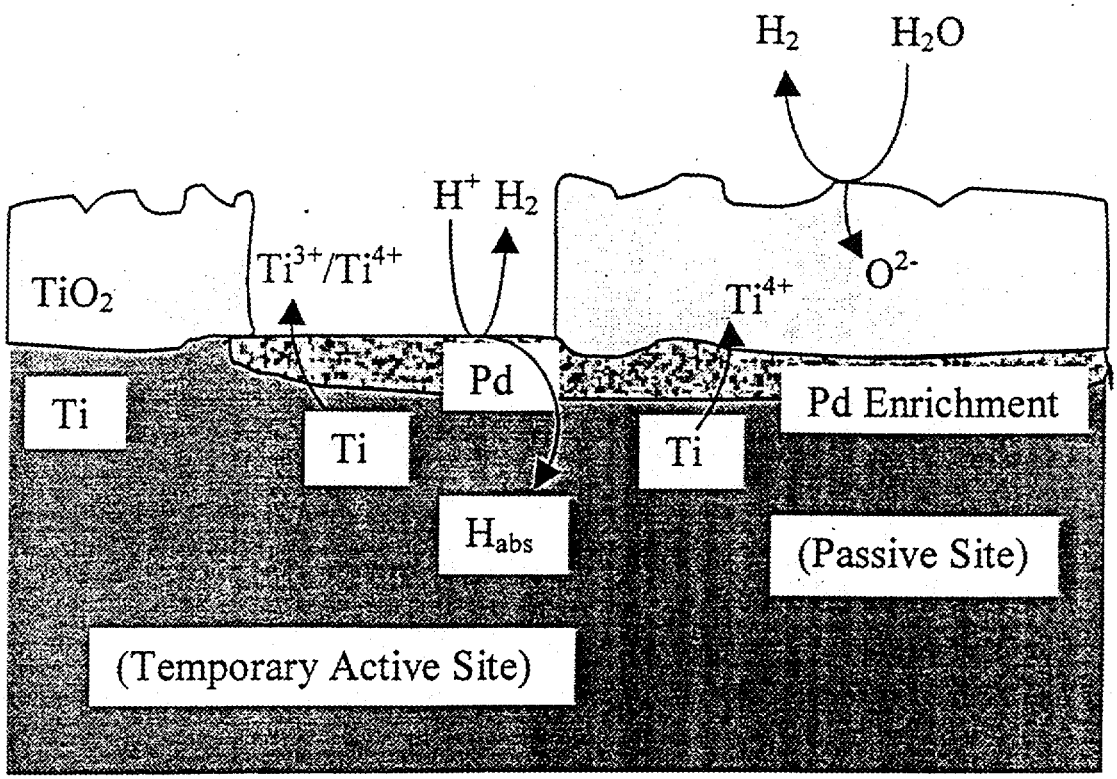
H2
H2O
H+ H2
TiO2
Ti3+/Ti4+
Ti4+
O2-
Pd
Ti
Ti
Ti
Pd Enrichment
Habs
(Passive Site)
(Temporary Active Site)

Figure 7

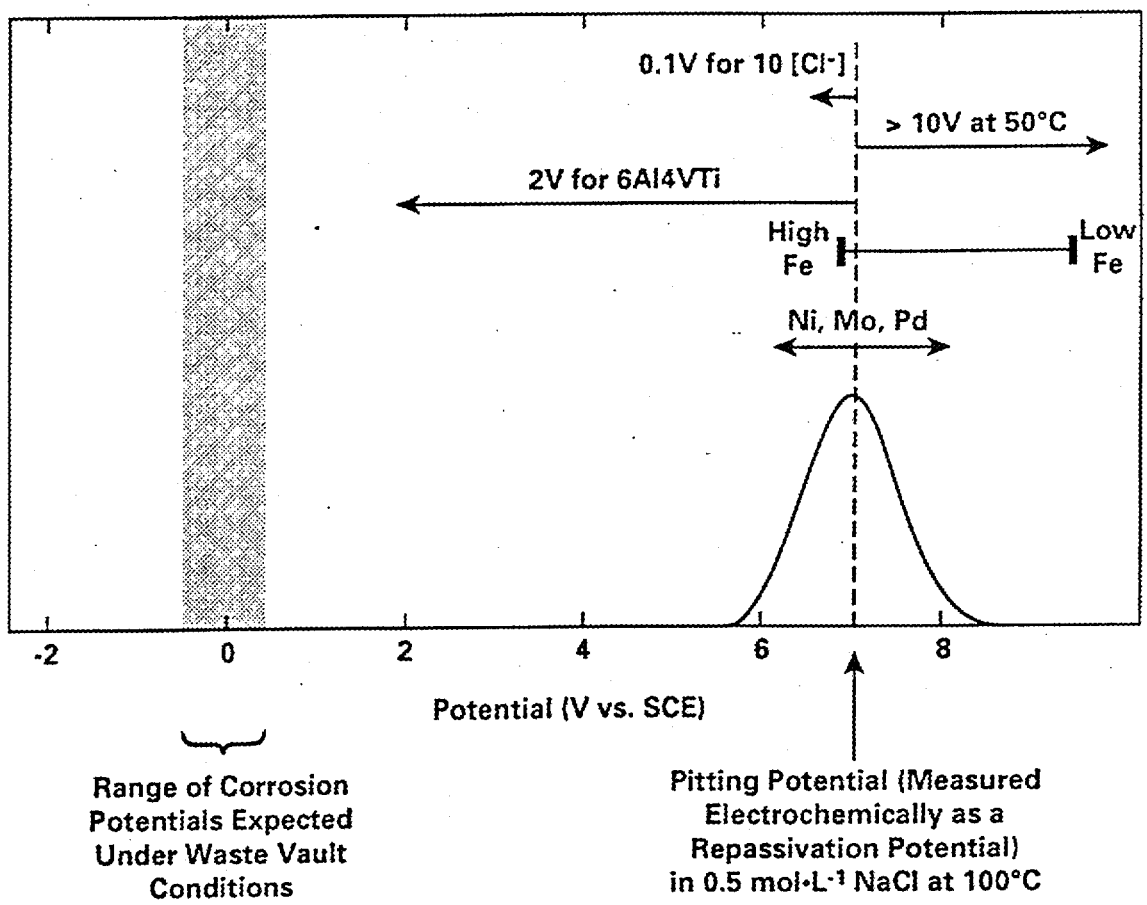
0.1V for 10 [Cl-]
> 10V at 50°C
2V for 6Al4VTi
High Fe
Low Fe
Ni, Mo, Pd
-2
0
2
4
6
8
Potential (V vs. SCE)
Range of Corrosion Potentials Expected Under Waste Vault Conditions
Pitting Potential (Measured Electrochemically as a Repassivation Potential) in 0.5 mol·L-1 NaCl at 100°C

Figure 8

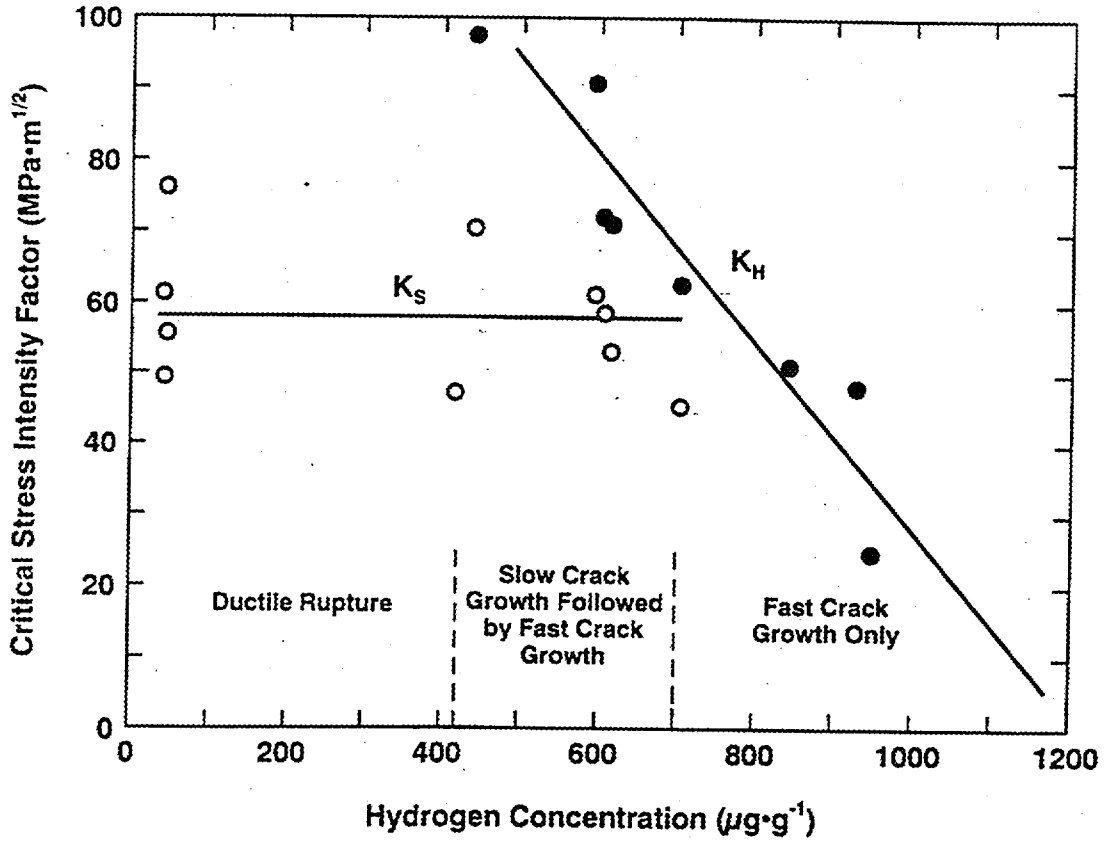
Critical Stress Intensity Factor (MPa•m^1/2)
100
80
60
40
20
0
0
200
400
600
800
1000
1200
Hydrogen Concentration (μg•g^-1)
K_S
K_H
Ductile Rupture
Slow Crack Growth Followed by Fast Crack Growth
Fast Crack Growth Only

Figure 9

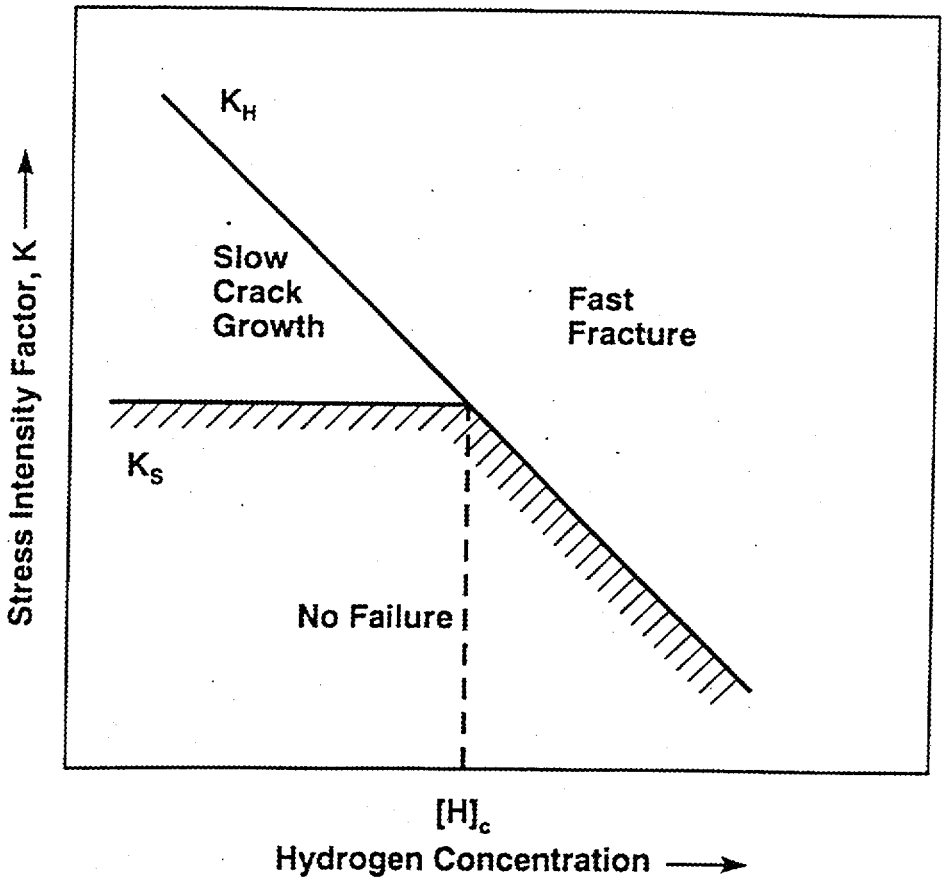
K_H
Slow
Crack
Growth
Fast
Fracture
K_S
No Failure
Stress Intensity Factor, K
$[H]_c$
Hydrogen Concentration

Figure 10

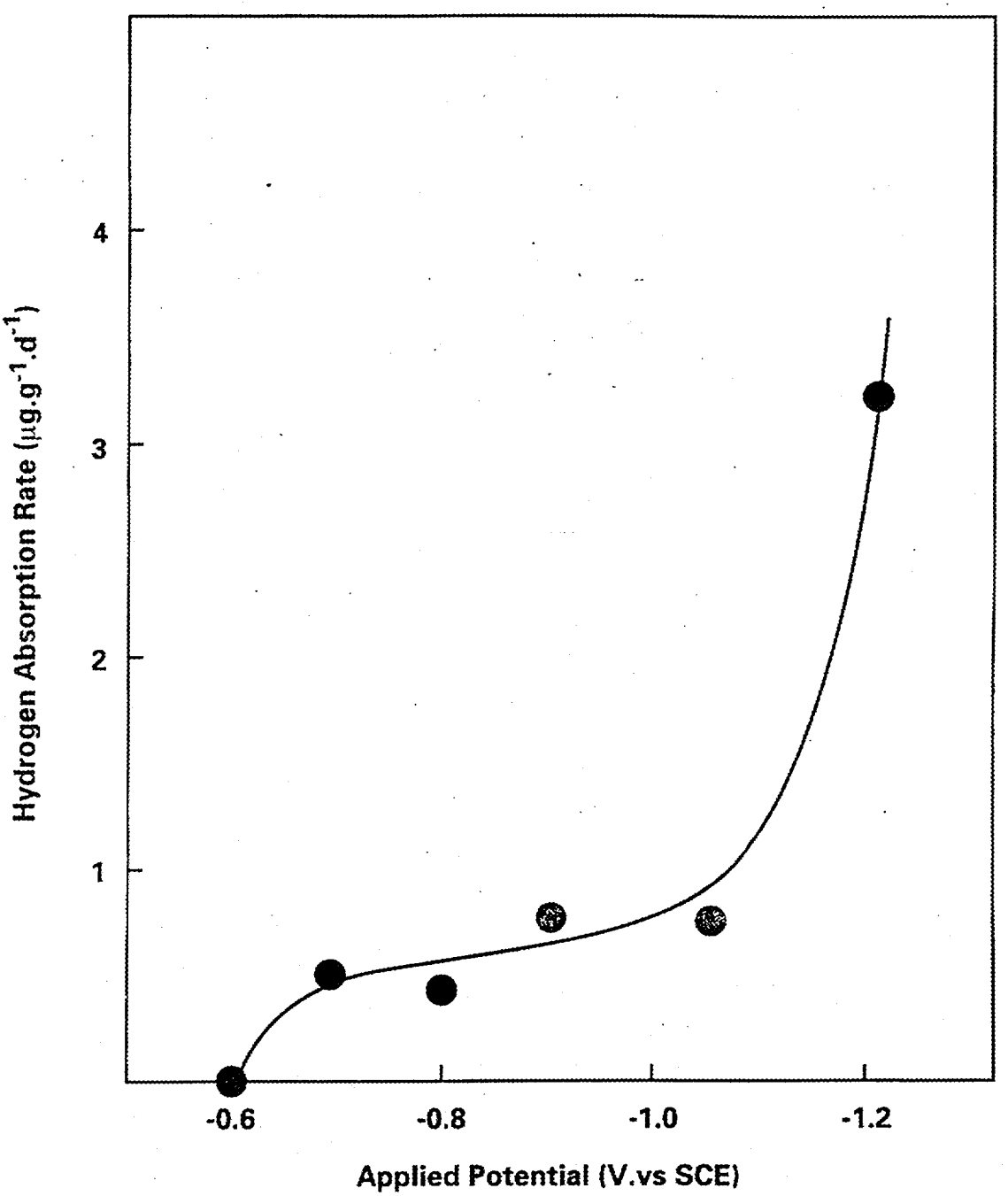
Hydrogen Absorption Rate (μg.g-1.d-1)
4
3
2
1
-0.6
-0.8
-1.0
-1.2
Applied Potential (V.vs SCE)

Figure 11

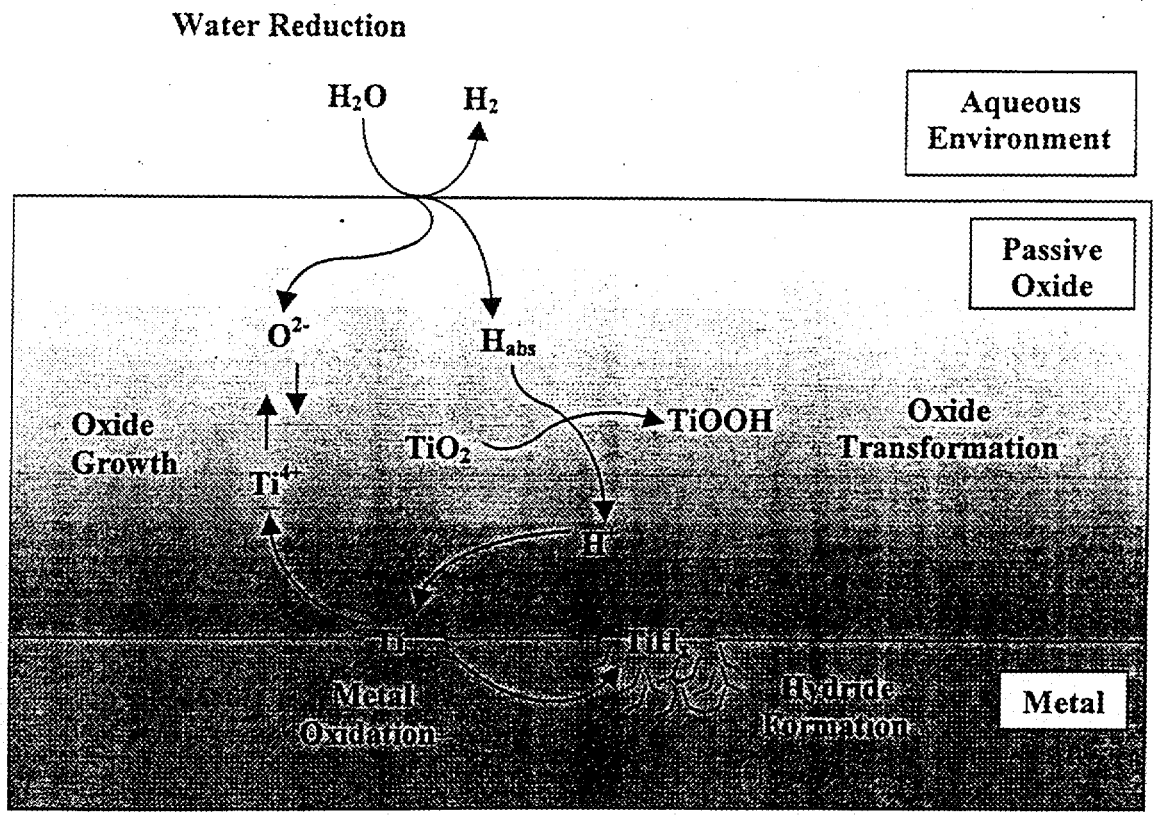
Water Reduction
H_2O
H_2
Aqueous Environment
Passive Oxide
O^{2-}
H_{abs}
Oxide Growth
TiO_2
TiOOH
Oxide Transformation
Ti^{4+}
H
Ti
TiH_x
Metal Oxidation
Hydride Formation
Metal

Figure 12

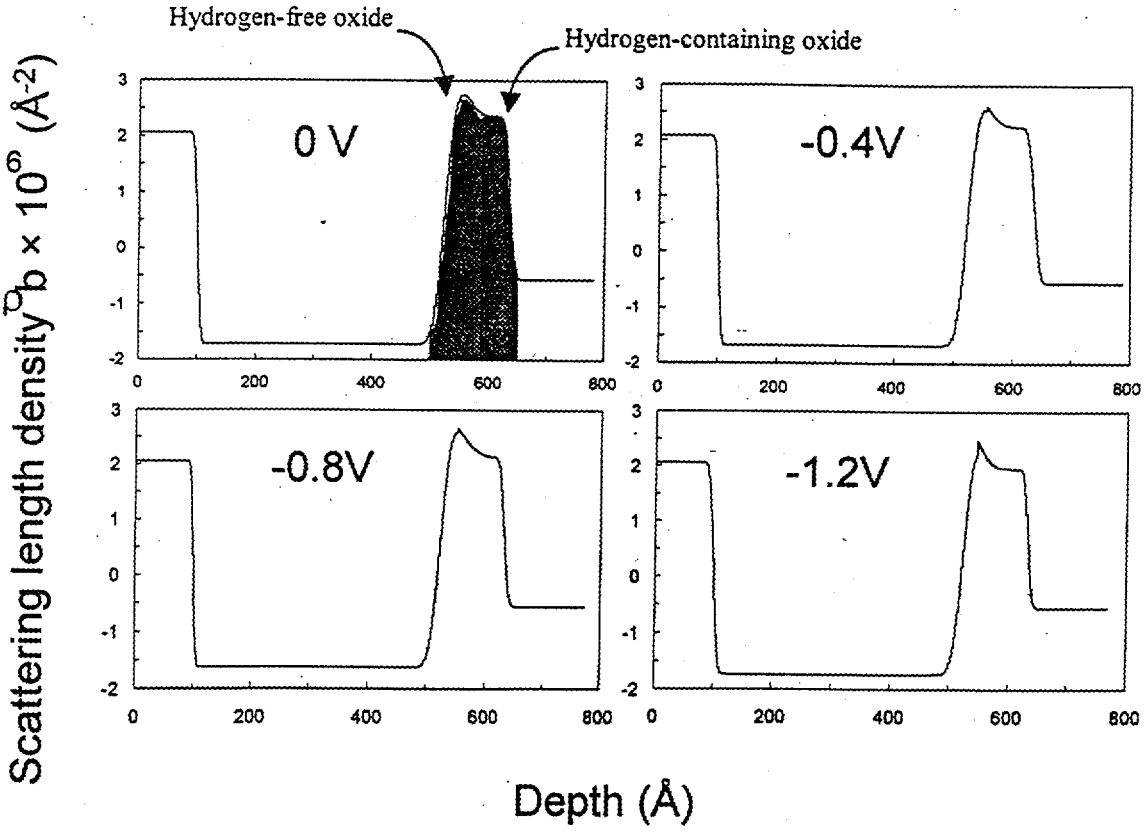
Hydrogen-free oxide
Hydrogen-containing oxide
0 V
-0.4V
-0.8V
-1.2V
Scattering length density ρb x 10^6 (Å^-2)
Depth (Å)

Figure 13

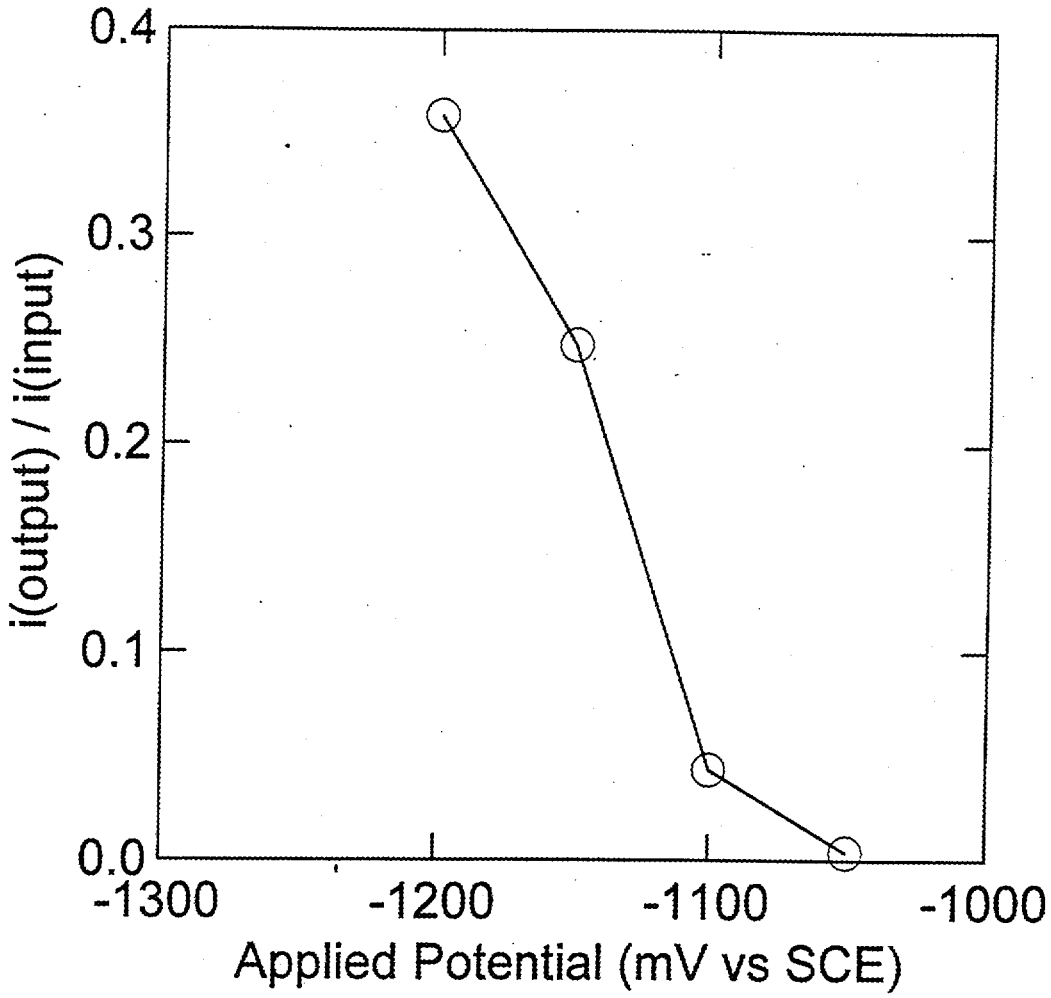
0.4
0.3
0.2
0.1
0.0
i(output) / i(input)
-1300
-1200
-1100
-1000
Applied Potential (mV vs SCE)

Figure 14

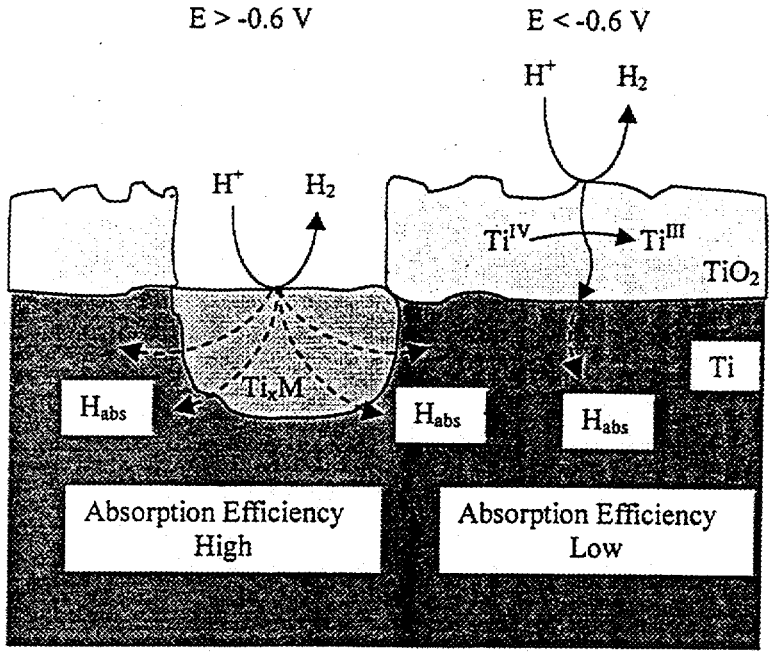
E > -0.6 V
E < -0.6 V
H+
H2
H+
H2
TiIV
TiIII
TiO2
Ti
TixM
Habs
Habs
Habs
Absorption Efficiency High
Absorption Efficiency Low

Figure 15

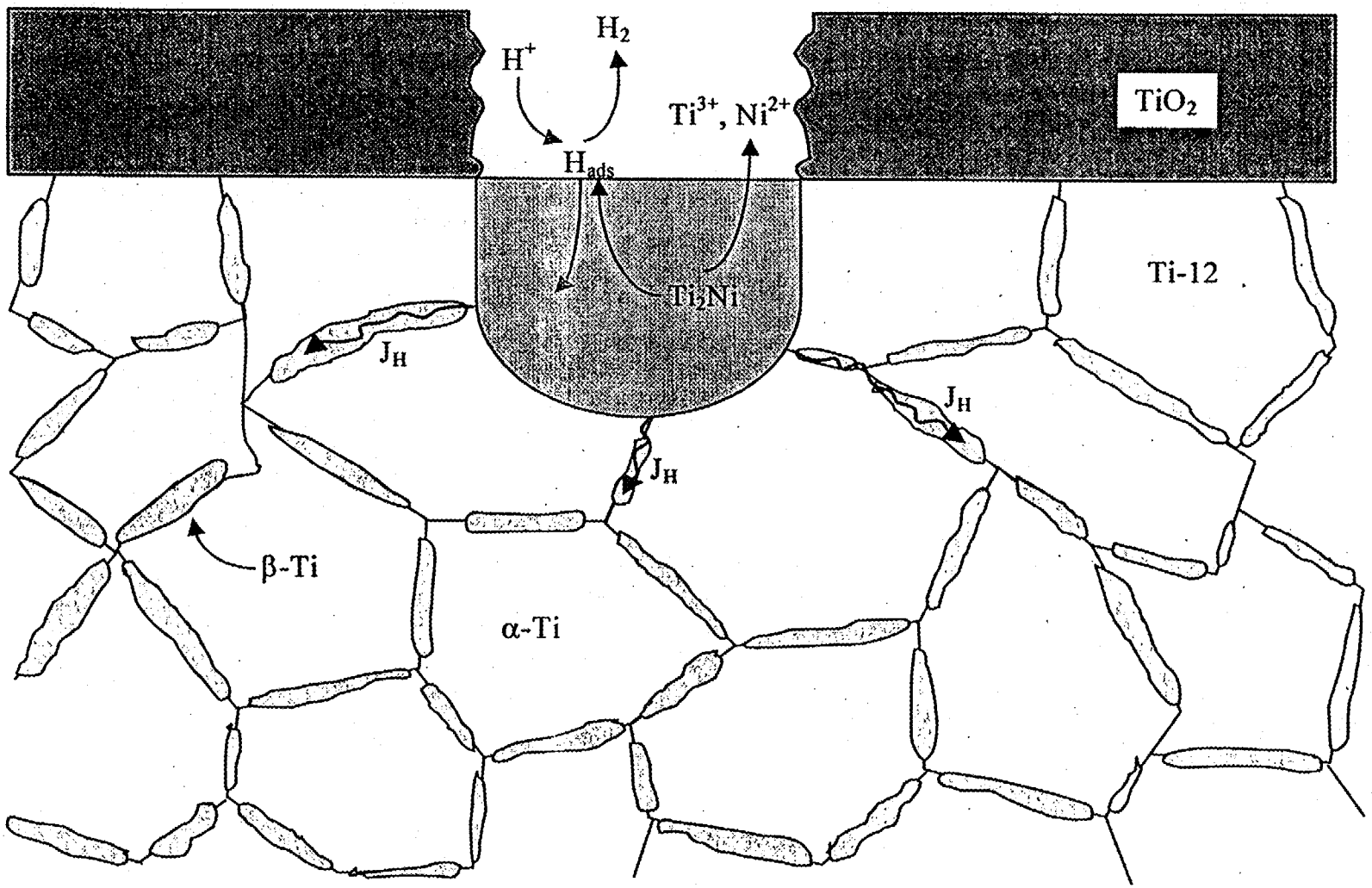

Figure 16

A. LOW TEMPERATURES

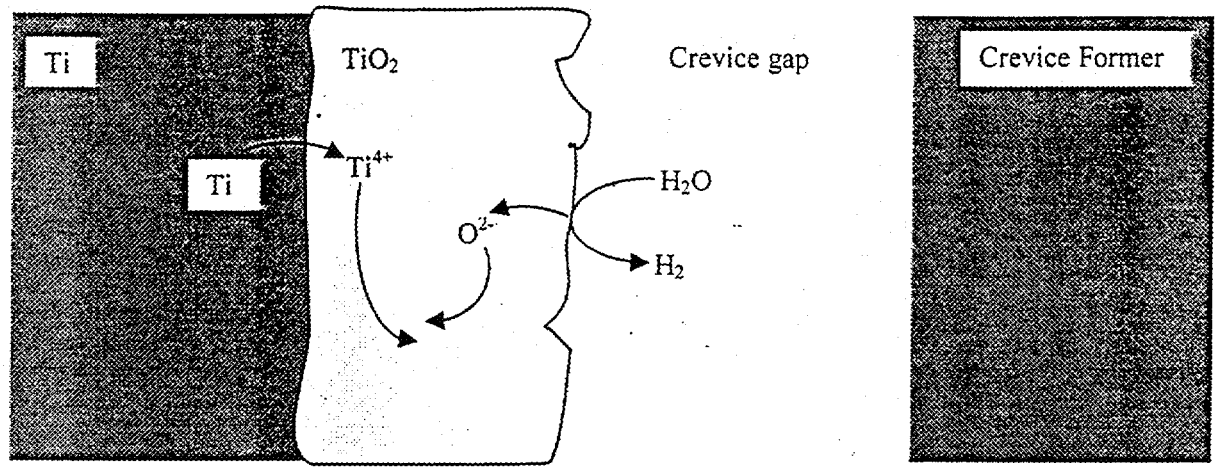

B. TEMPERATURE ≥ 65°C

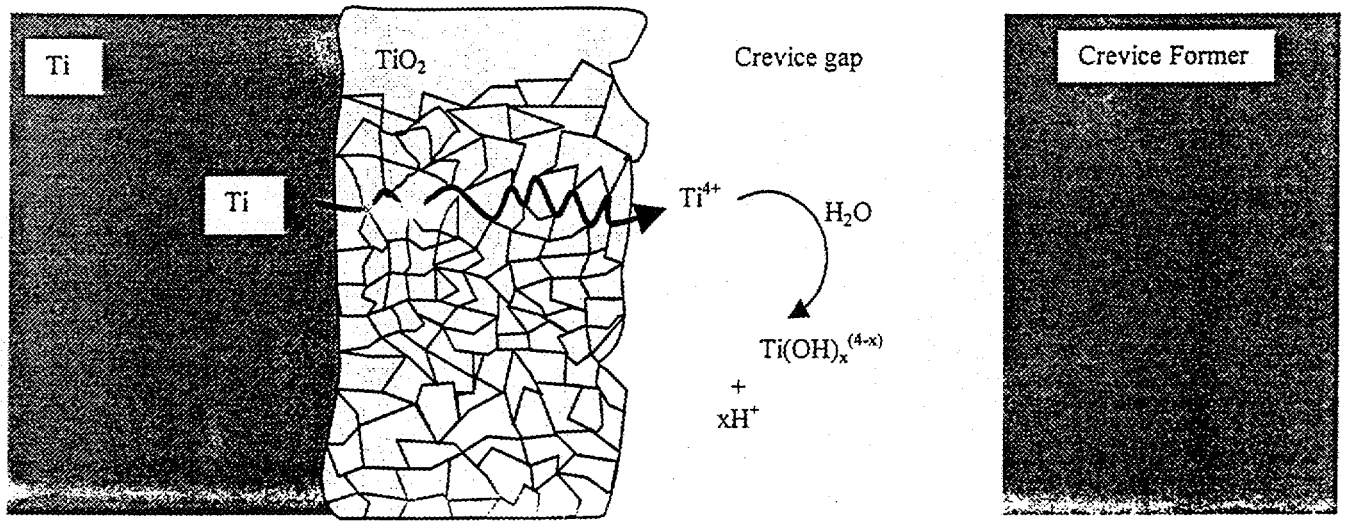

Figure 18

APPENDIX A

THE PROPERTIES OF ALLOYING ELEMENTS IN α-TITANIUM ALLOYS AND THEIR ABILITY TO CATALYZE HYDROGEN ABSORPTION

While the addition of alloying elements such as Ni (in Ti-12) and Pd (in Ti-16 and Ti-7) are generally beneficial in maintaining the passivity of the alloys their cathodic properties make them potential catalysts for hydrogen absorption into the alloy.

A substantial body of evidence exists to show that the presence of these alloying elements leads to the absorption of hydrogen. Based on polarization curves determined in acidic solutions, Figure A1, Glass (1983) clearly showed that Ti_2Ni and titanium could couple galvanically. In a subsequent experiment, in which commercially pure Ti was coupled to Ti_2Ni in boiling HCl, he showed that the dissolution of Ti was accompanied by the embrittlement of the Ti_2Ni, and concluded that the cathodic kinetics on Ti-12 (containing Ti_2Ni) would be dominated by Ti_2Ni providing a sufficient surface area of the intermetallic were available. Okada (1983) showed that Ni-plated (by electrodeposition) or Pt-coated (by sputter deposition) titanium electrodes readily absorbed hydrogen for pH □ 3, efficiencies of up to 60% being obtained in acidic solutions at 25°C, Figure A2.

electrochemical desorption step consistent with the catalytic behaviour observed on noble metals such as Pd (Greef *et al.* 1985). This observation of catalyzed proton reduction at less negative potentials is clear evidence that the need for redox transformations in the oxide is not a prerequisite for proton absorption into the metal matrix. The behaviour observed is consistent with the existence of intermetallics, rich in noble metal content, which can function as "hydrogen windows" in the oxide.

Schutz and Xiao (1993) observed similar effects for proton reduction on Ti-2, Ti-7, and Ti-16. The Tafel slope for Ti-16 (100 mV^{-1}) was larger than that obtained for Ti-7 (80 mV^{-1}) indicating that the ability to catalyze proton reduction decreases as the Pd content of the titanium decreases.

This is consistent with the observation of Fukuzuka *et al.* (1980), that the efficiency of H absorption into the Ti also decreases with decreasing Pd content, Figure A3. As shown in the figure, the difference in measured absorption efficiency between Ti-2 and Ti-7 is less than a factor of 5 over the measured region. An even lower difference would be expected between Ti-2 and Ti-16.

Our own cathodic polarization studies on Ti-2, Ti-12 and Ti-16 specimens have shown interesting differences in the hydrogen absorption behaviour of these alloys. Figure A4 shows cathodic polarization curves recorded potentiostatically on Ti-2 in 0.27 $mol \cdot L^{-1}$ NaCl (pH ~ 1) at 95°C (Noël *et al.* 1996). In a separate set of experiments, the amount of hydrogen absorbed as a function of applied potential was measured. The hydrogen absorption behaviour can be separated into two distinct regions, denoted A and B on the figure. In region A (> -0.6 V) no hydrogen absorption into the metal was observed, while

for more negative potentials in region B it was. This observation is consistent with the demonstrated existence of a hydrogen absorption threshold at (~ -0.6 V) (Murai *et al.* 1977) discussed above (Figure 11).

For Ti-12, absorption was observed at more positive potentials than -0.6 V consistent with the presence of hydrogen absorption windows which allow absorption to occur before redox transformations occur in the oxide. In view of the results of Fukuzuka *et al.* (1980) for Ti-1Pd and Ti-7, we would have anticipated similar behaviour for Ti-16. However, no absorption of hydrogen into the metal was observed until E was □ -1.0 V (vs. SCE). This observation was even more baffling since microscopic examination of the Ti-16 revealed the existence of a large number of randomly dispersed intermetallic particles, suggesting the separation of Pd into catalytic cathodes (Noël 1999), Figure A5.

A hypothesis advanced by Ikeda (private communication) is that the intermetallic particles act as point conductors within an insulating TiO_2 oxide. At cathodic potentials the low resistance to current flow at these sites prevents polarization of the surrounding oxide, and the potential at the intermetallic must reach -1.0 V before a potential of -0.6 V becomes applied across the oxide. For this situation to prevent H absorption into the alloy, the cathodic intermetallics must either be unable to absorb H or capable of saturating with H and rapidly forcing its absorption efficiency to zero. If behaving in the latter mode the intermetallics would be acting as hydrogen storage sites which in the absence of any β-phase in the bulk of the alloy retain the hydrogen at the surface of the alloy. Since they are small and few in number their hydrogen content may be undetectable by bulk analyses.

To date, the nature and properties of these intermetallics present in Ti-16 have not been elucidated. According to the phase diagram for Ti-Pd, a Pd content of 0.05 wt% is insufficient to exceed the Pd solubility and, hence, to cause phase separation as an intermetallic. This appeared to be confirmed by Kitayama *et al.* (1990) who showed that Ti-16 had a large grained equiaxed microstructure containing no separated intermetallics. However, when 0.3 wt% Co was added to the alloy, a much smaller grained equiaxed structure containing a fine dispersion of particulates was obtained. The presence of these particulates, assumed to be Ti_xCo led to further increases in the alloy's resistance to corrosion in hot reducing acid solutions.

The Ti-16 specimens used in impedance experiments (Figure B2) and cathodic polarization/hydrogen absorption experiments (Figure A4) contained ~0.1 wt% Fe, a concentration in excess of the ~0.03 wt% solubility limit above which Watanabe *et al.* 1988 showed Ti_xFe particles precipitated. As discussed in Appendix B, Ti_xFe would be a reactive intermediate and expected to behave in a manner similar to that observed for Ti_2Ni in Ti-12. However, the impedance results, discussed in Appendix B, clearly show the intermetallic precipitates present in Ti-16 to be inert.

Two alternative explanations appear possible. The particulates could be Ti_xFe and simply difficult to activate for hydrogen absorption as discussed by Wu (1984). This would not account for their inertness at temperatures (> 65°C) at which they would be expected to be reactive. Alternatively, the co-separation of Pd to yield a TiPdFe intermetallic particle could explain both their inertness and their ability to function as catalytic cathodes without causing significant H absorption. To function in this last

manner they would have to act as hydrogen saturated storage alloys with zero efficiency for the absorption of further hydrogen once saturated. Presently, no experimental evidence exists to evaluate these possibilities.

REFERENCES

T. Watanabe. T. Shindo and H. Naito. 1988. Effect of iron content on the breakdown potential for pitting of titanium in NaCl solutions. In Proceedings of the Sixth World Conference on Titanium, Cannes, France, 1988, June 6-9, 1735-1740.

S. Kitayama, Y. Shida and M. Oshiyama. 1990. Development of new crevice corrosion resistant Ti alloys. Sumitomo Search 41, 23-32.

J.B.C. Wu. 1984. Effect of iron content on hydrogen absorption and passivity breakdown of commercially pure titanium in aqueous solutions. In Titanium, Science and Technology, Proceedings of the Fifth International Conference on titanium, Munich, Germany, Sept. 10-14, 1984 (edited by G. Lütjering, U. Zwickler and W. Bunk), vol. 4., 2595-2602.

R. Greef, R. Peat, L.M. Peter, D. Pletcher, J. Robinson. 1985. Instrumental methods in Electrochemistry. Ellis Horwood Ltd. Chichester, U. K.

R. S. Glass. 1983. Effect of intermetallic Ti_2Ni on the electrochemistry of Ticode-12 in hydrochloric acid. Electrochimica Acta, 28 (11), 1507-1513.

T. Okada. 1983. Factors influencing the cathodic charging efficiency of hydrogen modified titanium electrodes. Electrochimica Acta, 28(8) 113-1120.

Y. J. Kim and R. A. Oriani. 1987. Corrosion properties of the oxide film formed on Grade-12 titanium in brine under gamma radiation. Corrosion. 43, 85-91.

T. Fukuzuka, K. Shimogori and H. Satoh. 1980. Role of palladium in hydrogen absorption of Ti-Pd alloy. In titanium '80, Science and Technology (edited by H. Kimura and O. Izumi), The metallurgical Society of AIME, Warrendale, PA.

J. J. Noël, M. G. Bailey, J. P. Crosthwaite, B. M. Ikeda, S. R. Ryan and D. W. Shoesmith. 1996. Hydrogen absorption by Grade-2 Titanium. Atomic Energy of Canada Ltd. Report, AECL-11608, COG-96-249.

T. Murai, M. Ishikawa and C. Miura. 1977. Absorption of hydrogen into titanium under cathodic polarization. Boshoku Gijutsu 26, 177-183.

D. W. Shoesmith and F. King. 1999. The effects of gamma radiation on the corrosion of candidate materials for the fabrication of nuclear waste packages. Atomic Energy of Canada Ltd. Report. AECL-11999.

R. W. Schutz and M. Xiao. 1993. Optimized Lean-Pd titanium alloys for aggressive reducing acid and halide service environments. Proceedings of 12th International Corrosion Congress, Sept. 1993, Vol. 3A, 1213-1225, NACE International, Houston, TX.

LEGENDS FOR FIGURES IN APPENDIX A

Figure A1. Polarization curves recorded (separately) for commercially-pure Ti (o, Ti-2) and the intermetallic compound Ti_2Ni (±) in boiling deaerated 1M HCl (from Glass 1983).

Figure A2. Effect of pH on the current efficiency for hydrogen absorption by Ti (o), Ni-modified Ti (ƒ) and Pt-modified Ti (±) recorded galvanostatically at a current density of 0.5 $mA \cdot cm^{-2}$ at 25°C for 2 hours (from Okada 1983).

Figure A3. Relationship between the amount of hydrogen absorbed and the corrosion rate of $Ti^{(o)}$ and titanium containing 1% Pd (±) and 0.15% Pd (•) (from Fukuzuka *et al.* 1980).

Figure A4. Potentiostatically recorded polarization curves for Ti-2 in 0.1 $mol \cdot L^{-1}$ HCl + 0.27 $mol \cdot L^{-1}$ NaCl at 95°C. The curves denoted by the symbols ∏ and o correspond to polarization curves recorded after an open-circuit transient in which the potential (E_{oc}) initially shifted to negative values before reclimbing to ~ -0.3 V. The curve denoted by the symbol ® was recorded after E_{oc} fell to negative values (~ -0.6 V) and did not subsequently reclimb. A and B indicate the two segments of the polarization curves discussed in the text (from Noël *et al.* 1996).

Figure A5. Photomicrograph showing the large number of randomly dispersed intermetallic particles in Ti-16 (from Noël 1999).

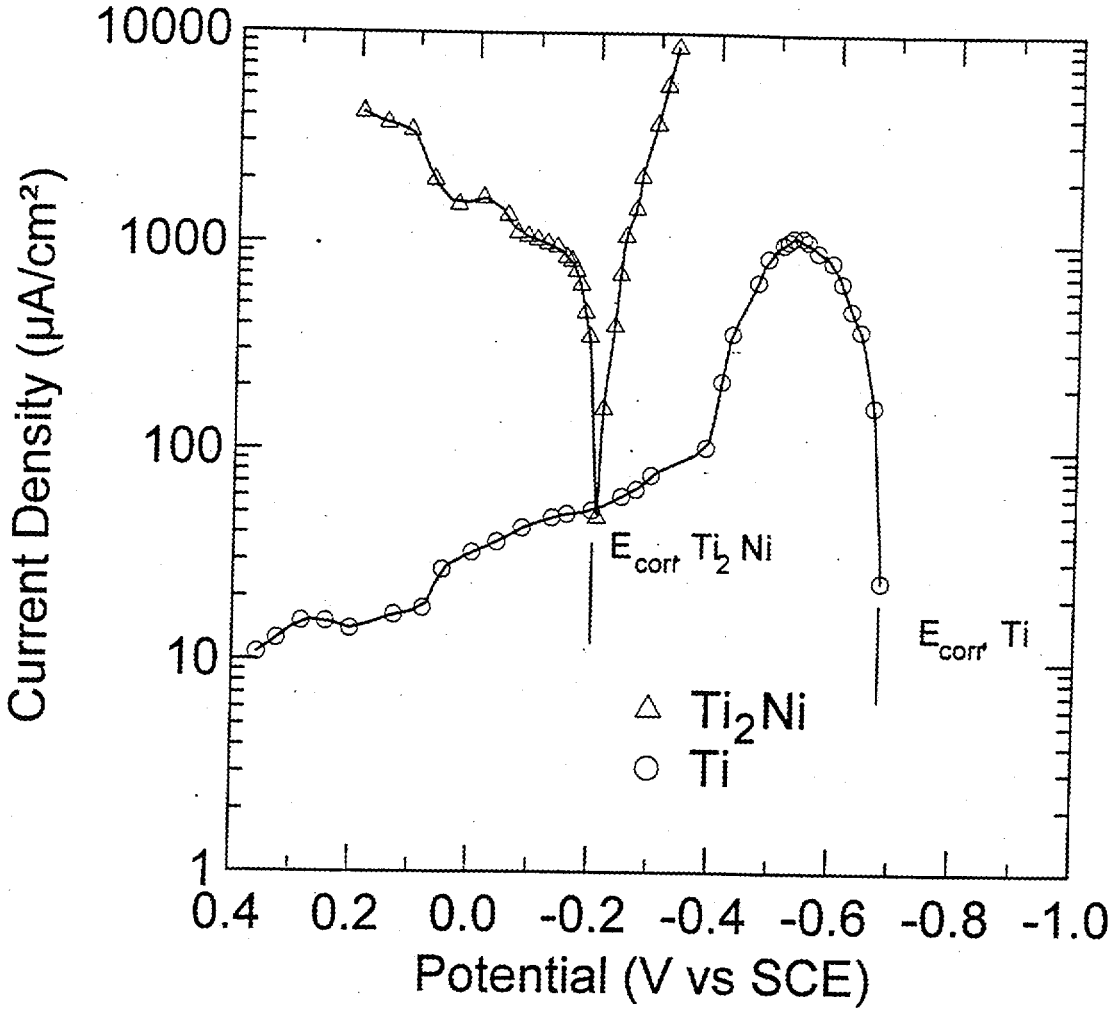
10000
1000
100
10
1
Current Density (μA/cm²)
0.4
0.2
0.0
-0.2
-0.4
-0.6
-0.8
-1.0
Potential (V vs SCE)
E corr Ti2 Ni
E corr Ti
Ti2Ni
Ti

Figure A1

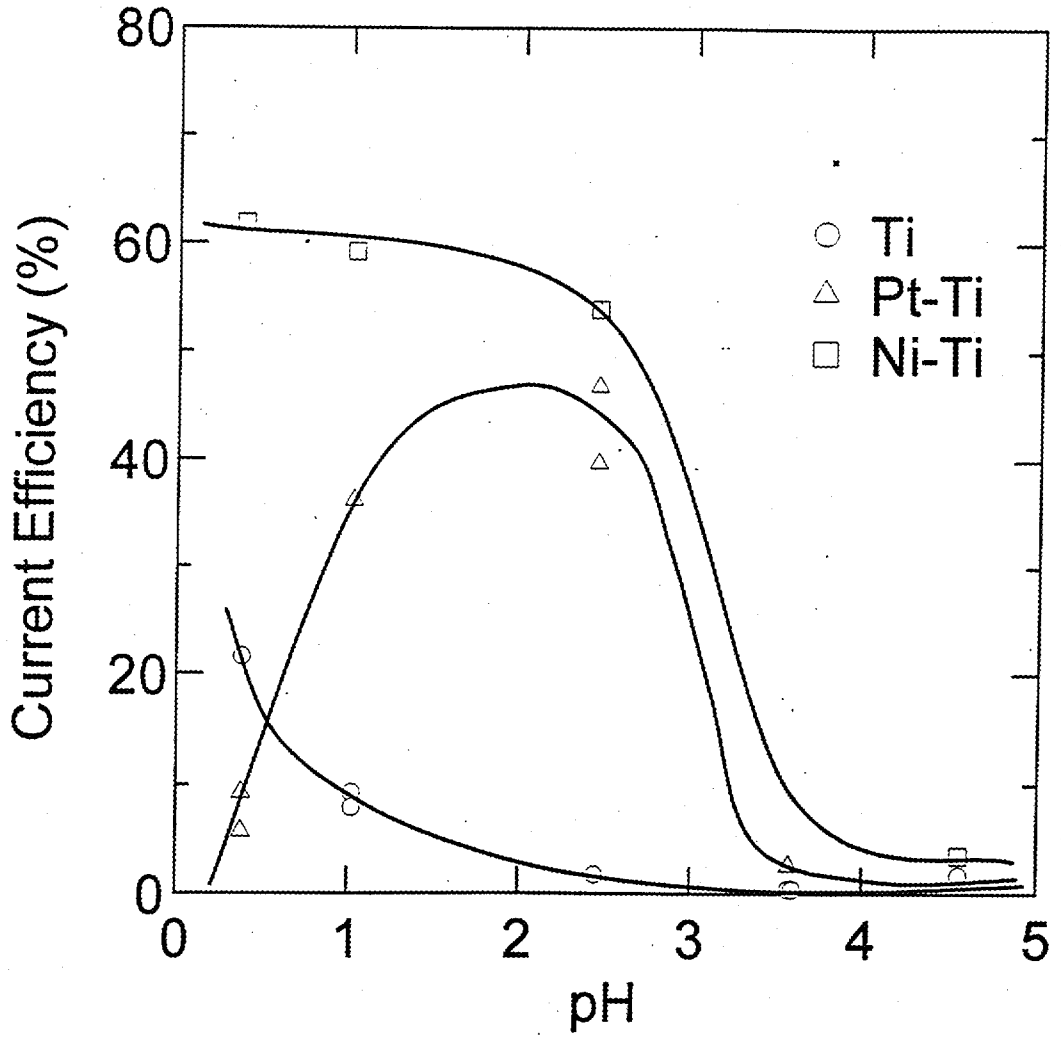

Figure A2

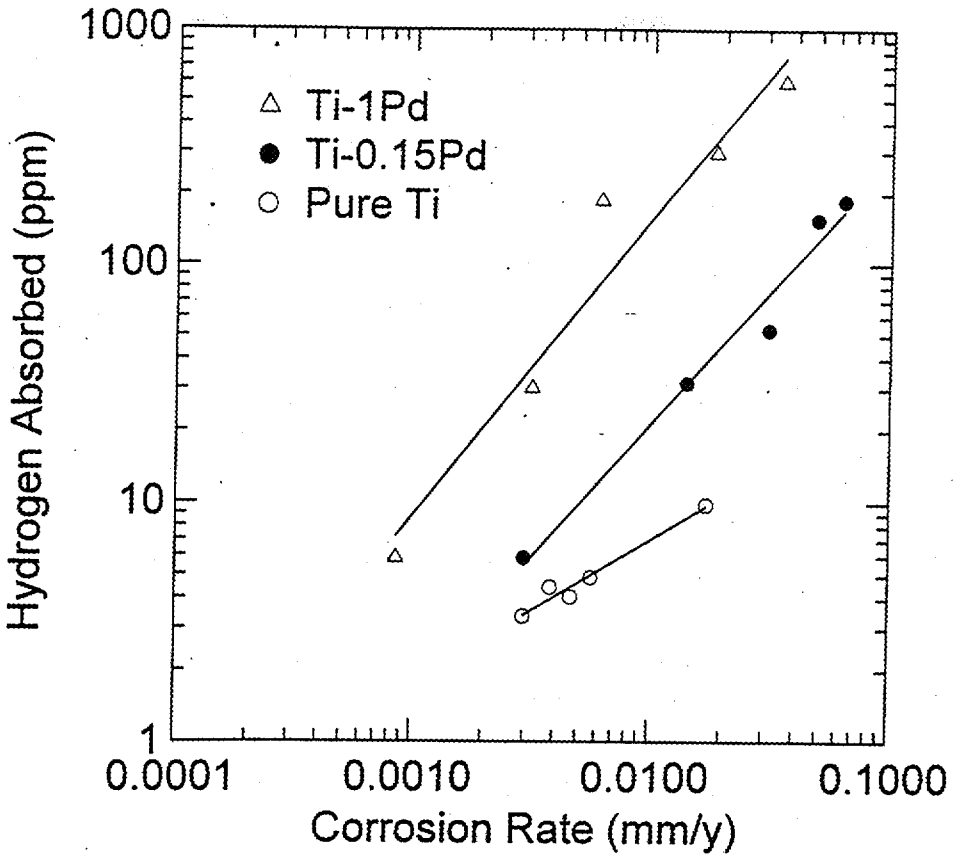
1000
100
10
1
Hydrogen Absorbed (ppm)
Ti-1Pd
Ti-0.15Pd
Pure Ti
0.0001
0.0010
0.0100
0.1000
Corrosion Rate (mm/y)

Figure A3

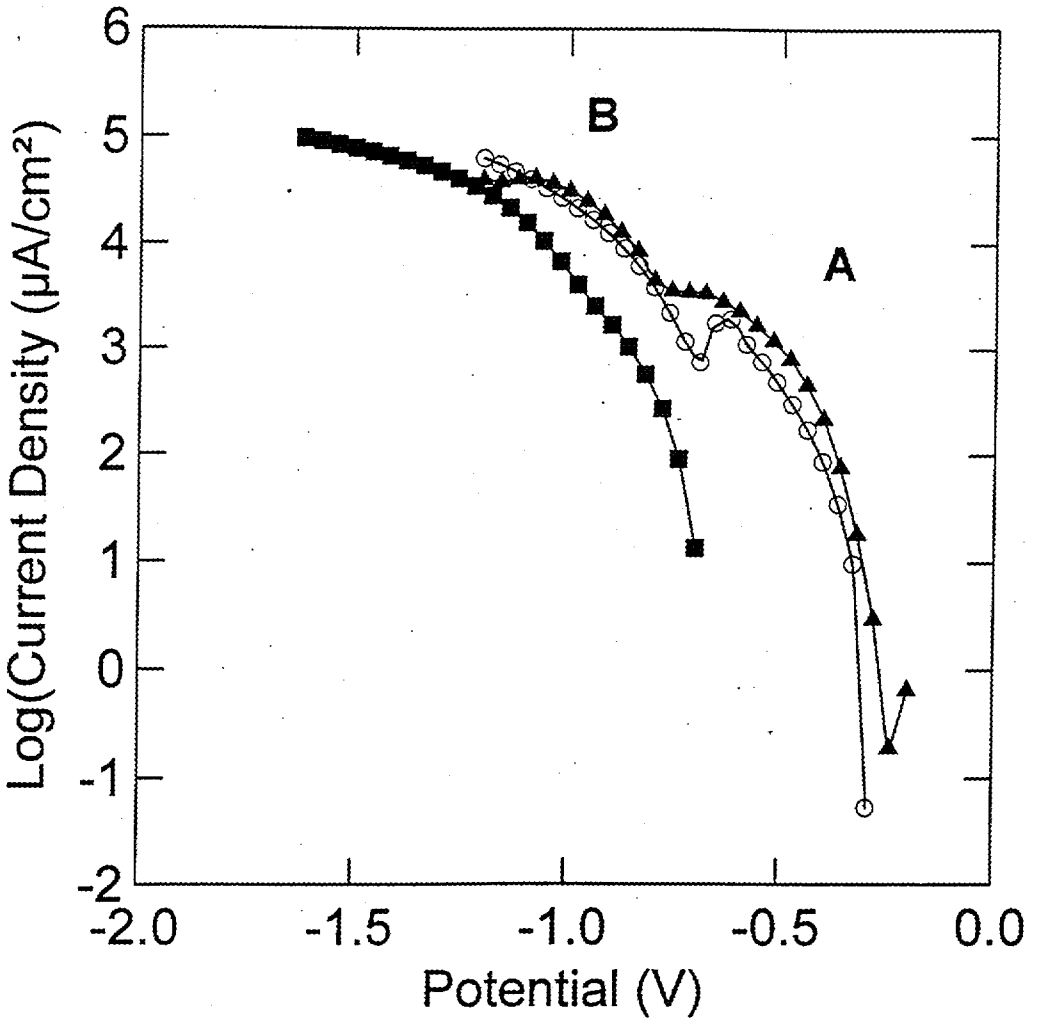
Log(Current Density (μA/cm²))
Potential (V)
B
A
6
5
4
3
2
1
0
-1
-2
-2.0
-1.5
-1.0
-0.5
0.0

Figure A4

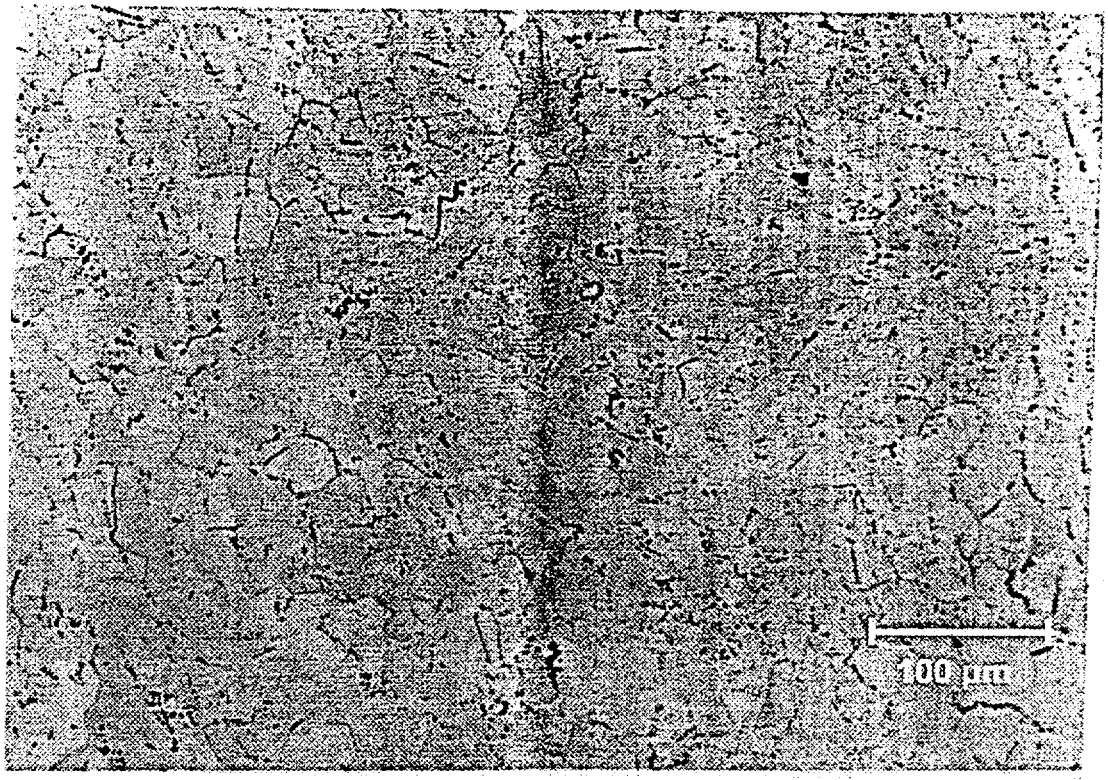

Figure A5

APPENDIX B

BEHAVIOUR OF THE ALLOYING ELEMENTS AND THE KEY IMPURITY, Fe, IN Ti-2, Ti-12, Ti-16

In an attempt to understand the properties of these alloys, in particular the properties of those sites at which the oxide film may be breached and hydrogen absorbed, we undertook an impedance study of a series of titanium alloys, including Ti-2, Ti-12 and Ti-16 in neutral 0.27 $mol \cdot L^{-1}$ NaCl as a function of temperature (ambient to 80°C) (Shoesmith *et al.* 1997, Noël 1999). For Ti-2, the impedance behaviour as a function of temperature showed a decrease in film resistance for T □ 65°C, and could be interpreted in terms of a simple equivalent circuit of a parallel combination of a capacitor and a resistance (*i.e.*, a single time constant circuit). The decrease in film resistance as the temperature increases is consistent with the film breakdown/recrystallization process known to occur for T □ 65°C (Shoesmith and Ikeda 1997). The absence of a second time constant in the impedance response indicates that this breakdown is general, e.g. the generation of many lower resistance pathways at grain boundaries in the recrystallized oxide, and not the formation of discrete breakdown sites.

For the Ti-12 and Ti-16 alloys, however, the impedance results fit a model in which it is assumed that pores (or cracks and other faults) existed in the passive oxide film protecting the alloy. These faults were modeled using an equivalent circuit comprising an interfacial impedance (Z_i) in series with a pore resistance (R_{PORE}) both in parallel with a capacitance used to represent the properties of the passive film on non-faulted sites in

the oxide, Figure B1. This model fitted the experimental data very well as discussed in detail elsewhere (Shoesmith *et al.* 1997, Noël 1999).

The calculated values of the interfacial resistance (the resistive component of Z_I which comprises a parallel combination of this resistance and a double layer capacitance), taken to be the polarization resistance (R_p) at the base of the pore, and the pore resistance are plotted in Figures B2A and B2B. For Ti-12, the polarization resistance decreases with temperature, especially above ~ 65°C. By contrast no significant drop in polarization resistance is observed for Ti-16 up to 80°C. For both alloys the pore resistance (R_{PORE}) decreases slightly with an increase in temperature, but the absolute values for Ti-16 are about an order of magnitude lower than those for Ti-12.

A rational conclusion from these results is that, as the temperature increases, Ti-12 develops reactive sites (low Z_i) at the bottom of relatively narrow, highly resistive pores (high R_{PORE}). By contrast, the sites at the bottom of relatively open pores/faults (low R_{PORE}) in Ti-16 remain inert (high Z_i) over the whole temperature range. This last interpretation is consistent with the photomicrograph in Figure A5. From the impedance results we would conclude that these particles are inert. For Ti-12, however, it is more reasonable to conclude that exposed sites within the passive oxide are reactive and that these sites coincide with the location of Ti_2Ni intermetallic particles or reactive β-phase in the underlying predominantly α-Ti matrix.

In support of this argument that the Ti_2Ni intermetallics in Ti-12 will be reactive if acidic conditions can be established are the results of Glass (1983) who has clearly shown in polarization experiments, Figure A1, that Ti_2Ni is very reactive in hot acidic solutions.

These polarization curves show that not only is Ti_2Ni a good catalyst for proton reduction but that it also does not passivate when anodically polarized and hence is susceptible to rapid corrosion under acidic conditions. A similar susceptibility to corrosion has been demonstrated for β-phase Ti when its Ni content is high (Hall *et al.* 1985).

We would conclude from this evidence that it is possible for hydrogen absorption into Ti-12 to be facilitated by the coexistence of anodes and cathodes located at Ti_2Ni or Ni-containing β-phase at imperfections in the passive TiO_2 film. In the situation analyzed in impedance experiments this acidity will be localized at the film breakdown sites which appear in the oxide as the temperature increases. As within any occluded site a combination of metal dissolution, dissolved cation hydrolysis and limited transport would yield acidity.

Since the solubility of hydrogen in Ti_2Ni, and to a lesser degree the β-phase, will be substantially higher than in the α-phase it would be expected that this reactivity would enhance hydrogen absorption into the titanium matrix. An additional feature of the Ti-12 which would aid this process is the presence of β-phase which tends to occur as ligaments along the α-Ti grain boundaries (Glass 1983). This geometry, coupled with the higher diffusion rate of H in the β–phase (reported to be 10^5 times that in the α-phase (Wang *et al.* 1999)) would facilitate the transport of H into the bulk of the alloy, Figure 16.

The most common impurity in titanium alloys with the potential to exert a major influence on H absorption behaviour is Fe. Many studies of the influence of Fe on the

corrosion of, and hydrogen absorption by, Ti have been undertaken with conflicting results (Cotton 1970, Covington and Schutz 1981, Schutz *et al.* 1984). Of particular interest in the present context is the ability of Fe-containing phases and intermetallic particles to absorb hydrogen. The influence of Fe would be expected to be similar to that of Ni in Ti-12 since it can both separate into intermetallic precipitates and stabilize the β-phase. It is likely that many of the inconsistencies for the influence of Fe on Ti corrosion can be attributed to variations in its distribution within the metal matrix.

Cotton (1970) clearly showed that H more rapidly diffused in Ti-2 as the Fe content was increased from 0.05 wt % to 0.12 wt %. This observation would be consistent with an increase in the β-phase content of the alloy with increasing Fe content. These results appear to be at odds with those of Covington and Schutz (1981) which showed that, for cathodic charging conditions (9.6 $mA \cdot cm^{-2}$ in 1% NaCl (pH = 1) at 90°C) the efficiency of H absorption decreased from ~ 30% for [Fe] < 0.04 wt % to ~ 15% for [Fe] □ 0.20%. While no attempt to explain this apparent inconsistency was offered, it is likely that the decreased efficiency can be attributed to the separation of the Fe into Ti_xFe intermetallic precipitates at the higher Fe contents. A number of authors (Wu 1984. Ikeda *et al.* 1990, Watanabe *et al.* 1988) have clearly shown that as the Fe content of Ti-2 increases the α-grain size decreases and Ti_xFe intermetallics are formed. According to Watanabe *et al.* (1988) this occurs once [Fe] is □ 350 μg/g (0.035 wt %).

While the intermetallic Ti_xFe has been shown to be a hydrogen absorber it is claimed to be difficult to activate for hydrogen storage (Wu 1984). Hence, despite its presence at higher Fe contents it could actually impede hydrogen absorption despite acting as a H^+

reduction catalyst. According to Wu, the hydride formed on this intermetallic possesses less lattice distortion than that formed on α-Ti, a feature which would retard the diffusion of hydrogen. Similar speculations have been offered by Schutz *et al.* (1984). Such mechanistic features would lead to decreased H absorption with increasing Fe content.

That Fe present in β-phase leads to enhanced susceptibility to corrosion has been demonstrated by Ikeda *et al.* (1994) for Ti-2 and by Ruppen *et al.* (1983) for Ti-12. In both cases it appeared that if the Fe were located in β-phase it led to an increase in anodic current, and in corrosion experiments, an increase in corrosion current. However, when separated into Ti_xFe intermetallics, corrosion rates decreased and passivity was easier to maintain.

From these results it is clear that the distribution and local concentration of the alloying element Ni and the impurity element Fe will have a major influence on both the corrosion behaviour of Ti-12 (containing both Ni and Fe) and Ti-2 (similarly contaminated with Fe) and their ability to absorb hydrogen. Both Ni and Fe containing β–phase and Ti_2Ni and Ti_xFe intermetallic particles are susceptible to anodic dissolution in acidic environments. While it remains to be demonstrated whether Ni/Fe β-phase can also act as catalytic cathodes, there is little doubt in the case of the intermetallics, or in their ability to absorb hydrogen. It is likely, however, that absorbed H would remain localized at the intermetallic site unless the predominantly α-phase alloy contains β-phase ligaments which enhance transport of hydrogen into the bulk of the alloy. In the absence of these

transport pathways the intermetallic particles may become saturated in H, a condition for which the efficiency of further H absorption approaches zero.

For the Ti-16 alloy the presence of Pd in intermetallic particles would be expected to provide excellent hydrogen absorption "windows" thereby allowing hydrogen absorption to occur at potentials less than the -0.6 V required to induce the redox transformations in the oxide which render it permeable to hydrogen. While the H absorption efficiency has been shown to decrease as the Pd content decreases (Fukuzuka *et al.* 1980, Figure A3) it was still surprising to discover that the absorption of H into this alloy was undetectable until potentials □ -1.0 V.

REFERENCES

T. Watanabe. T. Shindo and H. Naito. 1988. Effect of iron content on the breakdown potential for pitting of titanium in NaCl solutions. In Proceedings of the Sixth World Conference on Titanium, Cannes, France, 1988, June 6-9, 1735-1740.

R. W. Schutz, J. S. Grauman and J. A. Hall. 1984. Effect of solid solution iron on the corrosion behaviour of titanium. In Titanium, Science and Technology, Proceedings of the Fifth International Conference on Titanium, Sept 10-14 (1984), Munich, Germany, (edited by G. Lütjering, U. Zwickler and W. Bunk), 2617-2624.

J. A. Ruppen, R. B. Diegle, R. S. Glass and T. J. Headley. 1983. Some effects of microstructure and chemistry on corrosion and hydrogen embrittlement of Ti-12. Mat. Res. Soc. Symp. Proc. 15, 685-693.

J. J. Noël. 1999. The electrochemistry of titanium corrosion. Ph. D. Thesis, University of Manitoba.

L. C. Covington and R. W. Schutz. 1981. Effects of iron on the corrosion resistance of titanium. In Industrial applications of Titanium and Zirconium, ASTM 728, (ed. E. W. Kleefisch) 163-180.

J.B.C. Wu. 1984. Effect of iron content on hydrogen absorption and passivity breakdown of commercially pure titanium in aqueous solutions. In Titanium, Science and Technology, Proceedings of the Fifth International Conference on titanium, Munich, Germany, Sept. 10-14, 1984 (edited by G. Lütjering, U. Zwickler and W. Bunk), vol. 4., 2595-2602.

R. S. Glass. 1983. Effect of intermetallic Ti_2Ni on the electrochemistry of Ticode-12 in hydrochloric acid. Electrochimica Acta, 28 (11), 1507-1513.

T. Fukuzuka, K. Shimogori and H. Satoh. 1980. Role of palladium in hydrogen absorption of Ti-Pd alloy. In titanium `80, Science and Technology (edited by H. Kimura and O. Izumi), The metallurgical Society of AIME, Warrendale, PA.

D. W. Shoesmith, W. H. Hocking, B. M. Ikeda, F. King, J. J. Noël and S. Sunder. 1997. Application of electrochemical methods in the development of models for fuel dissolution and container corrosion under nuclear waste disposal conditions. Can. J. Chem. 75(11), 1566-1584.

D. W. Shoesmith and B. M. Ikeda. 1997. The resistance of titanium to pitting, microbially induced corrosion, and corrosion in unsaturated conditions. Atomic Energy of Canada Ltd. Report, AECL-11709, COG-95-557-1.

J. A. Hall, D. Banerjee and T. L. Wardlaw. 1985. The relationships of structure and corrosion behaviour of Ti0.3Mo0.8Ni (Ticode-12). In Titanium, Science and Technology, Proceedings of the Fifth International Conference of Titanium (edited by G. Lütjering, U. Zwickler and W. Bunk), Sept. 10-14 (1984), Munich, Germany, 2603-2610.

B. M. Ikeda, M. G. Bailey, D. C. Cann and D. W. Shoesmith. 1990. Effect of iron content and microstructure on the crevice corrosion of Grade-2 titanium under nuclear waste vault conditions; In Advances in Localized Corrosion (edited by H. S. Isaacs, U. Bertocci, J. Kruger and S. Smialowska), 439-444, NACE International, Houston, TX.

B. M. Ikeda, R. C. Styles, M. G. Bailey and D. W. Shoesmith. 1994. The effect of material purity on crevice corrosion of titanium in NaCl solution. In Compatibility of Biomedical Implants, (edited by P. Kovacs and N. S. Istephanous), Electrochemical Society Proceedings, Vol. 94-15, Electrochemical Society, Pennington, NJ, 368-380.

J. B. Cotton. 1970. Using titanium in the chemical plant. Chemical Engineering Progress, 66(10), 57-62.

FIGURE LEGENDS FOR APPENDIX B

Figure B1. Equivalent circuit used to analyze the electrochemical impedance spectroscopy data for titanium alloys.

Figure B2. The calculated values of the interfacial resistance, R_p, (the resistive component of Z_I (Figure B1) which comprises a parallel combination of this resistance and a double layer capacitance) and the pore resistance, R_{PORE} (Figure B1), as functions of temperature for Ti-12 (→) and Ti-16 (°). The impedance data were recorded in 0.27 mol·L^{-1} NaCl after 24 hours on open circuit.

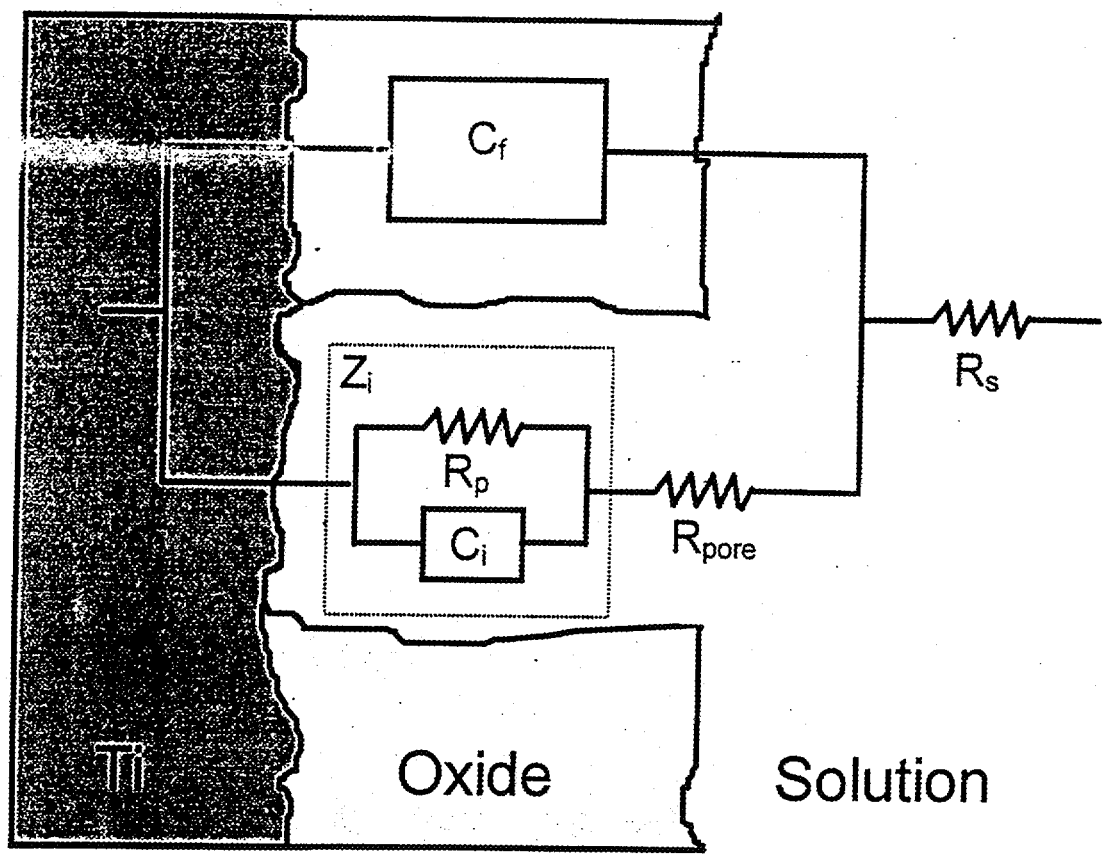

Figure B1

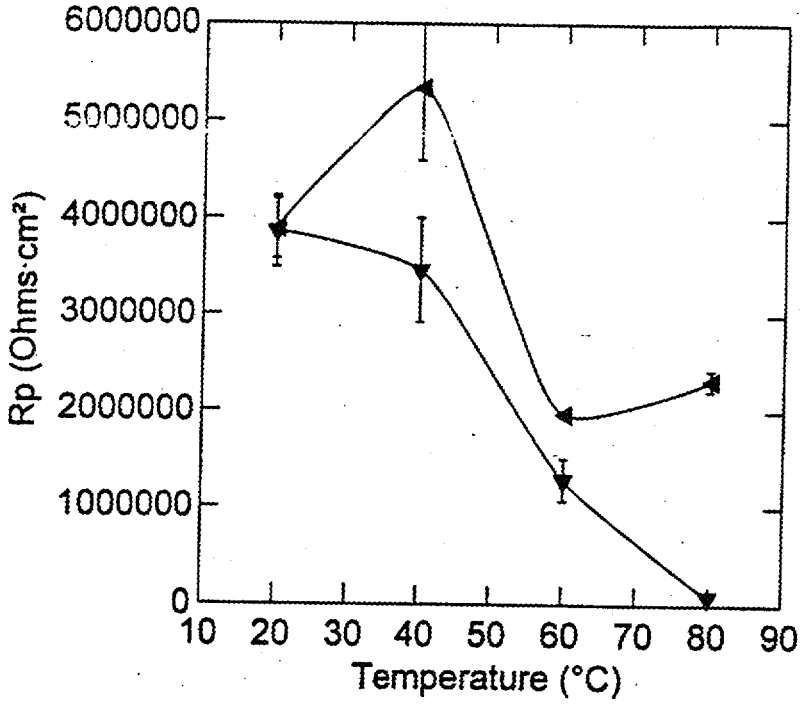
6000000
5000000
4000000
3000000
2000000
1000000
0
Rp (Ohms·cm²)
10 20 30 40 50 60 70 80 90
Temperature (°C)

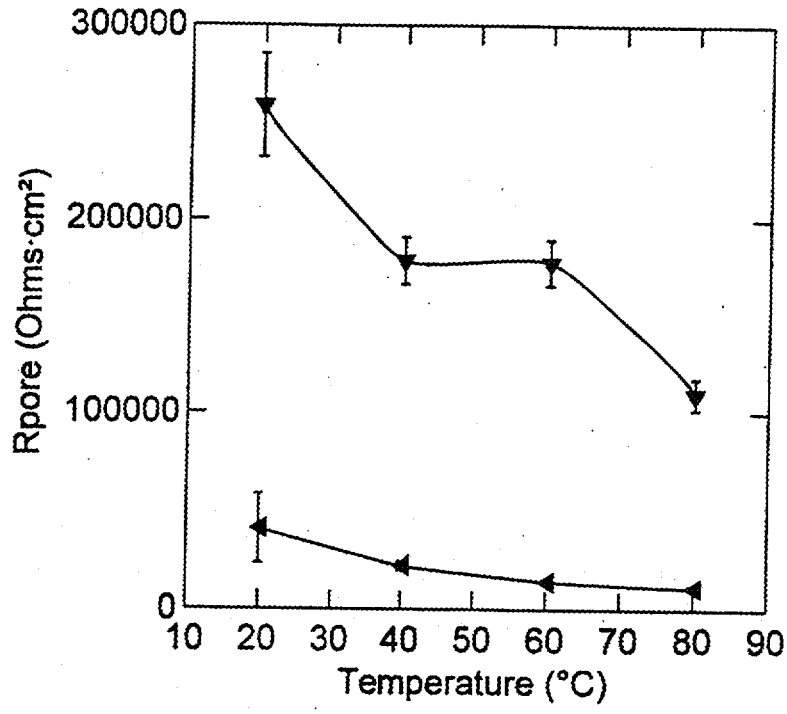
300000
200000
100000
0
Rpore (Ohms·cm²)
10 20 30 40 50 60 70 80 90
Temperature (°C)

Figure B2